University of Wollongong

Research Online

University of Wollongong Thesis Collection 2017+

University of Wollongong Thesis Collections

2023

Research on Information Flow Topology for Connected Autonomous Vehicles

Yan Yan

Follow this and additional works at: https://ro.uow.edu.au/theses1

University of Wollongong

Copyright Warning

You may print or download ONE copy of this document for the purpose of your own research or study. The University does not authorise you to copy, communicate or otherwise make available electronically to any other person any copyright material contained on this site.

You are reminded of the following: This work is copyright. Apart from any use permitted under the Copyright Act 1968, no part of this work may be reproduced by any process, nor may any other exclusive right be exercised, without the permission of the author. Copyright owners are entitled to take legal action against persons who infringe their copyright. A reproduction of material that is protected by copyright may be a copyright infringement. A court may impose penalties and award damages in relation to offences and infringements relating to copyright material. Higher penalties may apply, and higher damages may be awarded, for offences and infringements involving the conversion of material into digital or electronic form.

Unless otherwise indicated, the views expressed in this thesis are those of the author and do not necessarily represent the views of the University of Wollongong.

Research Online is the open access institutional repository for the University of Wollongong. For further information contact the UOW Library: research-pubs@uow.edu.au

UNIVERSITY
OF WOLLONGONG
AUSTRALIA

Research on Information Flow Topology for Connected Autonomous Vehicles

Yan Yan

Supervisors:
Senior Professor Haiping Du
Senior Professor Weihua Li
Associate Professor David Stirling

This thesis is presented as part of the requirement for the conferral of the degree:
Doctor of Philosophy

University of Wollongong

School of Electrical, Computer and Telecommunications Engineering

February 2023

This work © copyright by Yan Yan, 2023. All Rights Reserved.

No part of this work may be reproduced, stored in a retrieval system, transmitted, in any form or by any means, electronic, mechanical, photocopying, recording, or otherwise, without the prior permission of the author or the University of Wollongong.

This research has been conducted with the support of an Australian Research Council's Discovery Projects funding scheme.

Declaration

I, Yan Yan, declare that this thesis submitted in fulfilment of the requirements for the conferral of the degree: Doctor of Philosophy, from the University of Wollongong, is wholly my own work unless otherwise referenced or acknowledged. This document has not been submitted for qualifications at any other academic institution.

_____

Yan Yan

6th February 2023

Abstract

Information flow topology plays a crucial role in connected autonomous vehicles (CAVs). It describes how CAVs communicate and exchange information with each other. It predominantly affects the platoon's performance, including the convergence time, robustness, stability, and scalability. It also dramatically affects the controller design of CAVs. Therefore, studying information flow topology is necessary to ensure the platoon's stability and improve its performance. Advanced sliding mode controllers and optimisation strategies for information flow topology are investigated in this project.

Firstly, the impact of information flow topology on the platoon is studied regarding tracking ability, fuel economy and driving comfort. A Pareto optimal information flow topology offline searching approach is proposed using a non-dominated sorting genetic algorithm (NSGA-II) to improve the platoon's overall performance while ensuring stability.

Secondly, the concept of asymmetric control is introduced in the topological matrix. For a linear CAVs model with time delay, a sliding mode controller is designed to target the platoon's tracking performance. Moreover, the Lyapunov analysis is used via Riccati inequality to guarantee the platoon's internal stability and input-to-output string stability. Then NSGA-II is used to find the homogeneous Pareto optimal asymmetric degree to improve the platoon's performance. A similar approach is designed for a nonlinear CAVs model to find the Pareto heterogeneous asymmetric degree and improve the platoon's performance.

Thirdly, switching topology is studied to better deal with the platoon's communication problems. A two-step switching topology framework is introduced. In the first step, an offline Pareto optimal topology search with imperfect communication scenarios is applied. The platoon's performance is optimised using a multi-objective evolutionary algorithm based on decomposition (MOEA/D). In the second step, the optimal topology is switched and selected from among the previously obtained Pareto optimal topology candidates in real-time to minimise the control cost. For a continuous nonlinear heterogeneous platoon with actuator faults, a sliding mode controller with an adaptive mechanism is developed. Then, the Lyapunov approach is applied to the platoon's tracking error dynamics, ensuring the systems uniformly ultimately bounded stability and string stability. For a discrete nonlinear heterogeneous platoon with packet loss, a discrete sliding mode controller with a double power reaching law is designed, and a modified MOEA/D with two opposing adaptive mechanisms is applied in the two-step framework.

Simulations verify all the proposed controllers and frameworks, and experiments also test some. The results show the proposed strategy's effectiveness and superiority in optimising the platoon's performance with multiple objectives.

Publications

Journal

Yan, Yan, Du, Haiping, He, Defeng, Li, Weihua. (2022). A Pareto optimal information flow topology for control of connected autonomous vehicles. *IEEE Transactions on Intelligent Vehicles*, DOI: 10.1109/TIV.2022.3145343.

Yan, Yan, Du, Haiping, Wang, Yafei, Li, Weihua. (2022). Multi-Objective Asymmetric Sliding Mode Control of Connected Autonomous Vehicles. *IEEE Transactions on Intelligent Transportation Systems*, 23(9), 16342-16357, DOI: 10.1109/TITS.2022.3149985.

Yan, Yan, Du, Haiping, Wang, Yafei, Li, Weihua. (2022). Multiobjective Heterogeneous Asymmetric Sliding Mode Control of Nonlinear Connected Autonomous Vehicles. *IEEE Access*, 10, 50562-50577, DOI: 10.1109/ACCESS.2022.3171564.

Yan, Yan, Du, Haiping, Han, Qing-Long, Li, Weihua. (2022). Discrete multi-objective switching topology sliding mode control of connected autonomous vehicles with packet loss. *IEEE Transactions on Intelligent Vehicles*, DOI: 10.1109/TIV.2022.3215139.

Yan, Yan, Du, Haiping, Han, Qing-Long, Li, Weihua. (2022). Multi-objective switching topology adaptive sliding mode control of connected autonomous vehicles. *IEEE Transactions on Intelligent Transportation Systems*, under review.

Acknowledgements

I would like to express my profound appreciation to my supervisor, Senior Prof. Haiping Du. He always supports and encourages me when I lack confidence. He is very patient and provides lots of constructive feedback and guidance to my work. In addition, he shares his expertise with me and provides tangible support for my work. I could not have undertaken this journey without him.

I would like to extend my sincere thanks to my co-supervisors, Senior Prof. Weihua Li and Associate Prof. David Stirling. They also provided lots of advice and suggestions for my work, as well as moral support and inspiration. Special thanks to my colleague, Dr Wenxing Li. He helped me a lot when I needed it and always cared about my mental health and wellbeing.

Lastly, I would be remiss in not mentioning my family and friends. They believed in me during this journey and provided emotional support. Special thanks to my amazing boyfriend Justin for always being there for me and caring about me deeply.

List of Abbreviations and Notations

CAVs	Connected autonomous vehicles
MPC	Model predictive control
NSGA-II	Non-dominated sorting genetic algorithm II
MOEA/D	Multi-objective evolutionary algorithm based on decomposition
UB	Uniform boundedness
UUB	Uniform ultimate boundedness
V2V	Vehicle to vehicle
IFT	Information flow topology
CACC	Cooperative adaptive cruise control
LQG	Linear–quadratic–Gaussian
DoS	Denial-of-service
LQR	Linear quadratic regulator
HDVs	Human-driven vehicles
PPC	Prescribed performance control
FDI	False data injection
LMI	Linear matrix inequality
SVE	Velocity error sensitivity
SDE	Spacing error sensitivity
TI	Tracking index
FC	Fuel consumption
ASD	Acceleration standard deviation
DC	Direct current
I	Identical matrix of appropriate dimensions
$diag\{\cdots\}$	Diagonal matrix
$\mathbb{R}^{M\times N}$	Set of $M \times N$ real matrices
$\mathbb{R}^{n}$	n dimensional Euclidean space
$\lambda(A)$	The eigenvalue of Matrix A
1_N	A column vector of size N with all its entries being 1
$\otimes$	Kronecker product
$\|.\|$	Euclidean norm
$\|.\|_{l_2}$	l_2-norm
$\bar{\beta}$	The upper bound of β_i

List of Tables

List of Figures

Contents

Chapter 1

Introduction

1.1 Background and Motivation

CAVs are a group of vehicles that exchange information wirelessly with each other and the infrastructure. The platoon of CAVs improves traffic efficiency and releases traffic congestion. However, poor communication, such as packet loss, disturbance, and unstable wireless data transmission, affects the platoon negatively. Therefore, a dynamic information flow topology with a controller that supports it is essential to the platoon. Dynamic information flow topology selects alternative communication links and partners in real-time to eliminate the negative impact caused by poor communication. It also ensures the platoon's stability and robustness and improves its performance.

There are six types of common fixed information flow topologies: Predecessor-Leader Following Topology (PLF), Predecessor Following Topology (PF), Bidirectional Topology (BD), Bidirectional-Leader Topology (BDL), Two Predecessors Following Topology (TPF), and Two Predecessors-Leader Following Topology (TPLF) [1]. Most studies designed a controller that is based on one fixed information flow topology only. PLF and BDL are the most popular ones. Apart from fixed information flow topology, switching information flow topology is also a hot research topic. It mainly consists of two types. The first one is a topology that switches among a few fixed topologies mentioned above. A topology that switches based on a random or predefined switching signal is the second one. There are some advantages and limitations regarding all topologies. This study focuses on overcoming the limitations of the current fixed and switching topologies by providing a dynamic topology that improves the platoon's performance.

Previous research acknowledges the fact that information flow topology has an impact on CAVs. However, no research quantitatively investigates the influence of information flow topology on the platoon's performance. It motivates the author to study it systematically by considering the platoon's tracking ability, fuel economy, driving comfort, communication cost, and stability.

Sliding mode controller has been popular in the control of CAVs. However, there are also typical communication failures related to the platoon, such as packet loss, time delay, and actuator faults. Therefore, the application of designing an advanced sliding mode controller that not only supports all types of information flow topologies but also addresses the communication failures mentioned above in a nonlinear heterogeneous platoon also gains the author's interest.

Most previous switching topology research focuses on switching among fixed topologies or switching with a random signal only. However, switching information flow topology frequently and randomly poses unnecessary risks to the platoon's stability, making it undesirable in real-world applications. The author bridges the gap by using switching

topology as an optimisation tool to reduce the negative impact caused by poor communication.

In conclusion, there are a lot of essential research aspects of information flow topology for CAVs. Therefore, this thesis is inspired to design advanced sliding mode controllers and optimisation strategies for information flow topology to improve the platoon's performance with multiple objectives.

1.2 Research Objectives

The main aim of this thesis is to design advanced sliding mode controllers and optimisation strategies for information flow topology to improve the platoon's overall performance. Furthermore, simulations and experiments are conducted to prove the effectiveness of the proposed strategy.

The specific objectives of this thesis are listed as follows:

1. The influence of information flow topology on the platoon is investigated, and an offline Pareto optimal topology searching approach is proposed to improve the platoon's performance.
2. A sliding mode controller is proposed to deal with linear CAVs model with time delay, and a Pareto optimal homogeneous asymmetric degree searching approach is brought up to improve the platoon's performance.
3. A Pareto optimal heterogeneous asymmetric degrees searching approach and a sliding mode controller are designed for a nonlinear heterogeneous platoon.
4. A two-step topology switching framework is designed to optimise topology in real time with different communication failures. An adaptive sliding mode controller is designed to deal with actuator faults in a continuous nonlinear CAVs model.
5. A discrete sliding mode controller is designed to handle packet loss in a discrete nonlinear platoon. Modified MOEA/D with opposing adaptive mechanisms is used in a two-step topology switching framework to improve the platoon's performance.

1.3 Thesis Outline

The thesis outline is listed as follows:

Chapter 1 presents the background, motivation, research objectives, and thesis outline.

Chapter 2 provides a literature review of previous studies of information flow topology, including the linear and nonlinear model of CAVs, typical symmetric and asymmetric controllers, fixed and time-varying information flow topology, the multi-objective optimisation strategies of the platoon, some common communication failures, and some future suggestions.

Chapter 3 investigates the impact of information flow topology, and an off-line Pareto optimal information flow topology searching strategy is proposed to improve the platoon's performance.

In Chapter 4, a sliding mode controller is designed for a linear platoon with a time delay. Then, a homogeneous Pareto optimal asymmetric degree in information flow topology is obtained with

NSGA-II to improve the platoon's performance. Finally, a similar approach is also designed for a nonlinear heterogeneous platoon.

In Chapter 5, A two-step switching topology framework is introduced to find the Pareto optimal information flow topology in real-time with predicted communication failures to improve the platoon's performance. First, an adaptive sliding mode controller is designed to deal with actuator faults in a continuous nonlinear platoon. Second, A discrete sliding mode controller is proposed to handle a discrete nonlinear platoon with packet loss. A modified MOEA/D with opposing adaptive mechanisms is also in use.

Chapter 6 details the experiments of the project, including the experiment setup and the results.

Chapter 7 concludes the main contribution of this thesis and discusses future research directions.

Chapter 2

Literature Review

2.1 Introduction

The previous chapter introduces this thesis, which clarifies the background of information flow topology and what encourages the author to research advanced controller and optimisation strategy of information flow topology in a vehicular platoon. Then, the research objectives present the aim of this research, while the thesis outline shows the structure of this thesis. Finally, this chapter presents literature reviews about CAVs and information flow topology to conclude the past research and identify the limitations.

CAVs are a group of vehicles that use network communication to exchange information with each other and the infrastructure. As a result, it can perform automated motions and scheduled tasks on the route, such as platooning [2], intersection crossing, and lane changing. CAVs have the advantages of being able to perform complex tasks automatically and efficiently, improving overall traffic quality, reducing traffic congestion, and increasing road safety [3]. In recent years, the study of the platoon is gaining widespread attention due to its practical benefits in a real-world application. A platoon is a group of CAVs travelling in the same lane on the highway with a short inter-vehicle distance and the same velocity [4]. The following vehicles track the leading vehicle with a desirable velocity while maintaining a safe and comfortable inter-vehicle gap [5]. The platoon has many recognised benefits, including improved traffic mobility, safety, and emission reduction by forming a tight formation [6]. Information flow topology is one of the most important factors influencing the platoon's performance. It describes how CAVs send and receive information with each other, and it is commonly described by algebraic graph theory. Figure 2.1 shows a vehicular platoon with CAVs, where the communication links are indicated with dotted lines, indicating the information flow topology.

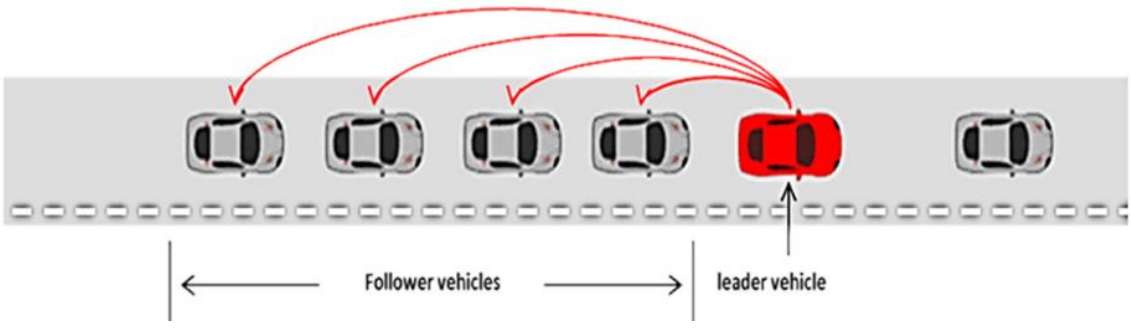

Figure 2.1 A vehicular platoon [7]

The control of CAVs consists of many aspects, including the dynamic model, control strategies, information flow topology, platoon multi-objective optimisation, and communication failures. Most early studies and current work focus on a third-order linear model, only considering the time lag in the powertrain dynamics. A nonlinear vehicle dynamic model is more practically desirable.

However, it increases the difficulty of controller design [8]. Common control strategy for CAVs includes the state-feedback controller, robust controller, and sliding mode controller. In addition, there has been growing interest in the asymmetric controller to improve the controller's behaviour [9]. The controller design is largely based on information flow topology. While most controllers are only constructed to suit one fixed information flow topology, an ever-increasing body of literature studied time-varying information flow topology and established the control strategy accordingly [10]. While researchers have been focusing on the platoon's tracking ability to assess its performance, multiple objectives are considered to improve the platoon's performance, such as fuel economy, driving comfort, stability, and string stability. MPC is one of the most common strategies to deal with the platoon with multiple optimisation objectives [11]. The weighted sum and dynamic tunning methods are also used when constructing the optimisation function. Finally, some common communication failure issues pose risks to the platoon, including time delay, actuator faults, and packet loss [12]. They are important and worth studying for practical applications.

2.2 Model of CAVs

Several dynamic models of CAVs have gained interest over the past decades. The third-order model is the most popular, describing the vehicle as a point mass. In addition, the time lag in the longitudinal acceleration is considered [4]. This section presents the commonly used third-order linear and nonlinear longitudinal dynamic models of CAVs, and their advantages and disadvantages.

2.2.1 Linear Model

The third-order linear longitudinal dynamic model is the most widely used vehicle dynamic model in past research [13-15]. It is based on the premise of the perfect knowledge of all dynamic parameters. For CAVs, the longitudinal dynamic model generally considers the engine, drive line, brake system, aerodynamics drag, tire friction, rolling resistance, and gravitational force. Assuming the longitudinal tire slip and the influence of pitch and yaw motions are negligible, with a rigid and symmetric vehicle body, the driving and breaking torques can be considered the control inputs. The general nonlinear vehicle longitudinal dynamic model is as follows [16]:

$$\begin{gathered} \dot{p}_i(t) = v_i(t) \\ \dot{v}_i(t) = \frac{1}{m_i}(\eta_i \frac{T_i(t)}{R_i} - C_{A,i} v_i(t)^2 - m_i g f) \\ \tau_i \dot{T}_i(t) + T_i(t) = T_{i,des}(t) \\ \text{for} \quad i = 1,2 \cdots N \end{gathered} \tag{2.1}$$

where $p_i(t)$ and $v_i(t)$ are the position and velocity of vehicle i, respectively. m_i is the vehicle mass. $C_{A,i}$ is the lumped aerodynamic drag coefficient, g is the acceleration due to gravity, f is the coefficient of rolling resistance, $T_i(t)$ is the actual driving or braking torque, $T_{i,des}(t)$ is the

desired driving or braking torque, τ_i is the inertial delay of the powertrain, also known as the engine time lag or engine time constant. R_i is the tire radius, η_i is the mechanical efficiency of drive line.

Then, the exact feedback linearisation technique is utilised to convert the nonlinear model into a linear model for simplicity [17]. The output of position with relative degree three is used to construct the feedback linearisation law as follows:

$$T_{i,des}(t) = \frac{1}{\eta_i}(C_{A,i}v_i(t)(2\tau_i\dot{v}_i(t) + v_i(t)) + m_i g f + m_i u_i(t))R_i \tag{2.2}$$

where $u_i(t)$ is the new input signal after linearisation. Then, a linear dynamic model for vehicle is obtained as follows:

$$\tau_i\dot{a}_i(t) + a_i(t) = u_i(t) \tag{2.3}$$

where $a_i(t)$ is the acceleration of vehicle i. A third-order state space model is established for each CAVs in the platoon:

$$\dot{x}_i(t) = A_i x_i(t) + B_i u_i(t) \tag{2.4}$$

where

$$x_i(t) = \begin{bmatrix} p_i(t) \\ v_i(t) \\ a_i(t) \end{bmatrix}, A_i = \begin{bmatrix} 0 & 1 & 0 \\ 0 & 0 & 1 \\ 0 & 0 & -\frac{1}{\tau_i} \end{bmatrix}, B_i = \begin{bmatrix} 0 \\ 0 \\ \frac{1}{\tau_i} \end{bmatrix}.$$

This model is preferable in most studies because of its simplicity. For example, it is widely used for Cooperative Adaptive Cruise Control (CACC) because it simplifies the stability analysis of the closed-loop system [18-19]. However, the vehicle's dynamic parameters may vary from the predicted ones. Therefore, it makes parameter mismatches and unmodelled nonlinearities unavoidable [4]. As a result, the platoon's stability and safety are at risk, making the linear dynamic model undesirable and impractical in real-world applications.

2.2.2 Nonlinear Model

Two types of third-order nonlinear models are commonly used in the study of CAVs. The first one is “Position-Velocity-Force”. This model satisfies Newton’s second law of motion and uses the driving or braking force $F_i(t)$ to approximate the vehicle’s dynamic. The throttle and the brake pedal give the control input. The mathematic expression is as follows [5]:

$$\begin{aligned} \dot{p}_i(t) &= v_i(t) \\ \dot{v}_i(t) &= \frac{1}{m_i}F_i(t)\frac{K_{di}}{m_i}v_i(t)^2 - \frac{d_{mi}}{m_i} \\ \dot{F}_i(t) &= \frac{1}{\tau_i}u_i(t) - \frac{1}{\tau_i}F_i(t) \end{aligned} \tag{2.5}$$

where K_{di} is the aerodynamic drag coefficient, d_{mi} is the mechanical drag.

The second one is “Position-Velocity-Acceleration”. It is equivalently normalized as the first

model. It simplified the controller design by using acceleration directly, an easily measurable parameter. Reducing all the nonlinear terms to the last-order equation also simplifies the control protocol. It is expressed as follows [5]:

$$\begin{aligned} \dot{p}_i(t) &= v_i(t) \\ \dot{v}_i(t) &= a_i(t) \\ \dot{a}_i(t) &= \frac{1}{m_i \tau_i} u_i(t) - \frac{2K_{di}}{m_i} v_i(t) a_i(t) - \frac{1}{\tau_i}\left(a_i(t) + \frac{K_{di}}{m_i} v_i(t)^2 + \frac{d_{mi}}{m_i}\right) \end{aligned} \tag{2.6}$$

The "Position-Velocity-Acceleration" model is more popular than the "Position-Velocity-Force" model. Third-order nonlinear vehicle longitudinal dynamic model captures the vehicle's dynamics more precisely [20-22]. Therefore, it is more desirable for real-world applications. However, it increases the difficulty of controller design, proving stability and string stability.

2.3 Control Strategies for the Platoon

The control structure has always been the most crucial aspect of the platoon. It influences the platoon's tracking ability, stability, and string stability directly. Therefore, many control strategies were proposed to solve different problems of the platoon. This section discusses the state-feedback controller, the robust controller, the sliding mode controller, and the asymmetric controller. Their advantages and disadvantages are also presented and compared in this section.

2.3.1 State-feedback Controller

Due to its simplicity, the state-feedback controller is one of the most popular control strategies used in CAVs. It does not burden the system with introducing additional zeros or poles [23]. Moreover, it improves the system's phase margin, dynamics, and steady-state tracking accuracy [24]. A state-feedback control protocol is established for a platoon under the influence of parameter uncertainty and communication delay [25]. Wang et al. [26] designed an optimal state-feedback linear–quadratic–Gaussian (LQG) control protocol for a vehicular platoon with time-correlated process noises. A state-feedback controller is proposed to ensure the platoon's secure tracking while dealing with denial-of-service (DoS) attack phenomena [27]. On the other hand, traditional state-feedback controller has its limitations. It is not ideal for systems with external disturbances and are sensitive to small variation [28]. Figure 2.2 illustrates the fundamental logic of the state-feedback controller.

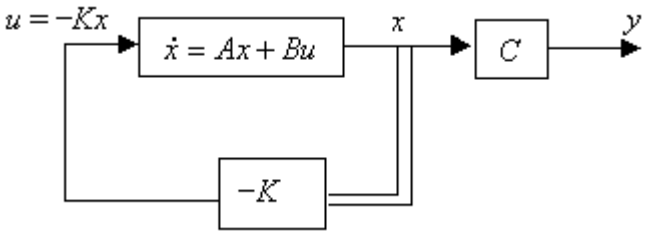

Figure 2.2 State-feedback controller [29]

2.3.2 Robust Controller

The robust controller handles uncertainty in the platoon. It deals with external disturbances, parameter uncertainty, and mismatches. It is essential and practical because uncertainty frequently occurs in the platoon. Therefore, the last few years have witnessed massive growth in the study of robust controllers. An innovative, robust coordinate control scheme is proposed to deal simultaneously with uncertain information flow topology, parameter mismatches, and external disturbances [30]. To deal with a platoon under the influence of parameter uncertainties, network-induced delay, and wireless communication delay, a robust H-infinity controller is designed to ensure the platoon's stability and string stability [31]. Apart from the uncertainties within the platoon, there are also uncertainties caused by human-driven vehicles (HDVs) since they may get in the way of the CAV's planned trajectory. Feng et al. [14] designed a robust platoon control framework based on tube MPC to deal with HDVs. However, the robust controller can sometimes be insensitive to changes in the system.

2.3.3 Sliding Mode Controller

The sliding mode controller gives a discontinuous signal that drives a nonlinear system into a predefined surface (sliding surface) in the state space. It has the advantages of fast convergence speed and effectiveness in tackling parameter uncertainties and external disturbances. It stands out due to its promising ability to handle nonlinear dynamics, actuator constraints and information flow topology diversity [32]. An adaptive fuzzy sliding mode controller is designed for the platoon's longitudinal and lateral vehicle dynamics [33], and it is shown to be beneficial in dealing with nonlinearity and external disturbances. To cope with unknown driving resistance and actuator saturation, Song and Ju developed a distributed adaptive sliding mode control algorithm [34]. Guo and Li combined a sliding mode controller with a set-point optimisation layer and a vehicle tracking control layer to address the issue of fuel-time efficient platooning control [35]. One of the remaining crucial questions is to determine the control parameters of the sliding mode controller. Figure 2.3 shows the theoretical structure of a sliding mode controller. Table 2.1 displays the comparison between different controllers [36]. It can be seen from the table that compared to other controllers, the sliding mode controller has several advantages, as mentioned above.

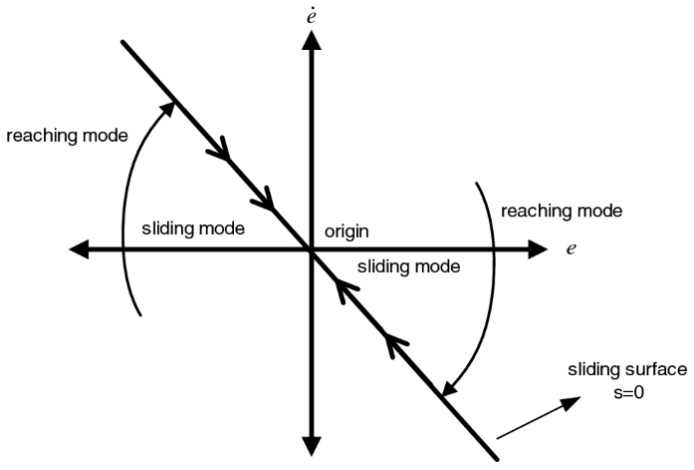

Figure 2.3 Sliding mode controller [37]

Parameters of Comparison	Direct Pole Placement	Voltage Mode Control	Current Mode Control	PID Control	Classical Half-Cycle Posicast Control	Hybrid Posicast Control	Sliding Mode Control	Fuzzy Logic Control	Neural Networks
Type of Control	Linear	Linear	Some non-linearity	Linear	Non-Linear	Non-Linear	Non-Linear	Artificial Intelligence	Artificial Intelligence
Overshoot	Moderate	Large	Negligible	Large	Moderate	Negligible	Negligible	Negligible	Negligible
Large Signal Dynamic response consistency	Average	Poor	Average	Average	Average	Good	Good	Excellent	Excellent
Sensitive to parameters and Load variations	Sensitive	Sensitive	Highly sensitive	Sensitive	Highly sensitive	Less sensitive	Not sensitive	Not sensitive	Not sensitive
Need of accurate mathematical modeling	Needed	Needed	Not Needed	Needed	Needed	Needed	Needed	Not Needed	Not Needed
Ease of Handling Complex System	Very Difficult	Difficult	Very Difficult	Difficult	Moderate	Moderate	Easy	Very Easy	Easy
Requirement of Current Sensing	Yes	No	Yes	No	No	No	Yes	May or may not be	May or may not be
Control Suitability	Lower Order System	Lower Order System	Lower Order System	Lower Order System	Lower Order System	Lower Order System	All types of system	All types of system	All types of system
Control Complexity	High	Less	Less	Medium	Medium	Medium	Higher	Less	High

Table 2.1 Comparison of different controllers [36]

2.3.4 Asymmetric Controller

The asymmetric controller has gained considerable attention over the past few years in the problem of CAVs. It primarily benefits the platoon by attenuating wireless communication's negative impact. Zheng et al. revealed that one of the most significant advantages of incorporating asymmetric control is that specific topologies' stability margins are independent of the platoon size while bounded away from zero [9]. As a result, asymmetric control obtains a scalable platoon with a constant stability margin. A similar regularity was also drawn by Herman et al. [38]. The asymmetry of inter-vehicular coupling with asymmetric bidirectional platoon control was investigated in the study. The result showed that even if harmonic instability exists for linear controllers, the Laplacian eigenvalues can still be bounded, which proved its superiority. Herman and Sebek established a Linear quadratic regulator (LQR) optimal distributed controller based on asymmetric topology [39]. The method was proved to be effective beyond the platoon's size. However, a limitation occurred as the scaling became exponential. Moreover, the asymmetric degree in all the research was selected randomly and artificially, and there was not enough evidence on how to choose the asymmetric degree.

2.4 Information Flow Topology

The information flow topology is one of the most critical factors influencing platoon performance. The communication links between vehicles, such as how they receive or exchange information,

are described by information flow topology. This section discusses the importance of information flow topology first, then introduces fixed topology and time-varying topology and the associated control strategies.

2.4.1 Importance of Information Flow Topology

Several studies acknowledged the significance of information flow topology and investigated its impact on vehicle platoon performance. Li et al. [40] investigated the effects of different topologies on CACC and the associated convergence time and robustness. A feedback-based platoon control protocol for CAVs that considers longitudinal and lateral gaps was proposed. It was discovered that while convergence time is related to network topologies, it has no significant effect on robustness. Zheng et al. [18] studied the influence of information flow topologies on the stability and scalability of the platoon, and it concluded that under bidirectional-leader topology, the stability margin of the platoon is always bounded and independent of the platoon size. Zheng et al. [1] also investigated the effect of topology on the platoon's closed-loop stability by comparing the spacing error of six typical types of topologies in both stable and unstable situations. However, only convergence time, stability, and scalability were studied, leaving out many other essential platoon properties. Secondly, previous research is limited to the six traditional information flow topologies. There is also a general lack of comprehensive and quantitative comparison.

2.4.2 Fixed Information Flow Topology

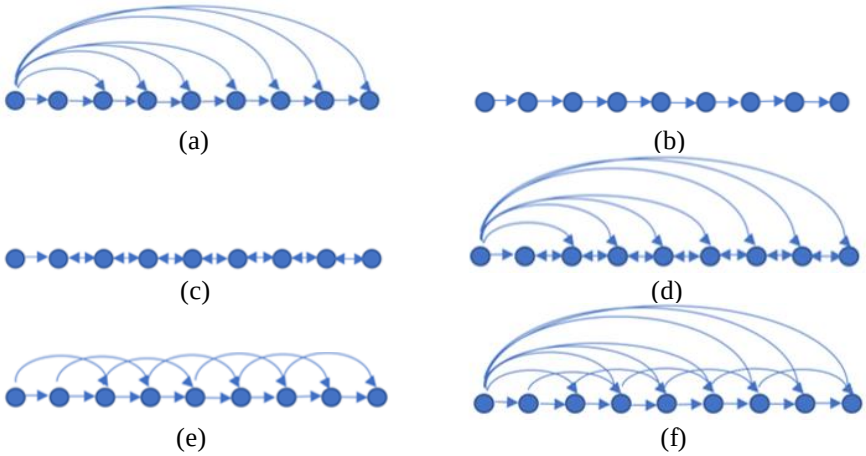

Figure 2.4 Fixed information flow topologies. (a) PLF; (b) PF; (c) BD; (d) BDL; (e) TPF; (f) TPLF

Figure 2.4 illustrates the six most commonly studied fixed information flow topologies. Most studies of CAVs are based on one particular fixed information flow topology due to its simplicity. Wu et al. [41] devised a method for solving the multi-lane platoon forming problem with a fixed information flow topology. A bump function is used in the potential function and applied to the control scheme. As a result, a multi-land platoon is formed with small fluctuations around desired velocities. Li et al. [42] created a CACC scheme targeting the multi-platoon problem with the Predecessor-Leader following topology. A four-layer framework was proposed to establish a

cooperative mechanism. As a result, the velocity and position consensus are guaranteed, and the method can achieve the desired cooperation pattern. In addition, the study discovered that, when compared to serial cooperation, parallel cooperation can increase road throughput. Chen et al. [43] concentrated on improving truck platooning on uphill grades with a fixed information flow topology. The feasibility analysis and the impact of the truck operation on truck platooning with varying uphill grades were examined. It revealed that the truck platoon could become asymptotically unstable above a critical grade. However, using a fixed information flow topology to solve a complex control problem is predominantly insufficient when the platoon is composed of heterogeneous vehicles with different dynamics and external disturbances.

2.4.3 Time-varying Information Flow Topology

Time-varying information flow topology is also known as switching topology and dynamic topology. It is more practically desirable. However, it adds difficulty to the controller design. The challenge is to construct a controller that supports different types of information flow topologies and ensures stability and string stability simultaneously.

Firstly, most research focused solely on switching between fixed traditional topologies. It limited the platoon's performance and lacked ability when dealing with poor communication. For instance, Li et al. [44] examined the stability of a platoon with a switching information flow topology, deriving a sufficient condition for stability utilising the Hurwitz criteria and the Riccati inequality. Chehardoli et al. [45] presented an adaptive control strategy incorporating parameter uncertainties to deal with a complex platoon structure, where the information flow topology switches between several traditional topologies.

Secondly, most switching topology designs were based on a random switching signal [46-47]. A nonlinear consensus-based control strategy incorporating car-following interactions between CAVs is proposed to deal with a platoon with switching topology [46]. A random switching signal switches the information flow topology from the predefined four topologies. Gao et al. [47] proposed a distributed H infinity control framework that supports undirected topologies in a platoon with bounded uncertainty. A uniform random switching signal is in use to describe the topology. However, switching topology randomly poses unnecessary risks to the platoon's stability.

Some studies focused on achieving stability for systems with switching signals [48-49]. For example, Li et al. [48] proposed an output feedback controller with a prescribed method for unknown and arbitrary switching signals in a nonlinear system. The simplified controller only needed one parameter tuning. Furthermore, Li et al. [49] designed a command-filtered-based fuzzy adaptive controller to deal with the same problem. The fuzzy controller avoided calculating partial derivatives, while the Lyapunov function guaranteed the platoon's stability.

2.5 Multi-objective Optimisation of The Platoon

Optimising the performance of the platoon has been the most significant goal of the control of

CAVs. Most studies consider the tracking ability as the most critical criterion to evaluate the platoon's performance [32]. It refers to the ability of the following vehicles to track the leading vehicle. In addition, there are some other criteria to assess the platoon, such as fuel efficiency [50], driving comfort [51], stability [52] and communication cost [53]. This section introduces MPC, which is one of the most common control strategies for multi-objective optimisation. In addition, this section discusses the construction of the optimisation function.

2.5.1 MPC Strategy

Previous studies have widely used MPC to deal with multiple control objectives. MPC is used in the platoon to predict the future behaviour of vehicles and take control actions, including forecast system dynamics and handling actuator and state constraints by optimising multiple objectives [54]. The control input is obtained by numerically optimising a finite horizon optimal control problem and dealing with nonlinearity and constraints. For instance, Wang et al. [55] designed a centralised cooperative MPC for a platoon's signalised isolated intersections. Three optimisation objectives are considered: intersection throughput, fuel consumption and safety. As a result, the linear quadratic control problems are effectively solved. Yang et al. [56] proposed an eco-driving control framework for the platoon based on optimising travel time, fuel consumption, and safety. The proposed strategy, which uses two-stage control logic and an embedded traffic flow model, can reduce freeway congestion while lowering fuel consumption. Luo et al. [57] presented a new distributed economic MPC to improve the performance of the platoon with bidirectional information flow topology in terms of tracking, safety, stability, and string stability. As a result, it improved the platoon's fuel efficiency by 4.2 per cent. Zheng et al. [58] proposed a distributed MPC framework for heterogeneous vehicle platoons with unidirectional information flow topologies and a priori unknown desired set point. Therefore, the platoon is dynamically decoupled but constrained by spatial formation. Moreover, an equality-based terminal constraint is utilised to ensure the platoon's asymptotic stability. However, the centralised implementation of MPC is unsuitable for large-scale optimisation problems, and the formulation of ACC in most MPC research limits the information flow topology significantly [59]. Figure 2.5 displays the typical structure of MPC.

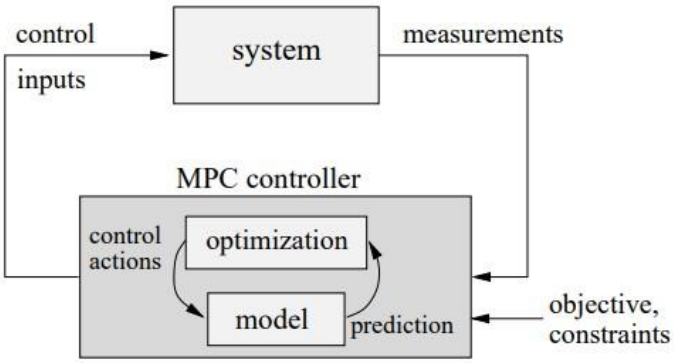

Figure 2.5 MPC [59]

2.5.2 Construction of The Optimisation Function

The weighted sum method is widely used in the optimisation function's construction. Fixed weighting coefficients are preferred in some studies. Yang et al. [56] recognise that the choice of weighting coefficients represents a trade-off between multiple objectives. The optimisation solutions are practically not desirable, with limited options for weighting coefficients. Using fixed weighting coefficients has its drawbacks [60] because not only the optimal solution usually obtained is the corner solution on the Pareto front, but it also varies significantly when the weighting coefficients change slightly. Some studies developed a weighting coefficient tuning strategy to overcome these limitations. Yu et al. [61], for example, proposed a dynamic weight tuning optimisation technique in the study to improve ride comfort and reduce tracking errors using the MPC strategy. The results demonstrated its superiority over the conventional strategy. Zhao et al. [62] also proposed a similar real-time weight-tuning method. In both studies, because the weighting coefficients are heavily reliant on the inter-vehicle states, any feedback delay can compromise the platoon's stability to a large extent. To avoid the drawbacks, control strategies that are not based on weighted sum optimisation have also been suggested. For example, he et al. [63] proposed an innovative predictive cruise control method to optimise platoon fuel consumption, tracking ability and safety. The optimisation is weight-free because the utopia point is implemented using a sequential quadratic programming algorithm. However, since the utopia point cannot be reached with conflicting objectives, a compromise solution must be introduced. Because quadratically constrained problems are computationally expensive in general, they complicate the proposed strategy [60].

2.5.3 Evolutionary Algorithms

Besides MPC strategy and traditional optimisation function, evolutionary algorithms are also popular for multi-objective optimisation. NSGA-II [64] is a fast and elitist multi-objective genetic algorithm, and it is well known for its ability to search for an optimal solution fast without premature occurs. NSGA-II consists of six steps. Firstly, the population is initialised. Then, the initialised population is sorted based on non-domination order. The crowding distance is assigned to each individual in the population in the third step. Next, the selection is performed using a crowded-comparison-operator. After that, the offspring population is generated by a genetic operator, which includes a crossover operator and a mutation operator mimic chromosome. Finally, the offspring population and the current population are combined. The selection is performed again to select the next generation. The iteration only stops once reaching the maximum generation number. Then a Pareto front with a set of Pareto optimal solutions can be obtained. NSGA-II has been widely used to handle all different types of multi-objective optimisation problems. It avoids having a premature problem by assigning crowding distance to each individual in the population, then selecting the individual with the least rank and maximum crowding distance to largen the search area. MOEA/D is also a popular evolutionary algorithm for multi-objective optimisation [65]. It is a simple and generic evolutionary algorithm that finds a small

number of uniformly distributed Pareto solutions. Compared to NSGA-II, the computational cost of MOEA/D is significantly reduced because it optimises each subproblem by only using information from its several neighbouring subproblems. It also demonstrates its benefits in multi-objective 0–1 knapsack problem.

2.6 Common Communication Failures

In recent years, there has been growing interest in the communication failures of the platoon. Communication is essential to the platoon's performance. Time delay, actuator faults, and packet loss are typical. Therefore, they need to be considered in the control problem of CAVs. This section discusses them, and the control strategies proposed in past research.

2.6.1 Time Delay

Time delay in the platoon causes delayed output feedback, which is challenging for the controller design, stability, and string stability. Many studies deal with time delays in the platoon in different ways. For example, a parameter-space-approach-based CACC protocol is designed for a homogeneous platoon with communication time delays [66]. Selecting the feedback loop's gains from the feasible region in the parameter space ensures D-stability and string stability of the platoon. A distributed MPC strategy under the impact of communication time delay is solved using a Laguerre-based MPC design [67]. The analysis of the closed-loop poles showed the influence of time delay on the stability margin of the platoon. Yang et al. [68] use the Lyapunov-Razumikhin and Lyapunov-Krasovskii techniques to estimate the upper bound of time delay and establish sufficient conditions that ensure the platoon's stability and string stability. The proposed technique achieves the platoon's tracking consensus successfully.

2.6.2 Actuator Faults

An actuator is a crucial part of a vehicle. It converts electrical signals into physical motions. Actuator faults are an essential aspect of the study of CAVs because it leads to failure of motion in a vehicle. Some previous studies proposed various techniques to deal with actuator faults in the platoon. For instance, an innovative prescribed performance control (PPC) strategy combined with barrier Lyapunov function is proposed to deal with a platoon under false data injection (FDI) and actuator faults [69]. An adaptive threshold-based fault observer is constructed to eliminate the influence of actuator faults. Pan et al. [70] designed a quadratic spacing error policy to improve the platoon's stability with actuator faults. An adaptive estimation mechanism is established to handle the unknown actuator saturation. Han et al. [71] proposed a systemic anti-fault safety consensus method to deal with actuator faults. Firstly, a distributed observer is constructed as the fault detection. Then an innovative adaptive fault parameter estimation law is provided to achieve fault-tolerant control. As a result, the proposed technique deals with actuator faults effectively.

2.6.3 Packet Loss

Packet loss implies that a CAV may lose connections with other CAVs in the platoon due to packet dropping, making it unable to receive or send information. There are many studies focused on packet loss in the platoon. Ma et al. [14] presented a distributed optimised controller for actuator delay and packet loss. The linear quadratic regulator method ensured the platoon's string stability. The results demonstrated that the platoon performed better on the highway with the proposed controller. Halder et al. [12] designed a robust distributed state-feedback controller to deal with external disturbances and packet loss. Linear matrix inequality (LMI) ensures the platoon's stability. The results demonstrated the controller's effectiveness with two traditional topologies under random single packet loss. Wen et al. [72] suggested a unified framework of network access schedules and a cooperative controller to investigate the effect of packet loss and network access limitation. A sufficient condition was established for the platoon's string stability and schedulability. Elahi et al. [73] developed a consensus control protocol for packet loss. The Lyapunov-Krasovskii function was utilised to offer sufficient conditions for the platoon's asymptotic stability and disturbance attenuation. However, the linearised vehicle dynamic model is one of the limitations of past research [12, 14, 72-73] in platoon packet loss. It only considers powertrain time lag and ignores heterogeneous vehicle dynamics, making it not practical nor desirable in real-world applications.

2.7 Conclusion

CAVs perform tasks automatically and efficiently. As a result, it improves traffic quality and road safety and reduces traffic congestion. The control of CAVs has many aspects, such as the dynamic model of the platoon, common control strategies, information flow topology, multi-objective optimisation, and some common communication failures.

Compared to the linear model of CAVs, the third-order nonlinear longitudinal dynamic model is worth studying the most due to its practical value. Many control strategies have been investigated in past research, such as the state-feedback controller, robust controller, and sliding mode controller. However, the asymmetric controller has been overlooked chiefly and has excellent potential to improve control accuracy, which gains the author's attention. While most controllers are only constructed to suit one fixed information flow topology, time-varying information flow topology has gained considerable interest based on its importance to the platoon. Multiple objectives have been considered to improve the platoon's performance, such as tracking ability, fuel economy, driving comfort, stability, and string stability. MPC has been the most popular controller to deal with multi-objective optimisation of the platoon. However, the weighted sum and dynamic tunning methods have limitations in constructing the optimisation function, which motivates the author to use evolutionary algorithms to bridge the gap. Finally, common communication failures such as time delays, actuator faults, and packet loss are worth investigating because they greatly impact the platoon.

Chapter 3

Impact of Information Flow Topology

3.1 Introduction

The previous chapter introduces a literature review of the linear and nonlinear model of CAVs, some common control strategies for the vehicular platoon, different types of information flow topology, the multi-objective optimisation of the platoon, and some common communication failures, including time delay, actuator faults, and packet loss. This chapter investigates the impact of information flow topology systematically, and a Pareto optimal information flow topology method for CAVs is proposed.

The information flow topology has been considered one of the most critical features of CAVs, and several studies acknowledged its impact on the platoon's performance [39-41]. There are six types of traditional fixed information flow topology. It was discovered that the initial states of different information flow topology affect the platoon's convergence time but have no significant effect on the robustness of the platoon [39]. Some studies also investigated the convergence time, stability, and scalability of the six conventional information flow topologies by studying the platoon's closed-loop stability [40-41]. It found that with bidirectional leader topology, the stability margin of the platoon is always bounded and independent of the platoon's size. However, past studies left out many other indices of the platoon's performance, which are also very important. Moreover, most research is limited to the six traditional information flow topologies, leaving out many other possible information flow topologies. Finally, there is a general lack of comprehensive and quantitative comparison of all information flow topologies. Therefore, this chapter aims to fill the gap by investigating the impact of traditional and innovative topologies on the platoon in a systematic manner.

Most studies were based on the traditional fixed information flow topology only and designed the controller's gains based on it [42-43]. The limitation is that the designed controller only supports one or a few pre-defined information flow topologies, which is insufficient when dealing with a complex control problem. For example, a platoon consists of heterogeneous vehicles with various dynamics and external disturbances. Some research is now focused on novel information flow topology to improve the platoon's performance [11,32,74]. Musa et al. [11] proposed an MPC strategy to enable a smooth-moving, stable and comfortable vehicle convoy system. An innovative topology was designed with pre-defined desired spacing and communication links. Compared to the traditional two-lookahead topology, the new strategy can safely bridge the inter-vehicle distance while maintaining driving comfort. Wu et al. [32] proposed a distributed sliding mode control model for nonlinear heterogeneous platoons with positive definite topologies. The simulation was run under four types of topologies to verify the effectiveness of the proposed method in terms of tracking index, acceleration standard deviation and fuel economy. Orki et al. [74], on the other hand, proposed three innovative information flow topologies for a mixed platoon, which consists of both automated and manual vehicles. A

new distributed controller using the H infinity control method was brought up to address the control problem. The effectiveness and feasibility were verified. Although the proposed innovative topologies mentioned above have proven their effectiveness to a certain extent, some were created artificially without scientific proof. Furthermore, there was insufficient evidence on how and why these topologies were selected. This chapter seeks to fill the gap by presenting a scientific scheme for searching for the Pareto optimal topology using NSGA-II to deal with complex CAV control problems. The proposed strategy balances the platoon's tracking ability, fuel economy and driving comfort to improve the platoon's performance objectively. It also ensures the platoon's stability in the first place.

The main contributions of this chapter are listed below:

1) Rather than focusing solely on convergence time, stability, and scalability, as is the case in current research, this chapter examines the impact of both conventional and innovative topologies on the platoon's performance systematically and quantitatively, using multiple evaluation criteria to investigate the platoon's performance.

2) This chapter's originality and innovation are uncovered in the platoon's performance regularities, which were discovered and concluded in a broad view with clear evidence of consistency. For example, the smoothness of the velocity profile and fuel economy are consistent, whereas driving comfort, fuel efficiency and communication efficiency are in direct opposition to tracking ability.

3) Rather than artificially creating a new topology, as in current research, this chapter utilizes NSGA-II to find the Pareto optimal information flow topology. Since the influences of heterogeneous vehicle dynamic characteristics and external disturbances on information flow topology cannot be modelled with the approach used in state-of-the-art. The proposed method can overcome the barrier and resolve the problem sufficiently.

3.2 Information Flow Topology Model

The platoon discussed in this section has N+1 vehicles, including one leading vehicle and N following vehicles. Nine types of fixed information flow topologies are discussed in the study, including six typical topologies referring to [16], three innovative topologies referring to [74]. Figure 3.1 shows all 9 topologies, including:

(a) Innovative Topology1 (N1);

(b) Innovative Topology2 (N2);

(c) Innovative Topology3 (N3);

(d) Predecessor-leader Following Topology (PLF);

(e) Predecessor Following Topology (PF);

(f) Bidirectional Topology (BD);

(g) Bidirectional-leader Topology (BDL);

(h) Two predecessors Following Topology (TPF);

(i) Two predecessor-leader Following Topology (TPLF).

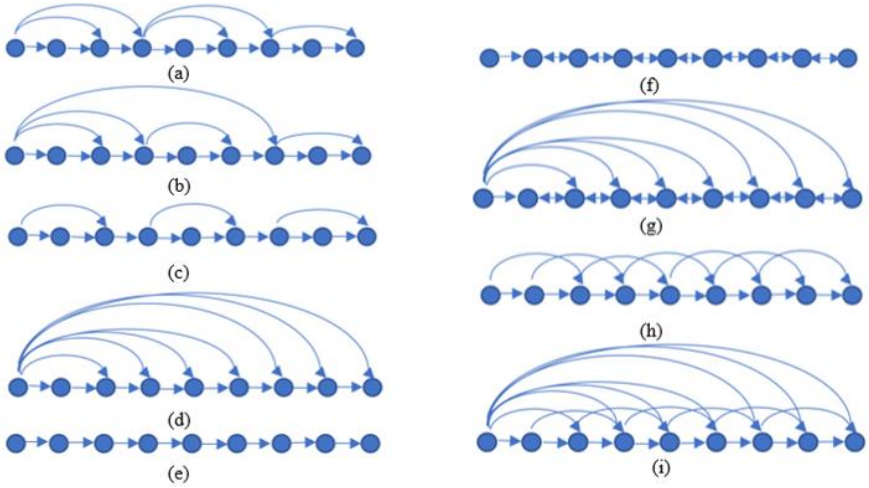

Figure 3.1 Information flow topologies for the platoon. (a) N1; (b) N2; (c) N3; (d) PLF; (e) PF; (f) BD; (g) BDL; (h) TPF; (i) TPLF

The fixed information flow topologies for nine CAVs, including one leader and eight followers, are described in Figure 3.1, where each vertex represents a CAV and each edge represents an active communication link. The information of each CAV can send and receive includes position, velocity and acceleration in both longitudinal and lateral directions. The mathematical description of the connection in a topology can be defined as [75]: $G = \{V, E, T\}$ where G is a weighted graph of order N consists of 3 elements: V represents the set of N nodes, $E \subseteq V \times V$ denotes the set of edges, which is also the communication link between vehicles; $T = [t_{ij}]$ represents the adjacency matrix of G. If there is a communication link from agent j to agent i, which means agent i can receive information from agent j, $t_{ij} = 1$, otherwise $t_{ij} = 0$. The in-degree of node i is defined as $d_i = \sum_{j=1}^{N} t_{ij}$. Denote $D = diag(d_1, d_2 \dots d_N)$, the Laplacian matrix L is defined as $L = D - T$. We define a neighbour set of node i in the following as:

$$\mathbb{N}_i = \{j \in V | t_{ij} = 1\}$$

N followers and one leader are contained in the weighted graph G. $P = diag(p_1, p_2 \dots p_N)$ is the linked matrix of G. If agent i receives information from the leader, $p_i = 1$, otherwise $p_i = 0$. We consider the information flow topologies discussed under the weighted graph G. The leader accessible set of node i is defined as

$$\mathbb{R}_i = \begin{cases} \{0\} & if\ p_i = 1 \\ \emptyset & if\ p_i = 0 \end{cases}$$

Therefore, the complete topology information set of node i is defined as

$$\Pi_i = \mathbb{N}_i \cup \mathbb{R}_i$$

The topological matrix in this section is represented by $T + P$. The maximum and minimum eigenvalue of a certain type of topology are calculated using the real numbers of the eigenvalues and expressed as $\lambda_{max}(L + P)$ and $\lambda_{min}(L + P)$ respectively, λ_{max} and λ_{min} for short.

3.3 Vehicle Dynamic Model

Applying the leader-follower approach, we consider the leader of the system as [76]:

$$\dot{x}_L(t) = v_L(t)$$
$$\dot{v}_L(t) = a_L(t)$$

(3.1)

where $x_L(t)$, $v_L(t)$ and $a_L(t)$ are the longitudinal position, velocity and acceleration of the leader vehicle. The model for vehicle *i* is considered as [76]:

$$\dot{x}_i(t) = v_i(t)$$
$$\dot{v}_i(t) = \frac{\widehat{M}}{M_i}u_i(t) - \frac{1}{M_i}C_e{v_a}^2 - gfcos(\theta) - gsin(\theta)$$

(3.2)

where $x_i(t)$ and $v_i(t)$ are the longitudinal position and of vehicle i. $u_i(t)$ is the control input of vehicle i. M_i(kg) is the mass of vehicle i. $\widehat{M}$(kg) is the nominal mass of all vehicles in the platoon. C_e is the aerodynamic resistance coefficient of vehicle *i*. v_a(m/s) is the wind speed. g is the gravitational acceleration, which is $9.8\,m/s^2$ in this section. f is the rolling resistance coefficient of vehicle i. $\theta(°)$ is the grade of the road. It should be noted that this second-order model is derived from a third-order model for simplification. It holds and only holds when the wind speed and road slope angle meet the conditions of energy bounded [76]. A second-order state space model is utilised for each vehicle:

$$\dot{X_i}(t) = AX_i(t) + B_1u_i(t) + B_2w_i(t) + B_2r_i(t)$$

(3.3)

where

$$X_i(t) = \begin{bmatrix} x_i \\ v_i \end{bmatrix};\ A = \begin{bmatrix} 0 & 1 \\ 0 & 0 \end{bmatrix};\ B_1 = \begin{bmatrix} 0 \\ \frac{\widehat{M}}{M_i} \end{bmatrix};\ B_2 = \begin{bmatrix} 0 \\ q \end{bmatrix};$$
$$w_i(t) = \frac{-C_e{v_a}^2}{M_iq} - \frac{gfcos(\theta) - gsin(\theta)}{q}$$

(3.4)

The uncertainty introduced by the vehicle dynamic is modelled as the disturbance $w_i(t)$ to simplify the problem. A sensitivity parameter q is introduced to the system to describe the sensitivity of the system to the disturbance, which is considered to be 1 in this section. $r_i(t)$ describes additional external disturbances vehicles experience.

3.4 Platoon's Performance Evaluation Criteria

To investigate the impact of different topologies on CAV platoon's performance, five performance indices are chosen to be the platoon's performance evaluation criteria. The first one is the tracking index (TI) [32] at indicates the ability of the vehicle tracking the preceding vehicle. TI for the *i*th vehicle is expressed as:

$$TI_i = \frac{1}{T}\int_0^T (|\Delta v_i(t)SVE| + |\Delta d_i(t)SDE|)\,dt$$

(3.5)

where T is the total simulation length, $\Delta v_i(t)$ is the velocity error, which is $v_i(t) - v_{i-1}(t)$. $\Delta d_i(t)$ is the spacing error, which is $d_i(t) - d_{i-1}(t)$. SVE=20 represents the velocity error sensitivity and SDE=50 represents the spacing error sensitivity [32]. The second index is the

acceleration standard deviation (ASD) [32] that indicates the degree of the smooth of the vehicle's velocity profile. ASD for the *i*th vehicle is expressed as:

$$ASD_i = std(a_i(t)) \tag{3.6}$$

where std represents the standard deviation in $t \in [0, T]$. The third index is fuel consumption [77] that indicates how much fuel the vehicle consumes. Fuel consumption for the *i*th vehicle is expressed as:

$$F_i(t) = \begin{cases} \xi_0 + \xi_1 P_i(t) + \xi_2 P_i(t)^2, P_i(t) \geq 0 \\ \xi_0, P_i(t) < 0 \end{cases} \tag{3.7}$$

$$P_i(t) = \left(\frac{R_i(t) + 1.04 M_i a_i(t)}{3600\eta}\right) v_i(t) \tag{3.8}$$

$$R_i(t) = \frac{\rho}{25.92} C_e C_h A_f v_i(t)^2 + g M_i f \frac{C_r}{1000} + g M_i sin\theta \tag{3.9}$$

where $F_i(t)(L/s)$ is fuel consumption rate of vehicle i, $P_i(t)$(kw) is the instantaneous power of vehicle i, $R_i(t)$(N) is the total resistance of vehicle i. ξ_0, ξ_1, ξ_2 are unitless parameters, η is the driveline efficiency of vehicle i. C_h is the correction factor. A_f is the vehicle frontal area of vehicle i. C_r is the road surface coefficient. The specific value of each parameter used in this section refers to Table 3.1 [77-78]. The fourth index is the time delay stability margin [52] that indicates the maximum time delay the system can endure while still remains stable and robust. Only the maximum eigenvalue of the topological matrix is required to reduce the computational burden. It is used as a constraint to ensure the platoon is robust against inevitable time delays. The time delay stability margin τ_i for the *i*th vehicle is expressed as:

$$\tau_i = \frac{\arctan\left(-\frac{ck_v\omega_i Re(\lambda_{max}) + ck_p Im(\lambda_{max})}{ck_v\omega_i Im(\lambda_{max}) - ck_p Re(\lambda_{max})}\right) + k\pi}{\sqrt{\frac{1}{2}(c^2 {k_v}^2 {\lambda_{max}}^2 + \sqrt{c^4 {k_v}^4 {\lambda_{max}}^4 + 4c^2 {k_p}^2 {\lambda_{max}}^2})}} \tag{3.10}$$

where $k \epsilon \{0,1\}$. The fifth index is the communication cost [53]. It is regarded as the required transmission rate at each node. The communication cost J_i for the *i*th vehicle is expressed as:

$$J_i = c|\Pi_i| \tag{3.11}$$

where c is the cost for enabling a communication link, which is selected to be 2.4 in this section [53]. $|\Pi_i|$ is the cardinality of set Π_i. Π_i is the complete topology information set of node i stated in Section 3.2. These five performance indices are chosen to be the platoon's performance evaluation criteria in the following chapters.

Table 3.1 Vehicle dynamics parameters for the platoon

Symbol	Quantity	Unit	Range
M	Vehicle mass	kg	1200-1700

C_e	aerodynamic resistance coefficient	-	0.2536
v_a	wind speed	m/s	-5-5
g	gravitational acceleration	m/s^2	9.8
f	rolling resistance coefficient	-	0.015-0.025
θ	grade of the road	°	0-3
η	driveline efficiency	-	0.8
C_h	correction factor	-	1
A_f	vehicle frontal area	m^2	2.08-2.45
C_r	Road surface coefficient	-	1.75
ξ_0	fuel economy index1	-	6×10^{-4}
ξ_1	fuel economy index2	-	1.9×10^{-5}
ξ_2	fuel economy index3	-	1×10^{-6}

3.5 Pareto Optimal Topology Searching Strategy

An H infinity controller proposed in [75] is modified then used in this section as follows:

$$u_i = -\sum_{j\in\Pi_i} \alpha[k_p(x_i - x_j - d_{i,j}) + k_v(v_i - v_j)] \tag{3.12}$$

$$K = [k_p, k_v]^T \tag{3.13}$$

where $d_{i,j}$ the desired longitudinal gap between vehicle i and vehicle j. α is the scalar, k_p and k_v are the controller's gains of the system. According to the LMI-based method proposed in [75], the following theory can convert the problem into a standard LMI problem:

Theorem 3.1: If there exist matrix $Q^T = Q > 0 \in \mathbb{R}^{2x2}$ such that:

$$\begin{bmatrix} AQ + QA^T - \alpha B_1 {B_1}^T & B_2 & Q{C_1}^T \\ {B_2}^T & -\gamma^2 I & 0 \\ C_1 Q & 0 & -I \end{bmatrix} \prec 0 \tag{3.14}$$

where scalar $\gamma > 0$ and $\alpha > 0$， then with the feedback gain K as defined as (3.13), (3.14) holds and

$$K^T = \frac{1}{2}{B_1}^T Q^{-1} \tag{3.15}$$

Proof of stability and consensus were established in [75]. It should be noted that *Theorem 3.1* holds for heterogeneous platoon because the platoon's closed-loop dynamic formulation is the same as indicated in [75] with various information flow topology.

Previous studies on the Pareto optimal information flow topology only considered homogeneous cases in which all vehicles have the same parameters and are subjected to the same disturbances [11,75,79-81]. Vehicle longitudinal models are typically simplified and linearised,

with essential properties like the rolling resistance coefficient and aerodynamic resistance coefficient being ignored [75,79-81]. These assumptions are unrealistic because vehicle parameters cannot be guaranteed the same in a platoon, and disturbances must be different in real-world situations due to different vehicle parameters. With current approaches, there are no suitable analytical methods for determining the optimal information topology for heterogeneous vehicles with various disturbances. Most existing topology switching techniques are limited to selecting from a collection of pre-defined topologies with only one or two goals [82-83], which cannot guarantee that the optimal topology in the CAVs control problem will be found.

The primary method used in this analysis is NSGA-II. NSGA-II [64] is a fast and elitist genetic algorithm for solving multi-objective problems. All five critical criteria discussed in Section 3.4 are considered when determining the Pareto optimal information flow topology. The primary goals of CAV control are to achieve consensus with excellent tracking ability, save resources with lower fuel consumption, and keep driving as pleasantly as possible. Three optimisation goals are chosen: tracking index, acceleration standard deviation, and fuel consumption. The platoon's stability is ensured by using a time delay stability margin as a constraint. Information flow topologies with a time delay stability margin less than the average are discarded during the operation. The platoon's communication cost is also calculated for further analysis.

There are six stages in NSGA-II. The population is first initialised. Next, The population is sorted into non-dominance order based on the calculation of objective values. Then, each individual in the population is allocated a crowding distance. Following that, a crowded-comparison-operator is used to make the pick. After that, a genetic operator, which involves a crossover operator and a mutation operator to imitate chromosomes, generates the offspring population. The crossover operator swaps parts of the parent solutions, and the mutation operator flips some string digits of the parent solution to produce a new solution. A single-point crossover operator with a crossover probability of 0.8 and a bitwise mutation operator with a mutation probability of 0.1 are implemented. Finally, the offspring population is merged with the existing population. The selection process is repeated to choose the next generation. The iteration continues until the maximum generation number is reached, at which point a Pareto front with a collection of Pareto optimal solutions is obtained.

The primary goal of using NSGA-II to search for the Pareto optimal information flow topology is to find the Pareto optimal topological matrix $T + P$. It should be noted that the elements of the topological matrix $T + P$ have a value of either 0 or 1. As a result, it can naturally use the binary chromosome in NSGA-II to represent the matrix. NSGA-II can provide Pareto optimal solutions to multiple objectives. The following summaries NSGA-II for the proposed Pareto optimal information flow topology strategy.

NSGA-II

Data: input: topological matrix $T + P$. n: generation number, $f_1(x)$: Tracking index; $f_2(x)$: Fuel consumption; $f_3(x)$: Acceleration standard deviation; $f_4(x)$: Time delay stability margin; $f_5(x)$: Communication cost. t: Average time delay stability margin constraint.

Generate random population

Calculate objective values: $f_1(x)$, $f_2(x)$, $f_3(x)$, $f_4(x)$, $f_5(x)$ using (3.5),(3.7),(3.6),(3.10),(3.11).

Eliminate candidates that does not satisfy the time delay stability margin constraint using $f_4(x)$

Sort the initial population with size N

Calculation the rank using $f_1(x)$, $f_2(x)$, $f_3(x)$ as objectives

Assign crowding distance to the initial population

For i=1:n

Perform selection

Create a mating pool (size: N/2)

Perform genetic operator: crossover and mutation

Combine the population

Eliminate candidates that does not satisfy the time delay stability margin constraint using $f_4(x)$

Perform selection

end

3.6 Simulation Results

MATLAB and Simulink are used to model the platoon. The simulation is conducted on an Intel Core i7-8550U laptop with 1.8GHz and a RAM of 8GB. The optimisation process is carried out using NSGA-II entirely offline. Each Case Study was simulated with three optimisation objectives and a population size of 40. Each iteration takes less than 30 seconds to complete. A Pareto front with 40 Pareto optimal solutions is obtained at the end of each iteration. In conclusion, the computational time required to complete 40 iterations is approximately 20 minutes. The computational time required at the moment is not suitable for online searching of the optimal topology. While the population size and number of iterations can be reduced to reduce computational costs, this introduces the risk of compromising the search result's optimality. A vehicular cloud [84] and fast programming language [85] could be used for future implementation to avoid the trade-off. Simulation conditions are as follows:

1) The kinematic model of the leader vehicle is described as follows:

$$a_L(t) = \begin{cases} 0 & 0 < t \leq 20s \\ 0.5\ m/s^2 & 20s < t \leq 30s \\ 0 & 30s < t \leq 70s \\ -1\ m/s^2 & 70s < t \leq 80s \\ 0 & 80s < t \leq 100s \end{cases} \tag{3.16}$$

$$v_L(t) = \begin{cases} 15\ m/s & 0 < t \leq 20s \\ 15 + 0.5 \times (t - 20)\ m/s & 20s < t \leq 30s \\ 20 m/s & 30s < t \leq 70s \\ 20 - 1 \times (t - 70)\ m/s & 70s < t \leq 80s \\ 10\ m/s & 80s < t \leq 100s \end{cases} \tag{3.17}$$

2) The time-varying wind speed and the grade of the road are viewed as external disturbances in this section. They are illustrated in Figures 3.2 and 3.3.

3) Each vehicle has a different set of control parameters due to the disturbance introduced by

the vehicle dynamics. The controller's parameters of each vehicle are obtained by solving (3.14) using MATLAB's LMIs toolbox.

4) The vehicle dynamic parameters are presented in Table 3.1, only the range of the parameters' value is provided. Each vehicle takes a random value within the range.

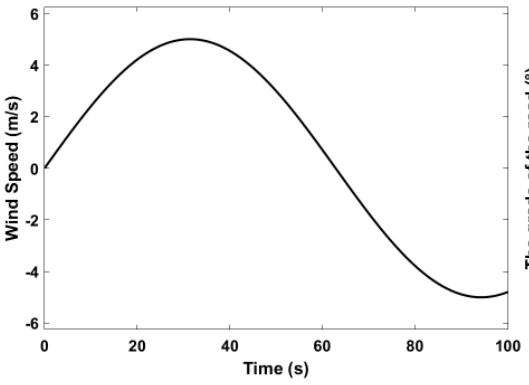

Figure 3.2 Wind speed

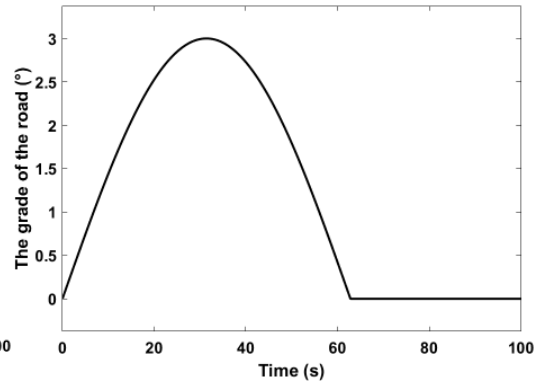

Figure 3.3 Grade of the road

Based on the simulation conditions stated above, this section first investigates the impact of different information flow topologies on the platoon's performance. Then it presents five case studies to prove the efficiency of the proposed strategy, using heterogeneous platoons of varying sizes in various scenarios. Finally, a Pareto front and the Pareto optimal solution topology are obtained and analysed using the proposed strategy.

3.6.1 Influence of Information Flow Topology

This section investigates a heterogeneous platoon of nine heterogeneous vehicles (one leader and eight followers). The platoon is interconnected by nine fixed information flow topologies, as depicted in Figure 3.1. Table 3.2 shows each vehicle's initial position and velocity states and the desired distance.

Table 3.2 The initial states and desired gaps of each vehicle

Vehicle	Position (m)	Velocity (m/s)	Desired gap (m)
Leader	0	15	0
Vehicle 1	-10	14	-10
Vehicle 2	-19	16	-20
Vehicle 3	-31	15.5	-30
Vehicle 4	-38	13	-40
Vehicle 5	-52	17	-50
Vehicle 6	-63	14.5	-60
Vehicle 7	-67	16.5	-70
Vehicle 8	-81	15	-80

Figure 3.4 demonstrates the spacing errors for information flow topologies (c) and (d). Figure 3.5 demonstrates the velocity errors for the same information flow topologies.

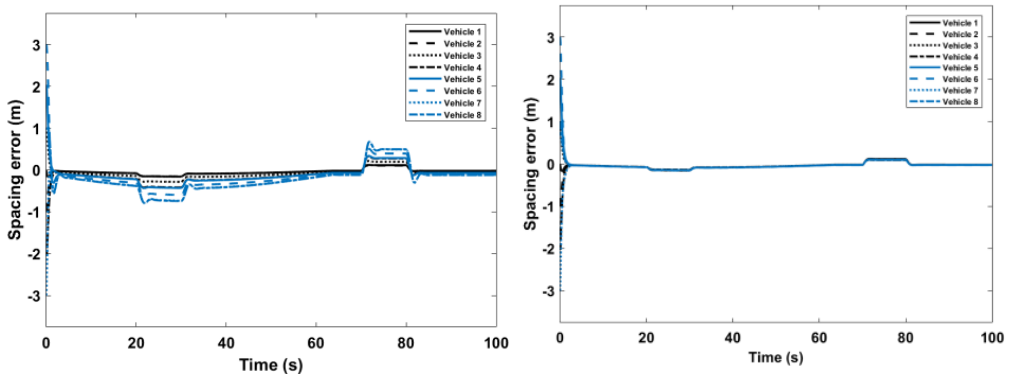

(a) (b)

Figure 3.4 Spacing error for platoon. (a): IFT(c)(N3). (b): IFT(d) (PLF)

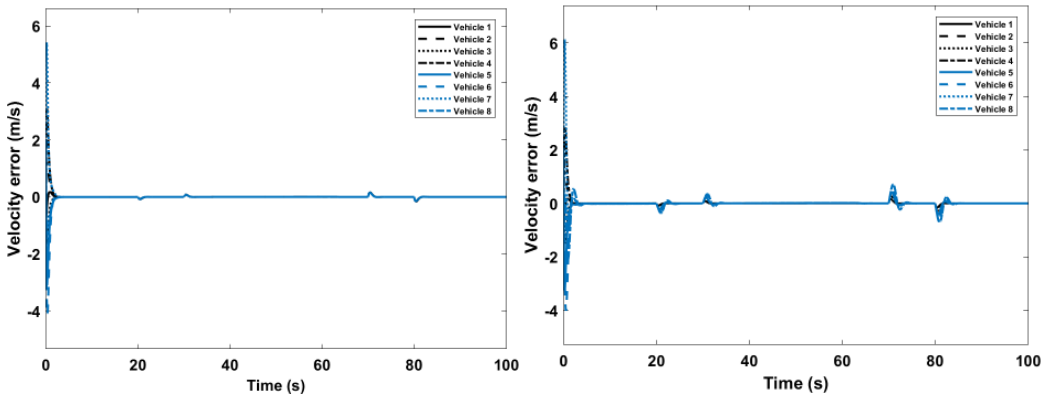

(a) (b)

Figure 3.5 Velocity error for platoon. (a): IFT(c)(N3). (b): IFT(d) (PLF)

The performance comparison of nine fixed information flow topologies in terms of the five performance indices is presented in Table 3.3. It depicts a comprehensive comparison of the impact of nine fixed information flow topologies on platoon performance.

Table 3.3 Qualitative performance comparisons for different information flow topologies

IFT	Tracking ability (TI)	Drive comfort (ASD)	Fuel efficiency (FC(L))	Ability to handle time delay (τ(s))	Communication Cost (J)
(a)	2.533 Medium	0.8476 High	1.223 High	0.14 Medium	31.2 Medium
(b)	2.67 Low	**0.8384** **Highest**	**1.209** **Highest**	0.14 Medium	31.2 Medium
(c)	3.366 Low	0.8617 High	1.288 High	0.14 Medium	26.4 Low
(d)	1.793 High	0.9305 Medium	1.336 Medium	0.14 Medium	36.0 High
(e)	4.773 Low	0.9067 Medium	1.330 Medium	**0.24** **Highest**	**19.2** **Lowest**
(f)	**94.07** **Lowest**	0.9880 Medium	**1.534** **Lowest**	**0.003** **Lowest**	36.0 Medium
(g)	1.727 High	**1.0782** **Lowest**	1.515 Low	0.06 Low	**52.8** **Highest**

(h)	2.499 Medium	0.9655 Medium	1.413 Low	0.14 Medium	36.0 Medium
(i)	**1.725** **Highest**	1.0618 Low	1.465 Low	0.10 Low	50.4 High

Table 3.3 provides a complete result for investigating the impact of topology on vehicle platoon performance. The ability to track the preceding vehicle has always been regarded as an essential criterion for assessing the performance of CAVs in a platoon. The tracking index evaluates how well a vehicle tracks and follows the preceding vehicle based on the spacing error, velocity error, spacing error sensitivity, and velocity error sensitivity. The lower the index number, the better the performance. IFT(i)(TPLF) has the smallest tracking index values and the most communication links among the nine fixed topologies, indicating that the two predecessor-leader following topology information flow topology is superior in tracking the preceding vehicle. IFT(d)(PLF) and IFT(g)(BDL) are excellent at tracking preceding vehicles. In addition, compared to other topologies, these information flow topologies have more communication links on average. The results overall show a consistent relationship between the number of communication links and the ability to track preceding vehicles. We can conclude that: 1) Information flow topology with more communication links has better tracking ability. 2) Bidirectional information flow topology performs the worst in tracking the preceding vehicles, while two predecessor-leaders following information flow topologies perform the best, performing 34.55% better than the average.

Another important criterion for evaluating platoon performance is the smoothness of the velocity profile. A smaller ASD indicates that the acceleration variation is relatively small during the sampling period, resulting in better driving comfort. IFT(b)(N2) has the smallest ASD value, demonstrating its superiority over all other information flow topologies. IFT(g)(BDL), on the other hand, has the least smoothness of the velocity profile. However, a low ASD value does not always imply better overall performance. A fast-converging rate can be caused by a more abrupt change in control input, which triggers a more abrupt change in acceleration values. Table 3.3 also illustrates that the vehicle's ability to track preceding vehicles and the smoothness of the vehicle velocity profile are complementary. A high ability to track preceding vehicles corresponds to low smoothness of the vehicle velocity profile, and vice versa. As a result, we can conclude that: 1) Innovative topology 2 has the smoothest velocity profile, with an ASD value 11% lower than the average, while bidirectional-leader information flow topology performs the worst, with an ASD value that is 14.45% higher than the average. 2) Information flow topology with better tracking ability possesses a less smooth velocity profile.

Another crucial evaluation of the platoon's performance is fuel efficiency. Fuel efficiency has always been one of the most valued advantages in the platoon of CAVs and has been viewed as an optimisation objective in many studies. It is clear from Table 3.3 that fuel efficiency is almost entirely consistent with the smoothness of velocity profiles and is contrary to the ability to track the preceding vehicle in different information flow topologies. The results also align with common sense that if less change occurs in the acceleration, less fuel will be consumed. IFT(b)(N2) consumes the least amount of fuel, with the highest fuel efficiency, while IFT(f)(BD) consumes

the most amount of fuel, with the lowest fuel efficiency. Thus, we can conclude that: 1) Bidirectional information flow topology has the least fuel efficiency, which is 12.13% less than average. In contrast, innovative information flow topology 2 has the best of it, which is 11.63% more than average.2) Information flow topology with a smoother velocity profile consumes less fuel.

A relatively new way of evaluating the platoon's performance is to compute the system's time delay stability margin, reflecting its ability to handle time delay without losing its string stability. The time delay stability margin is entirely determined by the topological matrix's maximum eigenvalue and the controller's gains. The time delay stability margin for IFT(a)(N1), IFT(b)(N2), IFT(c)(N3), IFT(d)(PLF), and IFT(h)(TPF) is 0.14s. It indicates that if a time delay greater than 0.14s occurs in the system, the system will no longer be stable. IFT(e)(PF) has the highest ability to deal with time delay among all information flow topologies but the lowest tracking ability. We can conclude that: 1) The predecessor following information flow topology is the least vulnerable to time delay, with a time delay stability margin that is 97.55% lower than the average, and the bidirectional information flow topology is the best, with a time delay stability margin that is 95.83% higher than the average. 2) Information flow topology with a high ability to track preceding vehicles has a low ability to deal with time delay.

Communication cost is also essential. High communication costs may result in wasted bandwidth and energy. Lower communication costs, however, can ensure lower channel contention and source broadcast rates, allowing for better data transmission. According to the definition, communication costs are lower when there are fewer communication links. Table 3.3 shows that IFT(g)(BDL) has the highest communication cost, whereas IFT(e)(PF) has the lowest. Information flow topology with a higher tracking index generally has a higher communication cost. The trade-off between tracking ability and communication burden in the platoon's control is unavoidable. We can conclude that: 1) Information flow topology with more communication links has higher communication costs. 2) Information flow topology with better tracking ability carries more communication burden.

In conclusion, this section demonstrates that different information flow topologies exhibit distinct characteristics. More communication links may result in improved platoon tracking ability. Furthermore, the velocity profile's smoothness, fuel economy and communication efficiency are consistent. All of them are antithetical to the tracking ability. Regarding dealing with time delays, the predecessor following information flow topology is the best, while the bidirectional information flow topology is the worst. The majority of the remaining information flow topologies are the same.

3.6.2 A Pareto Optimal Information Flow Topology for The Platoon

Case Study 1

The simulation conditions in the first case study are the same as in section 3.6.1. However, the proposed Pareto optimal information flow topology strategy is used to find the Pareto optimal

topology and make a comparison. In case study 1, a Pareto front with 22 valid Pareto optimal solutions is obtained using the proposed policy. Six solutions demonstrate complete superiority compared to the nine fixed information flow topology types. The obtained Pareto front is shown in Figure 3.6, where all valid solutions are depicted with dots.

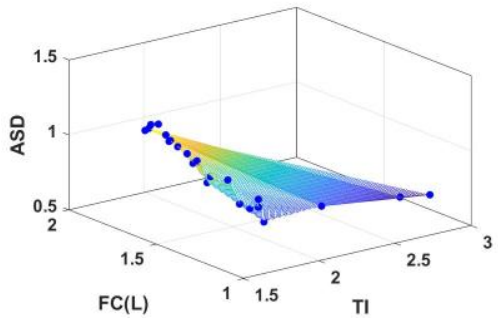

Figure 3.6 Pareto front in Case Study 1

A Pareto optimal topology in the Pareto front is chosen to be the solution, which is regarded as information flow topology(j). The topological matrix is:

$$\begin{bmatrix} 1 & 0 & 1 & 1 & 0 & 0 & 0 & 1 \\ 0 & 1 & 0 & 0 & 0 & 0 & 0 & 0 \\ 0 & 0 & 1 & 1 & 0 & 1 & 0 & 1 \\ 0 & 1 & 0 & 1 & 0 & 0 & 1 & 0 \\ 0 & 0 & 1 & 0 & 1 & 1 & 0 & 1 \\ 0 & 0 & 1 & 0 & 1 & 1 & 0 & 0 \\ 0 & 1 & 0 & 1 & 0 & 0 & 1 & 0 \\ 0 & 1 & 1 & 1 & 0 & 1 & 0 & 1 \end{bmatrix}$$

The tracking index, fuel consumption, and acceleration standard deviation for these six solutions are all lower than the average values for fixed information flow topologies. It demonstrated the proposed Pareto optimal information flow topology strategy's effectiveness in objectively improving the platoon's overall performance without sacrificing tracking ability, fuel economy, or driving comfort.

The tracking index for topology(j) is 1.700. Fuel consumption is 1.196L. The acceleration standard deviation is 0.860, and the time delay stability margin is 0.209s. The communication cost is 64.8, which is higher than traditional information flow topology. The proposed strategy improves the tracking ability by 35.50% more than average, and the tracking index is also 1.45% less than the minimum value in the nine fixed information flow topologies scenario. It also improves fuel economy by 11.6293% more than average and driving comfort by 8.70% more than average. The effectiveness is proven. The effectiveness of the proposed method can be better observed through Figure 3.7, which shows the platoon's spacing and velocity error under topology(j).

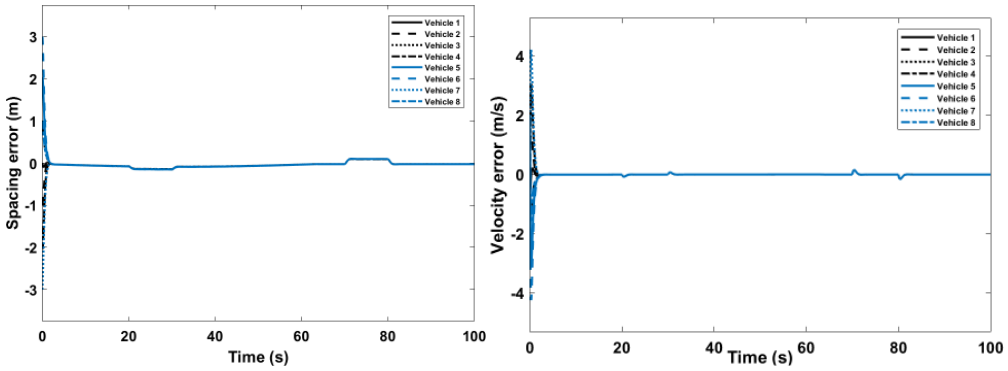

(a) (b)

Figure 3.7 IFT(j). (a): spacing error. (b): velocity error

Case Study 2

Based on the first case study, the second case study expands the platoon size to increase its practical value. Case Study 2 investigates a heterogeneous platoon of fifteen heterogeneous vehicles, including one leader and fourteen followers. The average time delay stability margin constraint is set to be 0.1637s. A Pareto front with 21 valid Pareto optimal solutions is obtained using the proposed policy. The fuel consumption measured in this section is the platoon's total fuel consumption. Five solutions outperform the previously discussed fixed information flow topologies regarding the tracking index and average fuel consumption. The obtained Pareto front is presented in Figure 3.8.

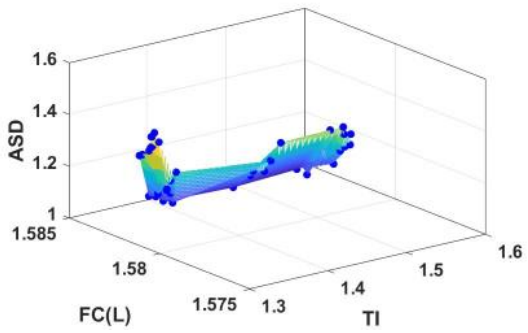

Figure 3.8 Pareto front in Case Study 2

Since convergence has always been the most critical part of the platoon, the Pareto optimal topology with the highest tracking index in the Pareto front is chosen to be the solution, which is regarded as information flow topology(k). It should be noted that with a Pareto front presenting superior valid Pareto optimal solutions, different information flow topologies can be chosen to suit different priorities under different scenarios. The topological matrix is:

$$\begin{bmatrix}
1 & 0 & 1 & 1 & 1 & 0 & 1 & 0 & 0 & 0 & 0 & 1 & 1 & 1 \\
0 & 1 & 1 & 1 & 0 & 0 & 1 & 0 & 1 & 0 & 0 & 0 & 1 & 0 \\
0 & 1 & 1 & 1 & 0 & 0 & 1 & 0 & 1 & 0 & 1 & 0 & 1 & 0 \\
0 & 1 & 1 & 1 & 0 & 0 & 1 & 1 & 1 & 1 & 0 & 1 & 1 & 1 \\
1 & 0 & 0 & 0 & 1 & 1 & 1 & 1 & 1 & 1 & 0 & 1 & 0 & 1 \\
0 & 1 & 1 & 0 & 1 & 1 & 1 & 1 & 0 & 0 & 1 & 0 & 1 & 1 \\
1 & 0 & 0 & 1 & 0 & 0 & 1 & 0 & 0 & 0 & 1 & 1 & 0 & 0 \\
1 & 1 & 1 & 0 & 1 & 0 & 0 & 1 & 1 & 0 & 1 & 0 & 1 & 1 \\
1 & 0 & 1 & 0 & 0 & 0 & 0 & 0 & 1 & 1 & 1 & 1 & 0 & 0 \\
0 & 1 & 0 & 0 & 0 & 0 & 0 & 1 & 1 & 1 & 1 & 0 & 1 & 0 \\
0 & 0 & 1 & 1 & 1 & 0 & 1 & 0 & 1 & 0 & 1 & 0 & 1 & 0 \\
1 & 0 & 1 & 0 & 0 & 0 & 0 & 1 & 0 & 0 & 0 & 1 & 0 & 1 \\
1 & 0 & 1 & 0 & 1 & 0 & 1 & 0 & 1 & 0 & 1 & 1 & 1 & 0 \\
0 & 1 & 0 & 0 & 0 & 0 & 1 & 0 & 1 & 0 & 0 & 0 & 1 & 1
\end{bmatrix}$$

The five performance indices of information flow topologies in Case Study 2 are indicated in Table 3.4.

Table 3.4 Performance indices for different information flow topologies in Case Study 2

IFT	TI	ASD	FC(L)	τ(s)	J
(a)	2.36	0.8712	1.616	0.1637	57.6
(b)	2.873	**0.8094**	1.59	0.1637	57.6
(c)	3.479	0.9426	1.727	0.1637	45.6
(d)	1.45	0.8979	1.583	0.1637	64.8
(e)	5.622	1.1541	**2.119**	**0.2671**	**33.6**
(f)	**36.3**	1.0753	1.906	0.091	64.8
(g)	1.399	1.0248	1.584	**0.074**	96.0
(h)	2.274	0.9542	1.615	0.1637	64.8
(i)	1.317	1.0271	1.581	0.1165	93.6
(k)	**1.315**	**1.4100**	**1.580**	0.1862	**240**

The platoon's spacing and velocity error under topology(k) are presented in Figure 3.9.

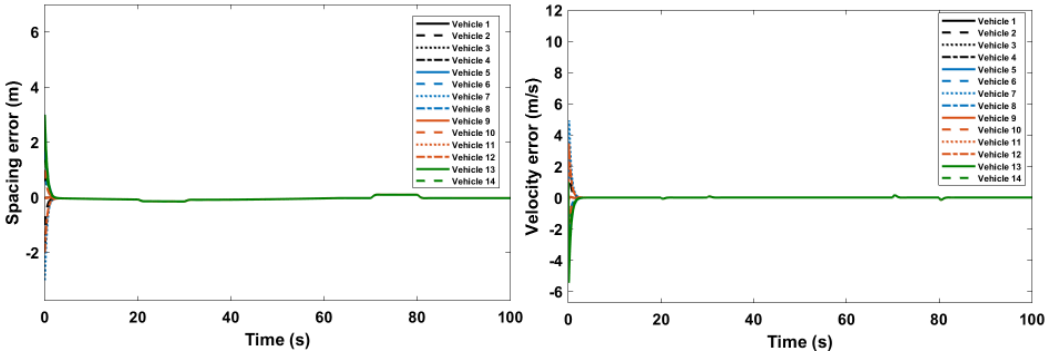

(a) (b)

Figure 3.9 IFT(k). (a): spacing error. (b): velocity error

The tracking index for topology(k) is 1.315. Fuel consumption is 1.58L. The acceleration standard deviation is 1.41, and the time delay stability margin is 0.1862s. The communication cost is 240, which is the highest among all topologies. The proposed strategy improves the tracking ability by 49.35% more than average. It also improves average fuel consumption by 7.181% more than average. Although it does not improve driving comfort, the result demonstrates superiority

because it significantly improves tracking ability and fuel economy.

Case Study 3

Based on the first case study. The size of the platoon remains unchanged. However, an additional external disturbance is introduced into the first case study specifically to vehicle number three and vehicle number six, which is:

$$r_i(t) = 0.5 \times \sin(t) \quad t \geq 5s \tag{3.18}$$

In Case Study 3, a Pareto front with 30 valid Pareto optimal solutions is obtained using the proposed policy. As a result, five solutions outperform the fixed information flow topologies among all valid solutions. The obtained Pareto front is presented in Figure 3.10.

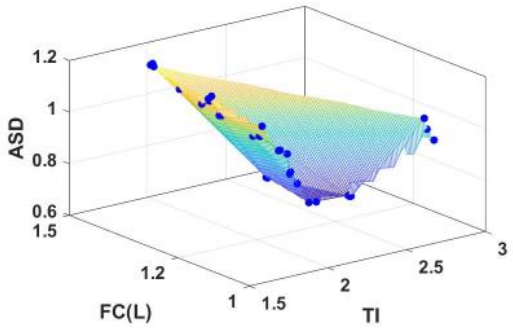

Figure 3.10 Pareto front in Case Study 3

A Pareto optimal topology in the above Pareto front is chosen to be the solution, which is regarded as information flow topology(l). The topological matrix is:

$$\begin{bmatrix} 1 & 0 & 0 & 0 & 0 & 0 & 1 & 1 \\ 1 & 1 & 0 & 1 & 1 & 0 & 1 & 1 \\ 1 & 0 & 1 & 1 & 1 & 1 & 0 & 1 \\ 0 & 0 & 0 & 1 & 0 & 0 & 1 & 0 \\ 0 & 0 & 1 & 0 & 1 & 0 & 1 & 1 \\ 0 & 1 & 1 & 1 & 0 & 1 & 1 & 1 \\ 0 & 0 & 0 & 0 & 0 & 0 & 1 & 0 \\ 0 & 0 & 0 & 0 & 0 & 0 & 1 & 1 \end{bmatrix}$$

The five performance indices of information flow topologies in Case Study 3 are indicated in Table 3.5

Table 3.5 Performance indices for different information flow topologies in Case Study 3

IFT	TI	ASD	FC(L)	τ(s)	J
(a)	2.798	0.8488	1.232	0.14	31.2
(b)	2.816	**0.8393**	1.217	0.14	31.2
(c)	3.657	0.8655	1.301	0.14	26.4
(d)	2.194	0.9308	1.354	0.14	36.0
(e)	5.088	0.9105	1.344	**0.24**	**19.2**
(f)	**18.06**	0.9961	1.547	**0.003**	36.0
(g)	2.027	**1.0784**	**1.556**	0.06	52.8
(h)	2.683	0.9661	1.438	0.14	36.0

(i)	1.992	1.0619	1.501	0.10	50.4
(l)	**1.930**	1.0750	**1.153**	0.159	**72**

To highlight the effectiveness of the proposed approach, comparisons between information flow topology (e) and (l) in terms of spacing error and velocity error in this case study are presented in Figures 3.11 and 3.12, respectively.

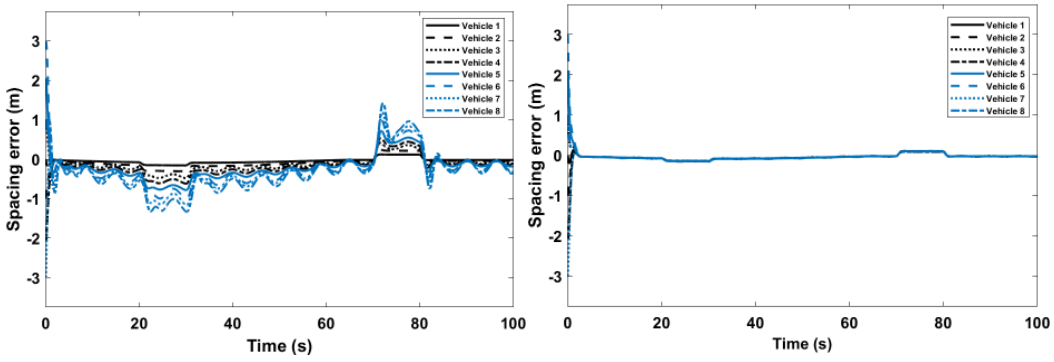

(a) (b)

Figure 3.11 Spacing error for the platoon. (a): IFT(e). (b): IFT(l)

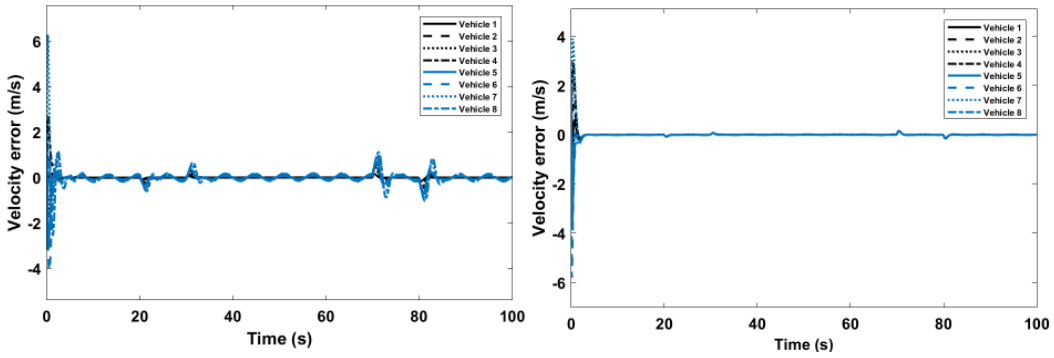

(a) (b)

Figure 3.12 Velocity error for platoon. (a): IFT(e). (b): IFT(l)

The average time delay stability margin constraint is set to be 0.14s. The tracking index for topology(l) is 1.930. Fuel consumption is 1.153L. The acceleration standard deviation is 1.075, and the time delay stability margin is 0.159s. The communication cost is 72. It remains the highest among all. The proposed strategy improves the tracking ability by 33.67% more than average, and the tracking index is also 3.11% less than the minimum value in the nine fixed information flow topologies scenario. It also improves fuel economy by 16.93% more than average, and fuel consumption is 5.26% less than the minimum value. Although driving comfort is not improved, the effectiveness is demonstrated by a significant improvement in tracking ability and fuel economy. When dealing with additional external disturbances, the proposed method is highly effective. The resulting topological matrix also shows that in the Pareto optimal topology, only the fifth and sixth vehicles receive information from the third vehicle, and only the third vehicle receives information from the sixth vehicle. Therefore, the communication links associated with vehicles experiencing external disturbance are significantly reduced.

Case Study 4

The fourth case study is based on the first case study as well. However, this case study considers a more dynamic environment in which the length of the platoon changes due to sensor failure. For $t\epsilon[0,85s]$, the length of the platoon is nine, with one leader, and eight followers. Vehicle number five to eight lose their connection with the vehicles ahead of it at $t = 85s$, causing the platoon to split into two platoons from $t = 85s$. For $t\epsilon(85s, 100s]$, the length of the platoon changes. The first platoon consists of five vehicles, including the leader and vehicles number one to four. The second platoon has four vehicles, including vehicle number five to eight, where they can only exchange information with each other. Vehicle number five is regarded as the leader, and travels at a constant speed.

In Case Study 4, the average time delay stability margin constraint is set to be 0.14s. Pareto fronts with 32 and 16 valid Pareto optimal solutions are obtained using the proposed policy for $t\epsilon[0,85s]$ and $t\epsilon(85s, 100s]$, respectively. They are presented in Figure 3.13.

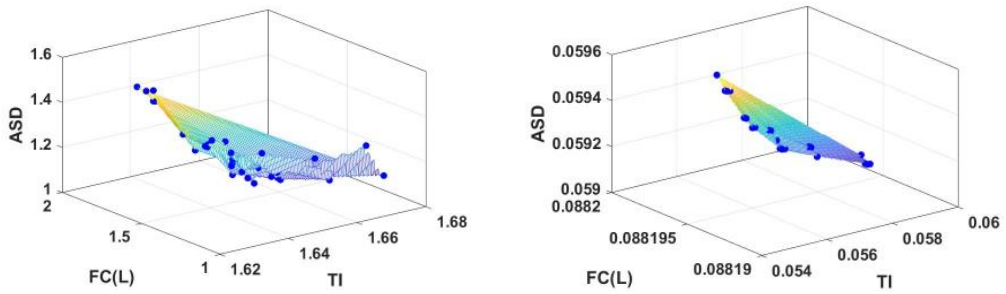

(a) (b)

Figure 3.13 Pareto front in Case Study 4. (a): $t\epsilon[0,85]$. (b): $t\epsilon(85,100]$

For $t\epsilon[0,85s]$, the Pareto optimal information topology for the platoon is regarded as information flow topology (m), the topological matrix is:

$$\begin{bmatrix} 1 & 1 & 1 & 1 & 1 & 1 & 0 & 0 \\ 0 & 1 & 1 & 0 & 1 & 0 & 1 & 1 \\ 1 & 1 & 1 & 1 & 1 & 0 & 0 & 1 \\ 0 & 0 & 0 & 1 & 1 & 0 & 1 & 0 \\ 0 & 1 & 1 & 1 & 1 & 0 & 1 & 1 \\ 0 & 0 & 1 & 0 & 1 & 1 & 1 & 0 \\ 0 & 0 & 0 & 0 & 0 & 0 & 1 & 0 \\ 1 & 0 & 0 & 0 & 0 & 1 & 1 & 1 \end{bmatrix}$$

For $t\epsilon(85s, 100s]$, the Pareto optimal information topologies are selected as information flow topology (n) and (o) for the first and second platoon, respectively, the corresponding topological matrices are:

$$\begin{bmatrix} 1 & 0 & 1 & 0 \\ 1 & 1 & 1 & 0 \\ 1 & 1 & 1 & 1 \\ 1 & 0 & 1 & 1 \end{bmatrix}, \begin{bmatrix} 1 & 0 & 0 \\ 1 & 1 & 1 \\ 0 & 1 & 1 \end{bmatrix}$$

Applying information flow topology (m), (n) and (o) to the platoon. The tracking index is 1.989. Fuel consumption is 1.226L. The acceleration standard deviation is 1.171. The time delay stability margins are 0.1629s, 0.2845s and 0.3133s for information flow topology (m), (n) and (o), respectively. The communication costs are 84, 12.8 and 14.4 for information flow topology (m), (n)

and (o), respectively. The spacing error and velocity error are illustrated in Figure 3.14.

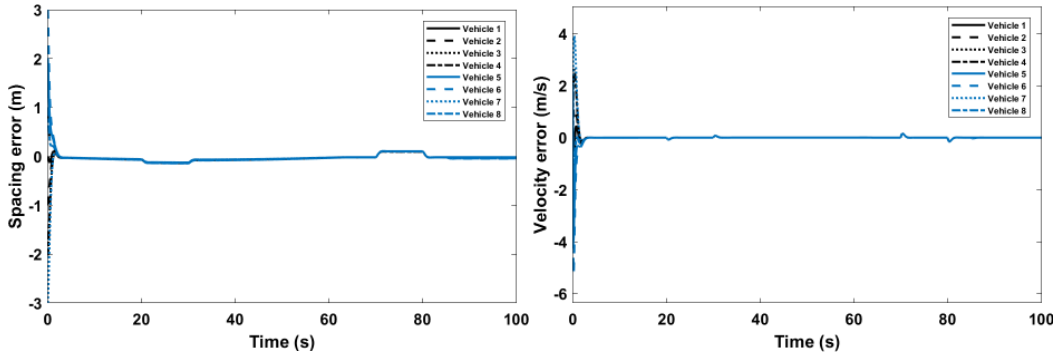

(a) (b)

Figure 3.14 IFT(m), (n) and (o). (a): Spacing error. (b): Velocity error

While traditional fixed information flow topology cannot deal with the length changing of a platoon, the proposed strategy can find Pareto optimal topologies in different time intervals for different platoon sizes and numbers. The tracking ability and the fuel efficiency are high, while the drive comfort is ensured by the acceleration standard deviation, which is within a reasonable range. There is a visible jerk in the velocity error at $t = 85s$, indicating the dynamic environment's impact. It can be seen from the above figures that the platoons can reach a consensus and maintain stability even in a dynamic environment. However, the spacing error does not converge to its best solution because of the uncertainty introduced by heterogeneous vehicle dynamics, which could be improved in future work.

Case Study 5

The fifth case study is based on the first case study too. This case study looks into the presence of missing information. In order to account for packet loss. The packet drop rate is defined in this section using the Bernoulli distribution [86]. The model is described as follows:

$$P_r[\mathrm{B} = 0] = p$$
$$P_r[\mathrm{B} = 1] = 1 - p \tag{3.19}$$

where B is a random Bernoulli process. When $\mathrm{B} = 0$, the communication experiences packet loss. When $\mathrm{B} = 1$, the communication remains normal. The packet loss ratio is denoted by p. In Case Study 5, the average time delay stability margin constraint is set to be 0.14s. As a result, a Pareto front with 40 valid Pareto optimal solutions is obtained. The Pareto front is illustrated in Figure 3.15.

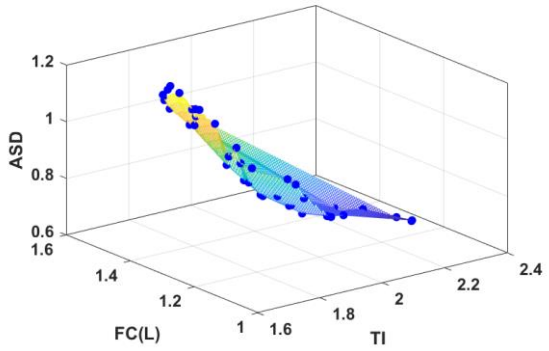

Figure 3.15 Pareto front in Case Study 5

The Pareto optimal information topology for the platoon is regarded as information flow topology(p), the topological matrix is:

$$\begin{bmatrix} 1 & 1 & 1 & 0 & 0 & 0 & 0 & 0 \\ 1 & 1 & 1 & 0 & 0 & 0 & 1 & 0 \\ 1 & 0 & 1 & 0 & 0 & 0 & 0 & 1 \\ 0 & 0 & 1 & 1 & 0 & 0 & 1 & 0 \\ 1 & 0 & 0 & 1 & 1 & 1 & 0 & 0 \\ 1 & 1 & 0 & 0 & 1 & 1 & 0 & 1 \\ 0 & 0 & 0 & 1 & 0 & 0 & 1 & 0 \\ 1 & 0 & 1 & 0 & 1 & 1 & 1 & 1 \end{bmatrix}$$

The five performance indices of information flow topologies in Case Study 5 are indicated in Table 3.6.

Table 3.6 Performance indices for different information flow topologies in Case Study 5

IFT	TI	ASD	FC(L)	τ(s)	J
(a)	2.842	0.8543	1.304	0.14	31.2
(b)	2.879	0.8470	1.303	0.14	31.2
(c)	3.653	0.8750	1.337	0.14	26.4
(d)	1.997	0.9237	1.437	0.14	36.0
(e)	5.299	**0.9063**	1.373	**0.24**	**19.2**
(f)	**20.32**	**1.3485**	**2.635**	**0.003**	36.0
(g)	1.93	1.0455	1.630	0.06	52.8
(h)	2.677	0.9528	1.451	0.14	36.0
(i)	1.885	1.0243	1.533	0.10	50.4
(p)	**1.831**	0.9337	**1.249**	0.1702	**69.6**

When Table 3.6 is compared to Table 3.3, it is clear that missing information harms the platoon's performance in general. The packet drop rate in communication links reduces tracking ability and drive comfort to a certain extent while slightly increasing fuel consumption.

With information flow topology(p), the tracking index is 1.831. Fuel consumption is 1.249L. The acceleration standard deviation is 0.9337. The time delay stability margin is 0.1702s. The communication cost is 69.6 for information flow topology(p). Figure 3.16 depicts the resulting spacing and velocity errors.

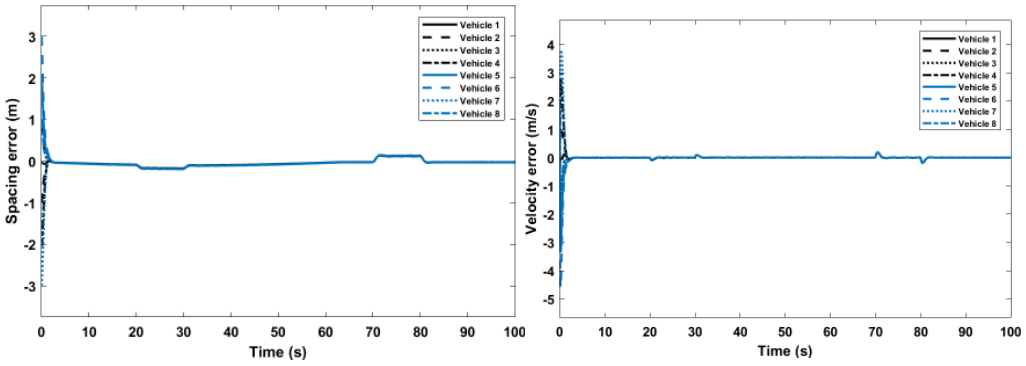

(a) (b)

Figure 3.16 IFT(p). (a): Spacing error. (b): Velocity error

As illustrated in Figure 3.16, the platoon can reach a consensus and remain stable after $t = 82s$. Although Figure 3.16 bears a strong resemblance to Figure 3.7. As can be seen from the data, both spacing and velocity errors are slightly increased as a result of the negative impact of packet drop rate. The cost of communication is 69.6, the highest of all topologies. The proposed strategy improved the tracking ability by 36.76% more than average. The tracking index is 2.95% less than the minimum value in all fixed topologies. The fuel economy is improved by 19.72% compared to the average value, and it is 4.3% better than the best performance obtained in fixed topology. On average, the drive comfort is increased by 14.9%. However, it is a smaller value compared to other fixed topologies. Comparing the above results to the results obtained in Case Study 1, the proposed strategy performs better when dealing with missing information in communication and packet drop rate.

The Pareto optimal topological matrices in the five case studies are asymmetrical. All Pareto optimal topologies exhibit some randomness, demonstrating their practical utility in complex CAVs control problems.

Designing controllers based on one or a few traditional topologies will compromise the platoon's performance and should be avoided. With the complex control problems illustrated in the preceding case studies, it is impossible to imagine the best information flow topology artificially without a scientific method or heuristically, which is the main impediment encountered by state-of-the-art researchers. The proposed Pareto optimal information flow topology strategy can sufficiently overcome this barrier. It can deal with complex control scenarios and provide a solution that can improve vehicle platoon overall performance without sacrificing tracking ability or fuel economy. However, the Pareto optimal topology's communication costs are the highest in all case studies. In addition, driving comfort is not improved in either Case Study 2 or Case Study 3. Given that tracking ability and fuel economy should be prioritised in CAVs, sacrificing driving comfort and communication cost to a reasonable extent to ensure safety and efficiency should be tolerated. The trade-off between communication efficiency and tracking ability is worth further investigation.

3.7 Conclusion

This section first demonstrated the impact of different information flow topologies on vehicle

platoon performance regarding tracking ability, velocity smoothness, fuel economy, ability to deal with time delay, and communication efficiency. The main results are as follows: More communication links lead to better tracking ability, and the smoothness of the velocity profile, fuel economy, and communication efficiency are consistent, contrary to tracking ability. This section then proposed an innovative Pareto optimal information flow topology method that uses NSGA-II to obtain the Pareto optimal topology offline and thus improves the overall performance of the vehicle platoon. The proposed method is tested using a platoon with heterogeneous vehicle dynamics and external disturbances in five case studies. The outcome demonstrates its efficacy and practicality. While ensuring the platoon's stability, it can improve the tracking ability by 33.67% to 49.35%, fuel economy by 7.181% to 16.93% and the acceleration standard deviation up to 14.9%. The next section introduces optimal asymmetric information flow topology and the sliding mode controller design.

Chapter 4

Optimal Asymmetric Information Flow Topology

4.1 Introduction

The previous chapter investigates the impact of information flow topology on the platoon regarding tracking ability, fuel economy, and driving comfort. Chapter 3 then proposes a Pareto optimal information flow topology searching method using NSGA-II to improve the platoon's performance overall. In this chapter, sliding mode controllers are proposed to deal with platoons with time delay and nonlinear model, then finding the optimal asymmetric degree in information flow topology.

Many control methods were proposed to deal with the control of CAVs. Distributed feedback controller has been popular due to its simplicity and direct response to tracking errors [44,87]. On the other hand, the sliding mode controller stands out based on the fast convergence speed and effectiveness in tackling parameter uncertainties and external disturbances. However, most approaches [5,88-89] used a simple strategy to choose the controller's gains, such as the transfer function method, which gives a wide range of feasible control parameters. The feedback coefficients were then selected artificially within the wide range, lacking scientific proof, and making the control method full of randomness. This paper aims to bridge the gap by incorporating a Riccati inequality via Lyapunov analysis in the sliding mode controller design to maintain superior conversing speed while ensuring the platoon's stability.

In terms of the modelling of the platoon, previous studies [14-15,90] considered a class of linearised third-order vehicle dynamic models in the control problem. However, it is based on the assumption that all vehicular parameters are precisely known, which is unrealistic. Therefore, several studies considered a nonlinear vehicle dynamic model to reflect the control problem more accurately [91-93]. In order to address the control problem more precisely, this paper considers a third-order nonlinear vehicle dynamic model in chapter 4.3.

Regarding information flow topology, most studies only focused on symmetric topological matrices. For example, Li et al. investigated different symmetric topologies on CACC and the corresponding convergence time and robustness [40]. A feedback-based platoon control method was in place to deal with both longitudinal and lateral gaps. The result showed that the symmetric network topologies affect the platoon's convergence time, but the robustness is not significantly related. Symmetric information flow topologies are considered in almost all control problems. However, due to the uncertainty of wireless communication, it is neither practical nor efficient.

The advantages of introducing asymmetric topology are also receiving attention in recent years. It is noticed that asymmetric topology can primarily benefit the platooning of CAVs with the attenuation of wireless communication's negative impact [9,38-39]. A study showed that one of the most significant advantages of incorporating asymmetric control is that specific topologies' stability margin can be independent of the platoon size while bounded away from zero [9]. As a result, asymmetric control can obtain a scalable platoon with a constant stability margin. A similar

regularity was also drawn by Herman et al. [38]. The asymmetry of inter-vehicular coupling with asymmetric bidirectional platoon control was investigated in the study. The result showed that even if harmonic instability exists for linear controllers, the Laplacian eigenvalues can still be bounded, which shows advantages. Herman et al. established an LQR optimal distributed controller to design the feedback gain based on the asymmetric topology [39]. The method was proved to be effective beyond the platoon's size. A limitation also occurred as the scaling became exponential and relied on the controller's tuning. However, the asymmetric degrees in all the research were selected randomly and artificially, and there needed to be more evidence on choosing the asymmetric degree. Therefore, this chapter is intended to fill the gap and fully exploit the benefit of asymmetric control by proposing a scientific method to find the optimal asymmetric degree for the platoon's topology.

The main contributions of this chapter are listed below:

1) In the context of the platoon's controller, the traditional distributed feedback controller suffers from slow convergence speed, and the traditional sliding mode controller lacks scientific evidence when choosing control parameters. Past studies selected the controller's gains arbitrarily within a wide range by the transfer function method. This chapter employs a Riccati inequality-based sliding mode control strategy to calculate the feasible controller's gains. As a result, A closed-loop stability theorem for a nonlinear heterogeneous platoon interconnected by the asymmetric topologies is derived using the Lyapunov analysis. Therefore, the advantage of fast convergence speed is preserved while the platoon's stability is ensured.

2) In the context of asymmetric degree, the state-of-the-art investigated platoon by choosing an asymmetric degree arbitrarily. This chapter proposes a strategy to find the optimal asymmetric degree in the topological matrix to achieve multiple objectives in complex control problems with different vehicle dynamics, information feedback delay, and external disturbances. The result proved the effectiveness of the proposed approach.

4.2 Homogeneous Optimal Asymmetric Topology with Time Delay

This chapter proposes a multi-objective asymmetric sliding mode control strategy to deal with time delay in the platoon. Firstly, the homogeneous asymmetric degree is introduced in the topological matrix. Then, a sliding mode controller is designed to target the platoon’s tracking performance. Moreover, Lyapunov analysis is used via Riccati inequality to find the controller’s gains and guarantee the platoon’s stability and Input-to-output string stability. Finally, NSGA-II is utilised to find the Pareto optimal homogeneous asymmetric degree regarding the overall performance of the platoon, including tracking index, fuel consumption, and acceleration standard deviation. Four different information flow topologies, including a random topology, are studied.

4.2.1 Vehicle Dynamic Model

The vehicle dynamic model of the leader is the same as (3.1) in Chapter 3. The model for vehicle i is given as

$$\dot{p}_i(t) = v_i(t)$$
$$\dot{v}_i(t) = a_i(t)$$
$$\dot{a}_i(t) = -\frac{a_i(t)}{\tau} + \frac{u_i(t-\chi)}{\tau} + \frac{w_i(t)}{\tau} \tag{4.1}$$

where $p_i(t)$, $v_i(t)$ and $a_i(t)$ are the longitudinal position, velocity, and acceleration of vehicle i. $u_i(t)$ is the control input of vehicle i. $w_i(t)$ is the external disturbance. τ is the inertial time constant. χ is the information feedback delay. χ is assumed to be bounded by a constant h. For the platoon control, the third-order state space model for each vehicle is:

$$\dot{x}_i(t) = Ax_i(t) + Bu_i(t-\chi) + Bw_i(t) \tag{4.2}$$

where

$$x_i = \begin{bmatrix} p_i \\ v_i \\ a_i \end{bmatrix}, A = \begin{bmatrix} 0 & 1 & 0 \\ 0 & 0 & 1 \\ 0 & 0 & -\frac{1}{\tau} \end{bmatrix}, B = \begin{bmatrix} 0 \\ 0 \\ \frac{1}{\tau} \end{bmatrix}$$

4.2.2 Homogeneous Asymmetric Degree Model

The information flow topology model is the same as in Chapter 3. Referring to [8], the asymmetric degree ε is introduced in the system, where $0 < \varepsilon < 1$. When an agent receives information from the agents ahead of it, the communications are regarded as more reliable, therefore the communication links are enhanced by ε, and vice versa. When $\varepsilon = 0$, the system becomes symmetric.

Here is the process of incorporating the asymmetric degree ε into the topological matrix. Firstly, the adjacency matrix T is separated into T_1 and T_2,where T_1 is an upper triangular matrix and T_2 is a lower triangular matrix. If $j < i$, the communication link is denoted by an adjacency matrix T_1, if $j > i$, the communication link is denoted by an adjacency matrix T_2.

Then, the asymmetric degree ε is introduced to the adjacency matrix T:

$$t_{ij} = \begin{cases} 1+\varepsilon & if\ t_{ij} = 1\ and\ t_{ij} \in T_1 \\ 1-\varepsilon & if\ t_{ij} = 1\ and\ t_{ij} \in T_2 \end{cases}$$

By enforcing the asymmetric degree ε, with the same example mentioned above, T_1 and T_2 can be obtained as:

$$T_1 = \begin{bmatrix} 0 & 0 & 0 & 0 & 0 \\ 1+\varepsilon & 0 & 0 & 0 & 0 \\ 1+\varepsilon & 1+\varepsilon & 0 & 0 & 0 \\ 0 & 1+\varepsilon & 1+\varepsilon & 0 & 0 \\ 0 & 0 & 1+\varepsilon & 1+\varepsilon & 0 \end{bmatrix}, T_2 = \begin{bmatrix} 0 & 1-\varepsilon & 0 & 0 & 0 \\ 0 & 0 & 1-\varepsilon & 0 & 0 \\ 0 & 0 & 0 & 1-\varepsilon & 0 \\ 0 & 0 & 0 & 0 & 1-\varepsilon \\ 0 & 0 & 0 & 0 & 0 \end{bmatrix},$$

$$T_\varepsilon = \begin{bmatrix} 0 & 1-\varepsilon & 0 & 0 & 0 \\ 1+\varepsilon & 0 & 1-\varepsilon & 0 & 0 \\ 1+\varepsilon & 1+\varepsilon & 0 & 1-\varepsilon & 0 \\ 0 & 1+\varepsilon & 1+\varepsilon & 0 & 1-\varepsilon \\ 0 & 0 & 1+\varepsilon & 1+\varepsilon & 0 \end{bmatrix}.$$

where T_ε is the adjacency matrix with the asymmetric degree. It can be seen that $T_\varepsilon = T_1 + T_2$. Therefore $D_\varepsilon$can also be separated into D_1 and D_2 corresponding to T_1 and T_2.

$$D_1 = diag(0, 1+\varepsilon, 2+2\varepsilon, 2+2\varepsilon, 2+2\varepsilon),$$

$$D_2 = diag(1-\varepsilon, 1-\varepsilon, 1-\varepsilon, 1-\varepsilon, 0),$$
$$D_\varepsilon = D_1 + D_2 = diag(1-\varepsilon, 2, 3+\varepsilon, 3+\varepsilon, 2+2\varepsilon).$$

The linked matrix with the asymmetric degree is $P_\varepsilon, P_\varepsilon = diag(1+\varepsilon, 1+\varepsilon, 0, 0, 0)$. By introducing the asymmetric degree, the Laplacian matrix becomes L_ε and topological matrix becomes H_ε.

$$L_\varepsilon = \begin{bmatrix} 1-\varepsilon & -1+\varepsilon & 0 & 0 & 0 \\ -1-\varepsilon & 2 & -1+\varepsilon & 0 & 0 \\ -1-\varepsilon & -1-\varepsilon & 3+\varepsilon & -1+\varepsilon & 0 \\ 0 & -1-\varepsilon & -1-\varepsilon & 3+\varepsilon & -1+\varepsilon \\ 0 & 0 & -1-\varepsilon & -1-\varepsilon & 2+2\varepsilon \end{bmatrix},$$
$$H_\varepsilon = \begin{bmatrix} 2 & -1+\varepsilon & 0 & 0 & 0 \\ -1-\varepsilon & 3+\varepsilon & -1+\varepsilon & 0 & 0 \\ -1-\varepsilon & -1-\varepsilon & 3+\varepsilon & -1+\varepsilon & 0 \\ 0 & -1-\varepsilon & -1-\varepsilon & 3+\varepsilon & -1+\varepsilon \\ 0 & 0 & -1-\varepsilon & -1-\varepsilon & 2+2\varepsilon \end{bmatrix}.$$

The neighbour sets of node i are divided into two sets, $\mathbb{N}_{i_1}$ and $\mathbb{N}_{i_2}$, which is defined as:

$$\mathbb{N}_{i_1} = \{j \in V | t_{ij} = 1+\varepsilon,\ t_{ij} \in T_1\}$$
$$\mathbb{N}_{i_2} = \{j \in V | t_{ij} = 1-\varepsilon,\ t_{ij} \in T_2\}$$

The leader accessible set of node i is defined as:

$$\mathbb{R}_i = \begin{cases} \{0\} & if\ p_i = 1+\varepsilon \\ \emptyset & if\ p_i = 0 \end{cases}$$

Therefore, the topology information sets of node i are also divided into two sections, which are defined as:

$$\Pi_{i_1} = \mathbb{N}_{i_1} \cup \mathbb{R}_i$$
$$\Pi_{i_2} = \mathbb{N}_{i_2}$$
$$\Pi_i = \Pi_{i_1} \cup \Pi_{i_2}$$

After introducing the asymmetric degree ε into the topological matrix, H_ε will be used in the following chapters when referring to the complete topology information set Π_i. Among all the vehicles that vehicle i receives information from, the first topology information set Π_{i_1}refers to the vehicles ahead of vehicle i, including the leader. The second topology information set Π_{i_2}refers to vehicles behind vehicle i. The maximum and minimum eigenvalues of a certain type of topology take the real part of the complex number and are expressed as $\lambda_{max}(H_\varepsilon)$ and $\lambda_{min}(H_\varepsilon)$ respectively.

4.2.3 Sliding Mode Controller Design

Firstly, this section presents the design of the sliding mode controller. Then it analyses the platoon's asymptotic stability with information time delay. Riccati inequality and Lyapunov analysis are used in the platoon's closed-loop error dynamic system. Finally, the input-to-output string stability of the platoon is proved.

Assuming the leader's trajectory is optimal. The tracking error $\gamma_i(t)$can be designed as the controller's prime goal, which is:

$$\gamma_i(t) = (1+\varepsilon)c_1 \sum_{j\epsilon\Pi_{i_1}} p_i(t) - p_j(t) - d_{ij} + (1+\varepsilon)c_2 \sum_{j\epsilon\Pi_{i_1}} v_i(t) - v_j(t)$$
$$+(1-\varepsilon)c_1 \sum_{j\epsilon\Pi_{i_2}} p_i(t) - p_j(t) - d_{ij} + (1-\varepsilon)c_2 \sum_{j\epsilon\Pi_{i_2}} v_i(t) - v_j(t) + c_3 a_i(t) \tag{4.3}$$

where $c_1, c_2, c_3 > 0$, and they are the error weights parameters, Π_{i_1} and Π_{i_2} are complete topology information sets of node i stated in previous chapter. d_{ij} is the desired spacing between vehicle i and vehicle j, a predefined nonzero constant. To converge the error to zero, the sliding surface is selected to be:

$$s_i(t) = \int \gamma_i(t)dt + \varsigma\gamma_i(t) \tag{4.4}$$

where ς is a positive sliding parameter. $s_i(t)$ can be rewritten as:

$$s_i(t) = (1+\varepsilon)c_1 \int \sum_{j\epsilon\Pi_{i_1}} (p_i(t) - p_j(t) - d_{ij})\,dt + (1+\varepsilon)(c_2 + \varsigma c_1) \sum_{j\epsilon\Pi_{i_1}} p_i(t) - p_j(t) - d_{ij}$$
$$+(1+\varepsilon)\varsigma c_2 \sum_{j\epsilon\Pi_{i_1}} v_i(t) - v_j(t) + (1-\varepsilon)c_1 \int \sum_{j\epsilon\Pi_{i_2}} (p_i(t) - p_j(t) - d_{ij})\,dt$$
$$+(1-\varepsilon)(c_2 + \varsigma c_1) \sum_{j\epsilon\Pi_{i_2}} p_i(t) - p_j(t) - d_{ij} + (1-\varepsilon)\varsigma c_2 \sum_{j\epsilon\Pi_{i_2}} v_i(t) - v_j(t)$$
$$+\varsigma c_3 a_i(t) + c_3 v_i(t) \tag{4.5}$$

Taking the time derivative of $s_i(t)$, then

$$\dot{s}_i(t) = \gamma_i(t) + \varsigma\dot{\gamma}_i(t)$$
$$= (1+\varepsilon)c_1 \sum_{j\epsilon\Pi_{i_1}} p_i(t) - p_j(t) - d_{ij} + (1+\varepsilon)(c_2 + \varsigma c_1) \sum_{j\epsilon\Pi_{i_1}} v_i(t) - v_j(t)$$
$$+(1+\varepsilon)\varsigma c_2 \sum_{j\epsilon\Pi_{i_2}} a_i(t) - a_j(t) + (1-\varepsilon)c_1 \sum_{j\epsilon\Pi_{i_2}} p_i(t) - p_j(t) - d_{ij}$$
$$+(1-\varepsilon)(c_2 + \varsigma c_1) \sum_{j\epsilon\Pi_{i_2}} v_i(t) - v_j(t) + (1-\varepsilon)\varsigma c_2 \sum_{j\epsilon\Pi_{i_1}} a_i(t) - a_j(t)$$
$$+c_3 a_i(t) + \varsigma c_3[-\tfrac{1}{\tau}a_i(t) + \tfrac{1}{\tau}u_i(t) + \tfrac{1}{\tau}w_i(t)] \tag{4.6}$$

When $\dot{s}_i(t) = 0$, the stability is reached, and $u_{eq_i}(t)$ can be found as:

$$u_{eq_i}(t) = -(1+\varepsilon)\frac{\tau c_1}{\varsigma c_3} \sum_{j\epsilon\Pi_{i_1}} p_i(t) - p_j(t) - d_{ij} - (1+\varepsilon)\frac{\tau c_2 + \tau\varsigma c_1}{\varsigma c_3} \sum_{j\epsilon\Pi_{i_1}} v_i(t) - v_j(t)$$
$$-(1+\varepsilon)\frac{\tau c_2}{c_3} \sum_{j\epsilon\Pi_{i_1}} a_i(t) - a_j(t) - (1-\varepsilon)\frac{\tau c_1}{\varsigma c_3} \sum_{j\epsilon\Pi_{i_2}} p_i(t) - p_j(t) - d_{ij}$$
$$-(1-\varepsilon)\frac{\tau c_2 + \tau\varsigma c_1}{\varsigma c_3} \sum_{j\epsilon\Pi_{i_2}} v_i(t) - v_j(t) - (1-\varepsilon)\frac{\tau c_2}{c_3} \sum_{j\epsilon\Pi_{i_2}} a_i(t) - a_j(t)$$
$$-\frac{\tau - \varsigma}{\varsigma} a_i(t) - w_i(t)$$

(4.7)

which can be further written as:

$$u_{eq_i}(t) = u_{eq}{}^{\circ}{}_i(t) + \widetilde{u_{eq}}_i(t)$$

(4.8)

where

$$\begin{aligned} u_{eq}{}^{\circ}{}_i(t) = &-(1+\varepsilon)\frac{\tau c_1}{\varsigma c_3}\sum_{j\epsilon\Pi_{i_1}} p_i(t) - p_j(t) - d_{ij} - (1+\varepsilon)\frac{\tau c_2 + \tau\varsigma c_1}{\varsigma c_3}\sum_{j\epsilon\Pi_{i_1}} v_i(t) - v_j(t) \\ &-(1+\varepsilon)\frac{\tau c_2}{c_3}\sum_{j\epsilon\Pi_{i_1}} a_i(t) - a_j(t) - (1-\varepsilon)\frac{\tau c_1}{\varsigma c_3}\sum_{j\epsilon\Pi_{i_2}} p_i(t) - p_j(t) - d_{ij} \\ &-(1-\varepsilon)\frac{\tau c_2 + \tau\varsigma c_1}{\varsigma c_3}\sum_{j\epsilon\Pi_{i_2}} v_i(t) - v_j(t) - (1-\varepsilon)\frac{\tau c_2}{c_3}\sum_{j\epsilon\Pi_{i_2}} a_i(t) - a_j(t) \\ &-\frac{\tau-\varsigma}{\varsigma}a_i(t) \end{aligned}$$

(4.9)

and

$$\widetilde{u_{eq}}_i(t) = -w_i(t)$$

(4.10)

where $w_i(t)$ is considered as bounded matched disturbance, $\max(|w_i(t)|) = \delta$. Thus, the final control law $u_i(t)$ is designed to be:

$$u_i(t) = u_{eq}{}^{\circ}{}_i(t) - (\left|\widetilde{u_{eq}}_i(t)_{max}\right| + \sigma)sgn(s_i(t))$$

(4.11)

where σ is another sliding parameter, and $\sigma > 0$, it represents the sliding speed. The control input $u_i(t)$ can be rewritten as:

$$\begin{aligned} u_i(t) = &-(1+\varepsilon)\frac{\tau c_1}{\varsigma c_3}\sum_{j\epsilon\Pi_{i_1}} p_i(t) - p_j(t) - d_{ij} - (1+\varepsilon)\frac{\tau c_2 + \tau\varsigma c_1}{\varsigma c_3}\sum_{j\epsilon\Pi_{i_1}} v_i(t) - v_j(t) \\ &-(1+\varepsilon)\frac{\tau c_2}{c_3}\sum_{j\epsilon\Pi_{i_1}} a_i(t) - a_j(t) - (1-\varepsilon)\frac{\tau c_1}{\varsigma c_3}\sum_{j\epsilon\Pi_{i_2}} p_i(t) - p_j(t) - d_{ij} \\ &-(1-\varepsilon)\frac{\tau c_2 + \tau\varsigma c_1}{\varsigma c_3}\sum_{j\epsilon\Pi_{i_2}} v_i(t) - v_j(t) - (1-\varepsilon)\frac{\tau c_2}{c_3}\sum_{j\epsilon\Pi_{i_2}} a_i(t) - a_j(t) \\ &-\tfrac{\tau-\varsigma}{\varsigma}a_i(t) - (\delta+\sigma)sgn(s_i(t)) \end{aligned}$$

(4.12)

Inspired by [31], asymptotic stability of the platoon with information feedback delay χ is proved using Lyapunov analysis and Riccati inequality, LMIs are computed subsequently.

Theorem 4.1: Considering information feedback delay, for given time delay upper bound $h \geq 0$, and scalar $\gamma > 0$, the system (4.2) is asymptotically stable, if there exist matrices $P, \bar{Q}_1, \bar{Q}_2, \bar{Q}_3 > 0$, and appropriately dimensioned matrices $\bar{D}, \bar{X}, W, \bar{K}$, such that the following inequalities hold:

$$\begin{bmatrix} \bar{O} + \bar{D}L_1 + (\bar{D}L_1)^T + h\bar{X} + W & \sqrt{h}\bar{M}^T \\ * & -\bar{Q}_3 \end{bmatrix} < 0$$

(4.13)

$$\begin{bmatrix} \bar{X} & \bar{D} \\ * & 2\bar{Q}_1 - \bar{Q}_3 \end{bmatrix} \geq 0$$

(4.14)

$$H_\varepsilon{}^T P + P H_\varepsilon - 2\lambda_{min}(H_\varepsilon) P > 0$$

(4.15)

where

$$\bar{O} = \begin{bmatrix} A\bar{Q}_1 + \bar{Q}_1 A^T + \bar{Q}_2 + W & -\frac{\lambda_{min}(H_\varepsilon)}{2} B\bar{K} & 0 & B_1 \\ * & 0 & 0 & 0 \\ * & * & -\bar{Q}_2 & 0 \\ * & * & * & -\gamma^2 \end{bmatrix}, \bar{M} = [A\bar{Q}_1, -\frac{\lambda_{min}(H_\varepsilon)}{2} B\bar{K}, 0, B_1\bar{Q}_1]$$

$$K = \bar{K}\bar{Q}_1{}^{-1}$$

(4.16)

Proof: The closed-loop error of the platoon is defined as $E(t)^T = [e_1(t)^T \dots e_N(t)^T]$ and $e_i(t) = [\Delta p_i(t) \quad \Delta v_i(t) \quad \Delta a_i(t)]^T$.

$$\Delta p_i(t) = p_i(t) - p_0(t) - d_{i0}$$
$$\Delta v_i(t) = v_i(t) - v_0(t)$$
$$\Delta a_i(t) = a_i(t) - a_0(t)$$

(4.17)

The closed-loop error dynamic is:

$$\Delta \dot{p}_i(t) = \Delta v_i(t)$$
$$\Delta \dot{v}_i(t) = \Delta a_i(t)$$
$$\Delta \dot{a}_i(t) = -\frac{\Delta a_i(t)}{\tau} + \frac{u_i(t-\chi)}{\tau} + \frac{w_i(t)}{\tau}$$

(4.18)

Thus, a third-order state space model can be established for the error dynamic as:

$$\dot{e}_i(t) = Ae_i(t) + Bu_i(t-\chi) + Bw_i(t)$$

(4.19)

Denoting the controller's gains as k_1, k_2, k_3, it can be obtained from (4.12) that:

$$k_1 = \frac{\tau c_1}{\varsigma c_3}$$
$$k_2 = \frac{\tau c_2 + \tau \varsigma c_1}{\varsigma c_3}$$
$$k_3 = \frac{\tau c_2}{c_3}$$

(4.20)

Therefore, the input with information feedback delay $u_i(t-\chi)$can be rewritten as:

$$u_i(t-\chi) = -(1+\varepsilon)k_1 \sum_{j \epsilon \Pi_{i_1}} p_i(t-\chi) - p_j(t-\chi) - d_{ij}$$

$$-(1+\varepsilon)k_2\sum_{j\epsilon\Pi_{i_1}} v_i(t-\chi)-v_j(t-\chi)-(1+\varepsilon)k_3\sum_{j\epsilon\Pi_{i_1}} a_i(t-\chi)-a_j(t-\chi)$$
$$-(1-\varepsilon)k_1\sum_{j\epsilon\Pi_{i_2}} p_i(t-\chi)-p_j(t-\chi)-d_{ij}-(1-\varepsilon)k_2\sum_{j\epsilon\Pi_{i_2}} v_i(t-\chi)-v_j(t-\chi)$$
$$-(1-\varepsilon)k_3\textstyle\sum_{j\epsilon\Pi_{i_2}} a_i(t-\chi)-a_j(t-\chi)-\frac{\tau-\varsigma}{\varsigma}a_i(t-\chi)-(\delta+\sigma)sgn(s_i(t-\chi))$$

(4.21)

$$K=[k_1\ k_2\ k_3]$$

(4.22)

Substitute (4.20) and (4.21) into (4.17) and (4.19), taking the time derivative of $E(t)$, $\dot{E}(t)$ can be obtained as:

$$\dot{E(t)}=(I_N\otimes A)E(t)-(H_\varepsilon\otimes BK)E(t-\chi)+(1_N\otimes B)\left[-(\delta+\sigma)sgn\big(s_i(t-\chi)\big)+w_i(t)-\frac{\tau-\varsigma}{\varsigma}\big(a_i(t-\chi)\big)\right]$$

(4.23)

Define the equivalent external disturbance as $\widehat{\omega}_i(t)$:

$$\widehat{\omega}_i(t)=-(\delta+\sigma)sgn\big(s_i(t-\chi)\big)+w_i(t)-\frac{\tau-\varsigma}{\varsigma}a_i(t-\chi)$$

(4.24)

$\dot{E}(t)$can be obtained as:

$$\dot{E}(t)=(I_N\otimes A)E(t)-(H_\varepsilon\otimes BK)E(t-\chi)+(I_N\otimes B_1)\varpi(t)$$

(4.25)

where $\varpi(t)=[\widehat{\omega}_1(t);\cdots;\widehat{\omega}_N(t)]\ \otimes[0;0;1], B_1=B[1,1,1]$.

Lemma 4.1 [94]: Given $\mathbb{Q}=\left[q_{ij}\right]\in\mathbb{R}^{N\times N}$, then all the eigenvalues of $\mathbb{Q}$ are located in the union of the N disks

$$\bigcup_{i=1}^{N}\left\{z\in\mathbb{C}||z-q_{ii}|\le\sum_{j=1,j\neq i}^{N}|q_{ij}|\right\}$$

(4.26)

Lemma 4.2 [94]: Given $A\in\mathbb{R}^{N\times N}$, then A is Hurwitz if and only if there exists a positive definite matrix $P>0$, such that:

$$AP+PA^T<0$$

(4.27)

Choose Lyapunov function to be:

$$V=V_1+V_2+V_3$$

(4.28)

$$V_1=E^T(t)(P\otimes Q_1)E(t)$$

(4.29)

$$V_2=\textstyle\int_{t-h}^{t}E^T(s)(P\otimes Q_2)E(s)ds$$

(4.30)

$$V_3=\textstyle\int_{-h}^{0}\int_{t+\theta}^{t}\dot{E}^T(s)(P\otimes Q_3)\dot{E}(s)\,dsd\theta$$

(4.31)

Based on Newton-Leibnitz formula:

$$E(t) - E(t-h) - \int_{t-h}^{h} \dot{E}(s)\, ds = 0$$

(4.32)

It can be obtained that:

$$2F^T(t)(P \otimes D)\left[E(t) - E(t-h) - \int_{t-h}^{h} \dot{E}(s)\, ds\right] = 0$$

(4.33)

where $F(t) = [E^T(t), E^T(t-\chi), E^T(t-h), \varpi^T(t)]^T$, D is any matrix with appropriate dimensions. Taking the time derivative of V_1:

$$\begin{aligned}\dot{V}_1 &= \dot{E}^T(t)(P \otimes Q_1)E(t) + E^T(t)(P \otimes Q_1)\dot{E}(t) \\ &= E^T(t)[P \otimes (A^T Q_1 + Q_1 A)]E(t) + E^T(t-\chi)\left[-{H_\varepsilon}^T P \otimes K^T B^T Q_1\right]E(t) + E^T(t) \\ &[-PH_\varepsilon \otimes Q_1 BK]E(t-\chi) + \varpi^T(t)\left[P \otimes {B_1}^T Q_1\right]E(t) + E^T(t)[P \otimes Q_1 B_1]\varpi(t)\end{aligned}$$

(4.34)

Based on LMI (4.15), for the second term in $\dot{V}_1$, the following inequality holds:

$$\begin{aligned}E^T(t-\chi)\left[-{H_\varepsilon}^T P \otimes K^T B^T Q_1\right]E(t) + E^T(t)[-PH_\varepsilon \otimes Q_1 BK]E(t-\chi) < E^T(t-\chi) \\ \left[-P \otimes \frac{\lambda_{min}(H_\varepsilon)}{2} K^T B^T Q_1\right]E(t) + E^T(t)\left[-P \otimes \frac{\lambda_{min}(H_\varepsilon)}{2} Q_1 BK\right]E(t-\chi)\end{aligned}$$

(4.35)

The time derivate of V_2 and V_3 can be obtained respectively:

$$\dot{V}_2 = E^T(t)(P \otimes Q_2)E(t) - E^T(t-h)(P \otimes Q_2)E(t-h)$$

(4.36)

$$\dot{V}_3 = h\dot{E}^T(t)(P \otimes Q_3)\dot{E}(t) - \int_{t-h}^{t} \dot{E}^T(s)(P \otimes Q_3)\dot{E}(s)\, ds$$

(4.37)

Therefore $\dot{V}$ can be expressed as:

$$\dot{V} = \dot{V}_1 + \dot{V}_2 + \dot{V}_3$$

(4.38)

It can be obtained that:

$$\begin{aligned}\dot{V} < {} & E^T(t)[P \otimes (A^T Q_1 + Q_1 A)]E(t) + E^T(t-\chi)\left[-P \otimes \frac{\lambda_{min}(H_\varepsilon)}{2} K^T B^T Q_1\right]E(t) \\ & + E^T(t)\left[-P \otimes \frac{\lambda_{min}(H_\varepsilon)}{2} Q_1 BK\right]E(t-\chi) + \varpi^T(t)\left[P \otimes {B_1}^T Q_1\right]E(t) + E^T(t)[P \otimes Q_1 B_1]\varpi(t) \\ & + E^T(t)(P \otimes Q_2)E(t) - E^T(t-h)(P \otimes Q_2)E(t-h) + h\dot{E}^T(t)(P \otimes Q_3)\dot{E}(t) \\ & - \int_{t-h}^{t} \dot{E}^T(s)(P \otimes Q_3)\dot{E}(s)\, ds + 2F^T(t)D\left[E(t) - E(t-h) - \int_{t-h}^{h} \dot{E}(s)\, ds\right]\end{aligned}$$

(4.39)

(4.39) can be further transformed into:

$$\dot{V} < E^T(t)[P \otimes (A^T Q_1 + Q_1 A)]E(t) + E^T(t-\chi)\left[-P \otimes \frac{\lambda_{min}(H_\varepsilon)}{2} K^T B^T Q_1\right]E(t)$$

$$+E^T(t)\left[-P\otimes\frac{\lambda_{min}(H_\varepsilon)}{2}Q_1BK\right]E(t-\chi)+\varpi^T(t)\left[P\otimes {B_1}^T Q_1\right]E(t)+E^T(t)[P\otimes Q_1B_1]\varpi(t)$$
$$+E^T(t)(P\otimes Q_2)E(t)-E^T(t-h)(P\otimes Q_2)E(t-h)+h\dot{E}^T(t)(P\otimes Q_3)\dot{E}(t)$$
$$-\int_{t-h}^{t}\dot{E}^T(s)(P\otimes Q_3)\dot{E}(s)\,ds+2F^T(t)(P\otimes D)L_1F(t)-2F^T(t)(P\otimes D)\int_{t-h}^{h}\dot{E}(s)\,ds \tag{4.40}$$

where $L_1=[I,0,-I,0]$. Define $\hat{F}^T(t,s)=[F^T(t),\dot{E}^T(s)]$, the following inequality holds:

$$\dot{V}+E^T(t)E(t)-\gamma^2\varpi^T(t)\varpi(t)\le F^T(t)\Phi F(t)-\int_{t-h}^{h}\hat{F}^T(t,s)\Psi\hat{F}(t,s)\,ds \tag{4.41}$$

where $\Phi<\mathrm{O}+\mathrm{D}L_1+(\mathrm{D}L_1)^T+M^T(hQ_3)M+hX+{L_2}^T L_2$, $L_2=[I,0,0,0]$,

$$\mathrm{O}=\begin{bmatrix}A^TQ_1+Q_1A+Q_2 & -\frac{\lambda_{min}(H_\varepsilon)}{2}Q_1BK & 0 & Q_1B_1\\ * & 0 & 0 & 0\\ * & * & -Q_2 & 0\\ * & * & * & -\gamma^2\end{bmatrix},M=[A,-\tfrac{\lambda_{min}(H_\varepsilon)}{2}BK,0,B_1],$$
$$\Psi=\begin{bmatrix}X & D\\ * & Q_3\end{bmatrix} \tag{4.42}$$

X is any matrix with appropriate dimensions. It is obvious that when $\Psi\ge 0$ and $\Phi<0$,

$$\dot{V}+E^T(t)E(t)-\gamma^2\varpi^T(t)\varpi(t)<0 \tag{4.43}$$

Converting $\Psi\ge 0$ and $\Phi<0$ into LMIs, it can be written as:

$$\begin{bmatrix}\mathrm{O}+\mathrm{D}L_1+(\mathrm{D}L_1)^T+hX+{L_2}^TL_2 & \sqrt{h}M^T\\ * & -{Q_3}^{-1}\end{bmatrix}<0 \tag{4.44}$$

$$\begin{bmatrix}X & D\\ * & Q_3\end{bmatrix}\ge 0 \tag{4.45}$$

Pre-multiply and post multiply the LMI (4.44) by Λ, where $\Lambda=\mathrm{diag}\{\Upsilon,I\}$, $\Upsilon=\mathrm{diag}\{{Q_1}^{-1},{Q_1}^{-1},{Q_1}^{-1},I\}$, and let $\bar{Q}_1={Q_1}^{-1}$, $\bar{D}=\Upsilon D\bar{Q}_1$, $\bar{X}=\Upsilon X\Upsilon$, $\bar{K}=K\bar{Q}_1$, $\bar{Q}_2=\bar{Q}_1Q_2\bar{Q}_1$. $W=\Upsilon{L_2}^TL_2\Upsilon$, $\bar{M}=\left[A\bar{Q}_1,-\frac{\lambda_{min}(H_\varepsilon)}{2}B\bar{K},0,B_1\bar{Q}_1\right]$. LMI (4.13) is obtained. Pre-multiply and post multiply the above LMI (4.45) by Ξ, where $\Xi=\mathrm{diag}\{\Upsilon,{Q_1}^{-1}\}$ and let $\bar{Q}_3={Q_3}^{-1}$, it can be derived that:

$$\begin{bmatrix}\bar{X} & \bar{D}\\ * & \bar{Q}_1{\bar{Q}_3}^{-1}\bar{Q}_1\end{bmatrix}\ge 0 \tag{4.46}$$

Since $(\bar{Q}_1-\bar{Q}_3){\bar{Q}_3}^{-1}(\bar{Q}_1-\bar{Q}_3)\ge 0$, it can be obtained that:

$$\bar{Q}_1{\bar{Q}_3}^{-1}\bar{Q}_1\ge 2\bar{Q}_1-\bar{Q}_3 \tag{4.47}$$

Substituting (4.47) into (4.46), LMI (4.14) is obtained. If feasible solutions exist, then the controller gain K can be calculated using (4.16). Asymptotic stability is established for the platoon with information feedback delay. The proof of Theorem *4.1* is completed.

By following [95], in which the input-to-output string stability is proposed, the input-to-output string stability of the platoon in this section is defined as below:

Definition 4.1 [31]: For the m dimensional space of piecewise continuous, square-integrable functions, the norm $\mathcal{L}_2$ is defined by

$$\| x \|_{\mathcal{L}_2} = \sqrt{\int_0^\infty \| x \|^2 \, dt} < \infty \tag{4.48}$$

where $\| x \| = \sqrt{x^T x}$, the space is denoted by $\mathcal{L}_2^m$.

Definition 4.2: For a platoon with external disturbances, the convergence performance is defined as:

$$J(\varpi) = \int_0^\infty E^T(t)E(t) - \gamma^2 \varpi^T(t)\varpi(t)\, dt \tag{4.49}$$

Lemma 4.3 [96]: The platoon system is input-to-output $\mathcal{L}_2$ string stable if all inputs belong to $\mathcal{L}_2$ space, i.e. $\| \varpi(t) \|_{\mathcal{L}_2} < \infty$, and the outputs are once again in the $\mathcal{L}_2$ space for any platoon length $m \in \mathbb{N}$, with the $\mathcal{L}_2$ gain bounded by γ, as shown in below:

$$\| \mathcal{G}_{\varpi E} \|_\infty \triangleq sup \frac{\|E(t)\|_{\mathcal{L}_2}}{\|\varpi(t)\|_{\mathcal{L}_2}} < \gamma \tag{4.50}$$

Theorem 4.2: Consider the platoon described by (4.2), and the controller designed as (4.21). If LMIs (4.13-4.15) are feasible, K and γ computed from (4.16) can guarantee the platoon being input-to-output $\mathcal{L}_2$ string stable and satisfies $J(\varpi) < 0$ for all nonzero $\varpi(t)$.

Proof: (4.43) is equivalent to:

$$\int_0^\infty E^T(t)E(t) - \gamma^2 \varpi^T(t)\varpi(t)\, dt < V(E(0)) - V(E(\infty)) \tag{4.51}$$

when under zero initial condition, such that $V\big(E(0)\big) = 0$ and $V\big(E(\infty)\big) > 0$. (4.51) is equivalent to:

$$\int_0^\infty E^T(t)E(t) - \gamma^2 \varpi^T(t)\varpi(t)\, dt < 0 \tag{4.52}$$

Therefore, $J(\varpi) < 0$ is proved. Based on (4.24), due to safety reason, the absolute value of acceleration of the vehicles in the platoon is bounded by $1\ m/s^2$. ς is selected to be within the range: $0.5\tau < \varsigma < \tau$, so that the coefficient $-\frac{\tau-\varsigma}{\varsigma}$ is bounded by 0 to 1. σ is selected to be larger than 1. Since $-\delta sgn\big(s_i(t-\chi)\big) + w_i(t) \approx 0$. $\widehat{\omega}_i(t)$ can be written as:

$$\widehat{\omega}_i(t) = \begin{cases} \sigma + g_i(t), & s_i(t-\chi) < 0 \\ g_i(t), & s_i(t-\chi) = 0 \\ -\sigma + g_i(t), & s_i(t-\chi) > 0 \end{cases}$$

(4.53)

where $g_i(t) = w_i(t) - \frac{\tau-\varsigma}{\varsigma} a_i(t-\chi)$. A maximum bound for $\widehat{\omega}_i(t)^T \widehat{\omega}_i(t)$ can be found at $(\sigma+\delta+1)^2$. Therefore, it can be derived that:

$$\| \varpi(t) \|_{\mathcal{L}_2} < \infty$$

(4.54)

Based on inequality (4.52) and *Lemma 4.3.* It can be obtained that:

$$\| E(t) \|_{\mathcal{L}_2}{}^2 < \gamma^2 \| \varpi(t) \|_{\mathcal{L}_2}{}^2$$

(4.55)

(4.55) can be transformed into:

$$sup \frac{\| E(t) \|_{\mathcal{L}_2}}{\| \varpi(t) \|_{\mathcal{L}_2}} < \gamma$$

(4.56)

The performance of disturbance propagation can also be represented by (4.56). Therefore, input-to-output $\mathcal{L}_2$ string stability is established for the platoon. The proof of *Theorem 4.2* is completed.

Configurable parameters ϵ, ς and σ are yet to be designed in the controller, the final chosen values after tuning are presented in Table 4.1. Here are some remarks regarding the above parameters.

Remark 1: ϵ is used in sgn function and is intended to reduce chattering of the controller. The selection of ϵ indicates a trade-off between control accuracy and chattering. Larger ϵ can improve chattering while compromising control accuracy to an extent.

Remark 2: ς is a positive sliding parameter that represents the importance of tracking error convergence in comparison to its integral form. ς is defined to be within the range of $0.5\tau < \varsigma < \tau$ to simplify the closed-loop error system. When ς is less than 1, the change in ς has no significant impact on controller's performance.

Remark 3: σ indicates the sliding speed of the controller. It is preferable to choose a relatively large σ to reach the stable point in the sliding surface rapidly. A small σ slows down the sliding speed with the risk of not reaching the stable point. However, if σ is too larger, the chattering increases.

Remark 4: The absolute value of acceleration of the vehicles in the platoon is limited to $1\ m/s^2$. If vehicles are not accelerated abruptly, it can not only improve safety, but also reduce wear on brake pads. However, it compromises controller's performance to some extent since the sliding range of the control input is limited.

Table 4.1 Asymmetric sliding mode controller's parameters

Symbol	Description	Unit	Value
ϵ	Chattering reduction parameter	-	5
σ	Sliding speed parameter	-	10
ς	Sliding surface's parameter	-	0.50

4.2.4 NSGA-II Based Homogeneous Asymmetric Degree Optimisation

Several studies have acknowledged the significance of introducing the asymmetric degree in the topological matrix. It is essential for complex control problems with large-size dynamic platoons. However, previous research selected the asymmetric degree randomly without any optimisation objectives. Furthermore, it is known that the minimum eigenvalue of the topological matrix is invariant to the change of basis. Therefore, introducing the asymmetric degree changes various topological matrix elements depending on the type of topology. Therefore, it is impossible to find the optimal asymmetric degree based on traditional methods since there is no linear mathematical model and regularity between the asymmetric degree and the resulting topological matrix eigenvalue. Thus, the problems of searching for the optimal asymmetric degree cannot use any heuristic solutions.

Thus, an evolutionary algorithm-based approach is proposed to solve this issue. As a metaheuristic method, the evolutionary algorithm has been famous for solving complex problems that cannot use heuristic solutions. The primary principle of the evolutionary algorithm is that only the fittest individual survives. Besides, evolutionary algorithms have many advantages, including flexibility, robustness, and human expertise independence.

NSGA-II is employed in this research to optimise the platoon's overall performance by selecting an optimal homogeneous asymmetric degree. Tracking index, acceleration standard deviation and fuel consumption are the three optimisation objectives in NSGA-II. They are defined the same as in Chapter 3 (3.5-3.9). The critical point of applying NSGA-II to the method is to search for the optimal homogeneous asymmetric degree. Then the asymmetric degree will be applied to the topological matrix. Thus, a new minimum eigenvalue of the matrix can be obtained. Based on the eigenvalue, the controller's gains can be solved using Riccati inequality. Therefore, the new control input and the resulting platoon performance indices can be obtained. The optimal information flow topology can be found after the evolutionary process to satisfy multiple objectives.

4.2.5 Simulation Result

The hardware setup is the same as in chapter 3. A platoon with eleven heterogeneous vehicles (one leader and ten followers) interconnected by asymmetric topologies is considered in the simulation. To show the superiority of the proposed method, a conventional sliding mode control method proposed in [87] is tested first. Then the proposed multi-objective asymmetric sliding mode control method is tested second.

This section considers two traffic scenarios. The first one is the urban road scenario, as most people drive on urban roads on a daily basis. According to Australia's velocity requirements on an urban road. Vehicle's maximum speed should be within 14 m/s. The desired gap between two consecutive vehicles should be $20m$. To emphasis the environmental disturbance the leader vehicle experiences, a sine wave is added to its acceleration profile. The kinematic model for the leader vehicle on urban road is described as:

$$a_0(t) = \begin{cases} 0 & 0 < t \leq 20s \\ 0.5 + 0.5\sin\left(\frac{\pi}{10}t\right) m/s & 20 < t \leq 30s \\ 0 & 30 < t \leq 50s \\ -0.5 + 0.5\sin\left(\frac{\pi}{10}t\right) m/s & 50 < t \leq 60s \\ 0 & 60 < t \leq 100s \end{cases}$$

(4.57)

Each vehicle's initial position, velocity, and the desired distance between itself and the leader vehicle are presented in Table 4.2. An information feedback delay of 0.1s [97] is applied to all vehicles in the platoon. Different external disturbances with different magnitude are applied to the following vehicles in the platoon:

$$w_i(t) = \delta\sin\left(\frac{\pi}{10}t\right)$$

(4.58)

where $0.1 \leq \delta \leq 0.7$.

Table 4.2 Initial states and desired gaps of each vehicle under urban road scenario

Vehicle	Position (m)	Velocity (m/s)	Desired gap (m)
Leader	0	4	0
Vehicle 1	-20	3	-20
Vehicle 2	-49	5	-40
Vehicle 3	-61	3.5	-60
Vehicle 4	-78	4.2	-80
Vehicle 5	-102	3.8	-100
Vehicle 6	-123	4.4	-120
Vehicle 7	-137	4.1	-140
Vehicle 8	-161	3.7	-160
Vehicle 9	-182	4.2	-180
Vehicle 10	-201	3.2	-200

The second scenario this section considers is the highway scenario, as platooning control is essential to releasing traffic congestion, especially on the highway. Referring to Australia's velocity requirements on the highway. Vehicle's maximum speed should be within $28m/s$. The desired gap between two consecutive vehicles should be $50m$ to ensure safety. The leader vehicle also experiences an amplified environmental disturbance due to the high speed. The kinematic model for the leader vehicle on highway is described as:

$$a_0(t) = \begin{cases} 0 & 0 < t \leq 20s \\ 1 + \sin\left(\frac{\pi}{10}t\right) m/s & 20 < t \leq 30s \\ 0 & 30 < t \leq 50s \\ -1 + \sin\left(\frac{\pi}{10}t\right) m/s & 50 < t \leq 60s \\ 0 & 60 < t \leq 100s \end{cases}$$

(4.59)

Each vehicle's initial position, velocity, and the desired distance between itself and the leader

vehicle are presented in Table 4.3. External disturbances and information feedback delay applied to the following vehicles are the same as in Urban Road Case Study.

Table 4.3 Initial states and desired gaps of each vehicle under highway scenario

Vehicle	Position (m)	Velocity (m/s)	Desired gap (m)
Leader	0	10	0
Vehicle 1	-51	11	-50
Vehicle 2	-99	9	-100
Vehicle 3	-152	9.5	-150
Vehicle 4	-205	8.8	-200
Vehicle 5	-251	10.6	-250
Vehicle 6	-297	11.5	-300
Vehicle 7	-345	11.3	-350
Vehicle 8	-402	10.8	-400
Vehicle 9	-449	9.3	-450
Vehicle 10	-497	9.1	-500

This section considers three traditional topologies and one random topology in each case study to investigate the impact of wireless communication and fully validate the proposed strategy's effectiveness. The three traditional topologies are two predecessors single following topology (TPSF), Predecessor-leader following topology (PLF) and Bidirectional-leader topology (BDL). They are shown in Figure 4.1 below:

(a) (b) (c)

Figure 4.1 Information flow topologies for the platoon. (a) TPSF; (b) PLF; (c) BDL

One random topology is also included in this section to prove the effectiveness of the proposed method. Random topology can be common in reality due to unstable wireless communication. This section uses the Bernoulli distribution to express the packet drop rate to consider packet loss. The packet loss probability increases when the distance between two vehicles increases. Therefore, a random topology can be obtained.

Figure 4.2 shows the platoon's spacing error when using the sliding mode control strategy [87] versus the proposed asymmetric control strategy under TPSF topology in the Urban Road Case Study. The figure shows that the traditional method is subject to information feedback delays and external disturbances, resulting in an inability to reach a consensus at the end. The proposed method can significantly reduce spacing error while reaching a consensus.

The most dramatic changes occurred in TPSF topology scenarios in both case studies. With the conventional control method, spacing errors fluctuated between -5m and 5m, but were reduced to within 0.1m with the proposed strategy. Moreover, PLF and BDL topologies perform the best. The spacing errors started at around 2m and were reduced to near zero with the proposed strategy.

Platoons performed better on highways than on urban roads, demonstrating the efficacy of the proposed method as the desired velocity and gap between vehicles increased. Overall, the proposed strategy reduces all spacing errors to less than $0.2m$, a reasonable threshold for ensuring consensus and stability. It can be concluded that the proposed strategy can reduce the platoon's spacing error significantly.

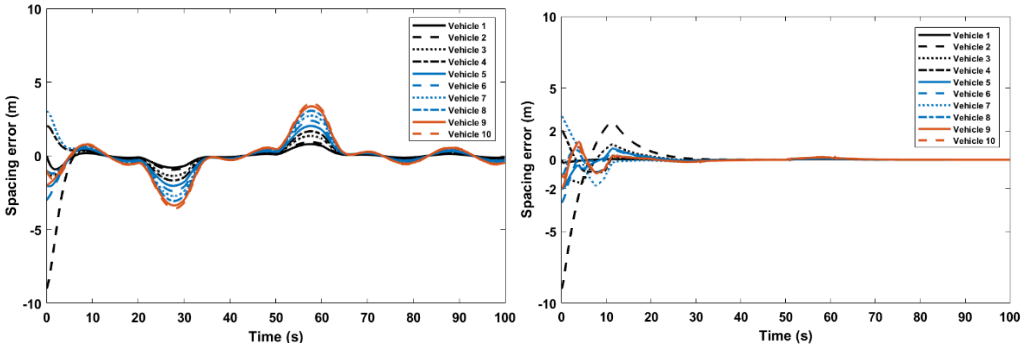

(a) Conventional (b) Asymmetric

Figure 4.2 Spacing error under Urban road Case Study with TPSF topology. (a) Conventional; (b) Asymmetric

Figure 4.3 illustrates the platoon's velocity under PLF topology for the Highway Case Study. The figure shows that the conventional method produces a more smooth velocity profile. However, it is still largely influenced by information feedback delays and external disturbances, resulting in a slight fluctuation from $t = 70s$. Nevertheless, the proposed method can guarantee convergence and reach a consensus much more quickly than the conventional method.

In both case studies, the proposed strategy significantly affects the TPSF and Random topologies, while the PLF topology outperforms the others. Although velocity errors are significantly reduced under all topologies in both cases, velocity errors were reduced to within 0.1 m/s, demonstrating that the proposed strategy can ensure the platoon's velocity consensus.

However, the velocity error fluctuates more significantly in the first four seconds under the proposed method compared to the conventional method. In addition, when the leader vehicle accelerates or decelerates, there are some jerks. The shortcomings listed above reflect the trade-off between control accuracy and chattering. Therefore, some measurements should be implemented in the future to eliminate the velocity error in the first few seconds.

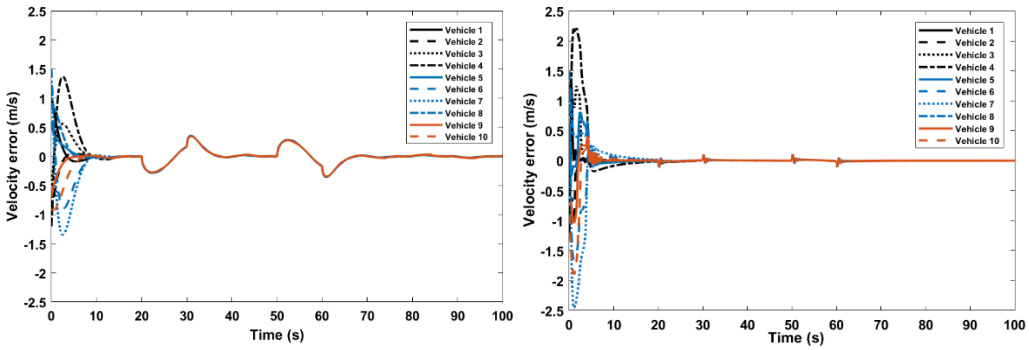

(a) Conventional (b) Asymmetric

Figure 4.3 Velocity error under Highway Case Study with PLF topology. (a) Conventional; (b) Asymmetric

Table 4.4 displays the obtained Pareto asymmetric degree and the resulting controller's gains under all topologies in the Urban Road and Highway Case Studies, respectively. As can be seen, the Pareto optimal homogeneous asymmetric degree varies between 89 and 96% depending on the road and topology scenarios considered. However, there is a clear consistency between the type of topology and the obtained Pareto optimal asymmetric degree.

Table 4.4 Controller's gains for different information flow topologies under both scenarios

Information flow topology	Scenario	Homogeneous Pareto asymmetric degree (%)	k_1	k_2	k_3
TPSF	Urban Road	96.0887	7.367	43.319	13.884
	Highway	96.4191	7.367	43.313	13.872
PLF	Urban Road	94	7.370	43.362	13.964
	Highway	94.7595	7.369	43.345	13.932
BDL	Urban Road	93.4403	7.371	43.378	13.990
	Highway	92.9496	7.474	43.917	14.326
Random	Urban Road	89.9333	7.514	44.299	14.874
	Highway	89.9524	7.514	44.298	14.873

Figure 4.4 illustrates the obtained Pareto front under BDL and Random topology in the Highway Case Study using the proposed strategy. The similarity between them is marginal, implying that there are no linear relationships between the asymmetric degree and the platoon's three primary performance indices, as the Pareto front varies according to the road and topology scenario. Additionally, it proved that while the optimal asymmetric degree cannot be obtained using a traditional mathematical formula, NSGA-II is well suited for this control problem.

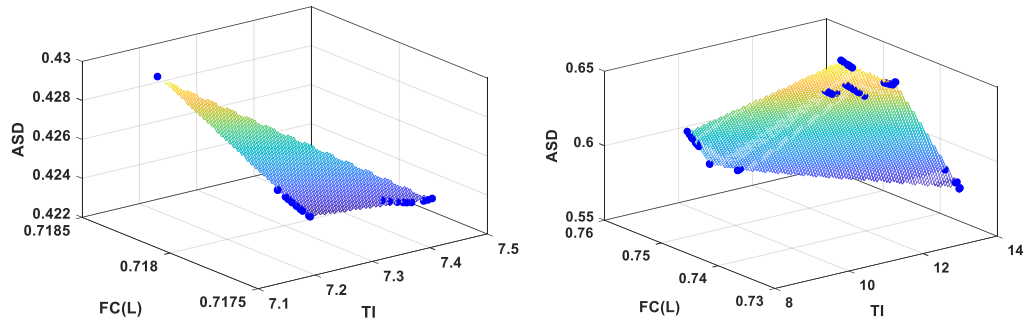

(a) (b)

Figure 4.4 Pareto front with asymmetric control under Urban Road Study. (a) BDL; (b) TPSF

The tracking index, fuel consumption, and acceleration standard deviation are the three performance evaluation criteria considered. These criteria reflect a platoon's ability to track, fuel economy, and driving comfort. As a result, they are used to conduct a systematic and comprehensive evaluation of a platoon's performance.

The tracking index indicates a vehicle's ability to track its preceding vehicles in the platoon. Because it is formulated in terms of spacing and velocity errors, the smaller the tracking index, the better the tracking ability. The tracking index for four different topologies under the Urban Road Case Study is shown in Table 4.5, using Vehicles 1, 5, 10, and the platoon as examples. The

platoon's tracking index increased by an average of 54.61% with the asymmetric control. The proposed method has the most significant effect on the TPSF topology, increasing its tracking index by 72.16% while only increasing the tracking index of the BDL topology by 44.07%. The tracking index for the Highway Case Study is also shown in Table 4.6. The platoon's tracking index increased by an average of 75.17% with asymmetric control. Compared to the Urban Road Case Study, the proposed method increased the tracking ability of TPSF and PLF topologies by 84.86% and 71.27%, respectively. Therefore, the proposed strategy is more effective in dealing with platoons travelling at a relatively high velocity and requiring large inter-vehicle gaps.

Table 4.5 Tracking index for different information flow topologies under urban road scenario

Information flow topology	Control Strategy	Vehicle 1	Vehicle 5	Vehicle 10	Platoon Overall
TPSF	Conventional	1.282	3.101	5.036	33.42
	Asymmetric	**0.1182**	**0.738**	**0.7785**	**9.305**
PLF	Conventional	1.084	1.237	1.181	13.01
	Asymmetric	**0.08572**	**0.5253**	**0.2106**	**7.096**
BDL	Conventional	1.083	1.225	1.189	13.01
	Asymmetric	**0.1476**	**0.521**	**0.2094**	**7.276**
Random	Conventional	1.713	2.175	2.2	21.23
	Asymmetric	**0.2018**	**0.6782**	**0.6813**	**9.182**

Table 4.6 Tracking index for different information flow topologies under highway scenario

Information flow topology	Control Strategy	Vehicle 1	Vehicle 5	Vehicle 10	Platoon Overall
TPSF	Conventional	1.951	4.788	8.587	54.47
	Asymmetric	**0.1757**	**0.4784**	**1.184**	**8.247**
PLF	Conventional	1.619	1.3	1.856	19.11
	Asymmetric	**0.177**	**0.4094**	**0.5376**	**5.491**
BDL	Conventional	1.635	1.627	1.864	19.41
	Asymmetric	**0.1761**	**0.4139**	**0.537**	**5.52**
Random	Conventional	3.054	3.561	3.982	36.56
	Asymmetric	**0.2645**	**0.4718**	**1.183**	**9.88**

Fuel economy is also a significant platoon property, quantified in fuel consumption: the less fuel consumed, the more efficient the vehicle. The fuel consumption for different topologies under the Urban Road and Highway Case Study is shown in Tables 4.7 and 4.8. It can be seen from the tables that almost all vehicles' fuel consumption decreased, and the platoon consumed more fuel on the highway compared to the urban road in general. At the same time, changes in fuel consumption are less sensitive to changes in the control strategy. The fuel economy increased by

an average 0.78% and 6.34% under the Urban Road and Highway Case Study, respectively. In conclusion, the proposed method can improve the platoon's fuel economy, especially on highways. Additionally, the proposed method has the most excellent effect on the fuel efficiency of the TPSF topology. It is improved by 0.92% and 16.54% under the Urban Road and Highway Case Study, respectively.

Table 4.7 Fuel consumption for different information flow topologies under urban road scenario

Information flow topology	Control Strategy	Vehicle 1	Vehicle 5	Vehicle 10	Platoon Overall
TPSF	Conventional	0.06432	0.06755	0.07825	0.7608
	Asymmetric	**0.0644**	**0.06748**	**0.07822**	**0.7539**
PLF	Conventional	0.06428	0.06697	0.06613	0.7252
	Asymmetric	**0.06452**	**0.06617**	**0.06605**	**0.7188**
BDL	Conventional	0.06439	0.06698	0.06613	0.7252
	Asymmetric	**0.06432**	**0.06612**	**0.06589**	**0.7179**
Random	Conventional	0.06443	0.06631	0.06543	0.7177
	Asymmetric	**0.06429**	**0.06606**	**0.06521**	**0.7157**

Table 4.8 Fuel consumption for different information flow topologies under highway scenario

Information flow topology	Control Strategy	Vehicle 1	Vehicle 5	Vehicle 10	Platoon Overall
TPSF	Conventional	0.1078	0.1414	0.2334	1.628
	Asymmetric	**0.1091**	**0.1407**	**0.1365**	**1.397**
PLF	Conventional	0.1087	0.1326	0.1202	1.321
	Asymmetric	**0.1079**	**0.1318**	**0.1203**	**1.321**
BDL	Conventional	0.1087	0.1325	0.1201	1.323
	Asymmetric	**0.1078**	**0.1317**	**0.1202**	**1.320**
Random	Conventional	0.1102	0.1365	0.1236	1.347
	Asymmetric	**0.1076**	**0.1318**	**0.1196**	**1.317**

The acceleration standard deviation (ASD) is used to quantify the platoon's driving comfort, indicating the profile's smoothness. Smooth and comfortable driving has long been regarded as a critical feature of the intelligent vehicle system: the smaller the ASD, the more comfortable driving. The ASD for four different topologies under the Urban Road and Highway Case Study are presented in Table 4.9 and Table 4.10. Driving comfort is not improved in both case studies. Figures 4.2 and 4.3 show that the traditional controller creates smooth and slow changes in both spacing and velocity profiles, whereas the proposed controller causes more abrupt changes. There is an unavoidable trade-off between the platoon's convergence speed and driving comfort. The proposed method ensures convergence and increases platoon convergence speed at the expense of

a certain amount of driving comfort. The trade-off is worth investigating, and future research should focus on improving platoon convergence without sacrificing driving comfort.

Table 4.9 Acceleration standard deviation for different information flow topologies under urban road scenario

Information flow topology	Control Strategy	Vehicle 1	Vehicle 5	Vehicle 10	Platoon Overall
TPSF	Conventional	0.3880	0.3970	0.4197	0.4035
	Asymmetric	**0.4272**	**0.4810**	**1.0457**	**0.6111**
PLF	Conventional	0.3864	0.3837	0.3880	0.3866
	Asymmetric	**0.4514**	**0.4090**	**0.4858**	**0.4338**
BDL	Conventional	0.3871	0.3839	0.3878	0.3867
	Asymmetric	**0.4099**	**0.4052**	**0.4763**	**0.4237**
Random	Conventional	0.3928	0.3922	0.3973	0.3949
	Asymmetric	**0.4044**	**0.3950**	**0.3974**	**0.3974**

Table 4.10 Acceleration standard deviation for different information flow topologies under highway scenario

Information flow topology	Control Strategy	Vehicle 1	Vehicle 5	Vehicle 10	Platoon Overall
TPSF	Conventional	0.7642	0.7944	0.8393	0.8080
	Asymmetric	**0.7808**	**0.8560**	**1.4990**	**1.0183**
PLF	Conventional	0.7616	0.7603	0.7600	0.7686
	Asymmetric	**0.7808**	**0.7804**	**0.7856**	**0.8091**
BDL	Conventional	0.7614	0.7595	0.7599	0.7682
	Asymmetric	**0.7794**	**0.7790**	**0.7843**	**0.8074**
Random	Conventional	0.7724	0.7767	0.7789	0.7836
	Asymmetric	**0.7667**	**0.7682**	**0.7639**	**0.7852**

4.3 Heterogeneous Optimal Asymmetric Topology with Nonlinear Model

This section proposes a multi-objective heterogeneous asymmetric sliding mode control strategy. Firstly, a nonlinear vehicle dynamic model is considered. Then, a sliding mode controller is designed to achieve consensus. Moreover, Riccati inequality and Lyapunov analysis are used to find the controller's gains and guarantee the platoon's Lyapunov stability and string stability. Finally, NSGA-II is used to find the Pareto optimal heterogeneous asymmetric degrees regarding the overall performance of the platoon, including tracking index, fuel consumption and acceleration standard deviation.

The vehicle dynamic model of the leader is the same as (3.1) in Chapter 3. A third-order

nonlinear model is used to express the dynamic properties of vehicle i, it is the same as (2.6) in Chapter 2. It can be further expressed as:

$$\dot{a}_i(t) = -\frac{a_i(t)}{\tau_i} + \frac{u_i(t)}{m_i\tau_i} - \theta^T\omega \tag{4.60}$$

where

$$\theta = \begin{bmatrix} \frac{2K_{di}}{m_i} \\ \frac{K_{di}}{m_i\tau_i} \\ \frac{d_{mi}}{m_i\tau_i} \end{bmatrix}, \omega = \begin{bmatrix} v_i(t)a_i(t) \\ v_i(t)^2 \\ 1 \end{bmatrix}$$

Heterogeneous vehicle dynamic parameters referred to Table 3.1.

4.3.1 Sliding Mode Controller Design

Referring to [9], heterogeneous asymmetric degrees ε_i are introduced in the system. The Heterogeneous asymmetric degrees model is based on Section 4.2.2, where heterogeneous asymmetric degrees ε_i are used instead of homogenous asymmetric degree ε. The rest of the definitions are the same as in Section 4.2.2

The sliding mode controller is proposed in this section as follows; the sliding surface is selected to monitor the tracking errors:

$$\begin{aligned} s_i(t) = a_i(t) &+ (1+\varepsilon_i)k_1 \sum_{j\epsilon\Pi_{i_1}} p_i(t) - p_j(t) - d_{ij} + (1-\varepsilon_i)k_1 \sum_{j\epsilon\Pi_{i_2}} p_i(t) - p_j(t) - d_{ij} \\ &+(1+\varepsilon_i)k_2 \sum_{j\epsilon\Pi_{i_1}} v_i(t) - v_j(t) + (1-\varepsilon_i)k_2 \sum_{j\epsilon\Pi_{i_2}} v_i(t) - v_j(t) \end{aligned} \tag{4.61}$$

where $k_1, k_2 > 0$, and they are controller's gain, $\Pi_{i_1}$and Π_{i_2} are complete topology information sets of node i stated before. d_{ij} is the desired spacing between vehicle i and vehicle j, a predefined nonzero constant. Considering the convergence of the spacing error and velocity error, the exponential reaching law is selected to be:

$$\dot{s}_i(t) = -\gamma s_i(t) \tag{4.62}$$

where $\gamma > 0$, and it is the sliding parameter, it determines the convergence speed of the sliding surface. Taking the time derivative of $s_i(t)$ described in (4.61), then $\dot{s}_i(t)$ can be obtained as:

$$\begin{aligned} \dot{s}_i(t) = \dot{a}_i(t) &+ (1+\varepsilon_i)k_1 \sum_{j\epsilon\Pi_{i_1}} v_i(t) - v_j(t) + (1-\varepsilon_i)k_1 \sum_{j\epsilon\Pi_{i_2}} v_i(t) - v_j(t) \\ &+(1+\varepsilon_i)k_2 \sum_{j\epsilon\Pi_{i_1}} a_i(t) - a_j(t) + (1-\varepsilon_i)k_2 \sum_{j\epsilon\Pi_{i_2}} a_i(t) - a_j(t) \end{aligned} \tag{4.63}$$

Therefore $\dot{a}_i(t)$ can be rewritten as:

$$\dot{a}_i(t) = -\gamma s_i(t) - (1+\varepsilon_i)k_1 \sum_{j\epsilon\Pi_{i_1}} v_i(t) - v_j(t) - (1-\varepsilon_i)k_1 \sum_{j\epsilon\Pi_{i_2}} v_i(t) - v_j(t)$$
$$-(1+\varepsilon_i)k_2 \sum_{j\epsilon\Pi_{i_1}} a_i(t) - a_j(t) \; - (1-\varepsilon_i)k_2 \sum_{j\epsilon\Pi_{i_2}} a_i(t) - a_j(t)$$

(4.64)

Combining (4.60), (4.61) and (4.64), the equivalent control input $u_i(t)$ can be obtained:

$$u_i(t) = m_i\tau_i[-\gamma s_i(t) - (1+\varepsilon_i)k_1 \sum_{j\epsilon\Pi_{i_1}} v_i(t) - v_j(t) - (1-\varepsilon_i)k_1 \sum_{j\epsilon\Pi_{i_2}} v_i(t) - v_j(t)$$
$$-(1+\varepsilon_i)k_2 \sum_{j\epsilon\Pi_{i_1}} a_i(t) - a_j(t) - (1-\varepsilon_i)k_2 \sum_{j\epsilon\Pi_{i_2}} a_i(t) - a_j(t) + \hat{\theta}^T\omega] + m_i a_i(t)$$

(4.65)

Define $K = [k_1 \; k_2]$. $\hat{\theta}$ is the estimated value of θ. Considering the fact the vehicle's parameters can be hard to obtain in reality. $\hat{\theta}$ is used for estimation, it refers to the nominal values in θ . $\hat{\theta}$ creates parameter mismatches, which adds practical value to this section.

Theorem 4.3: When the control law in (4.65) is implemented to the vehicle dynamics in (4.60), the sliding surface satisfies with the Lyapunov stability, the stability of the platoon can be guaranteed, and the tracking error converges to zero asymptotically.

Proof: The Lyapunov function candidate is selected to be:

$$V_i(t) = \frac{1}{2}s_i(t)^2$$

(4.66)

The time derivative of the Lyapunov function can be described as:

$$\dot{V}_i(t) = s_i(t)\dot{s}_i(t)$$

(4.67)

Based on (4.61), (4.62) and (4.63), $\dot{V}_i(t)$ can be obtained as:

$$\dot{V}_i(t) = s_i(t)\dot{s}_i(t)$$
$$= [-\frac{a_i(t)}{\tau_i} + \frac{u_i(t)}{m_i\tau_i} - \hat{\theta}^T\omega + (1+\varepsilon_i)k_1 \sum_{j\epsilon\Pi_{i_1}} v_i(t) - v_j(t) + (1-\varepsilon_i)k_1 \sum_{j\epsilon\Pi_{i_2}} v_i(t) - v_j(t)$$
$$+(1+\varepsilon_i)k_2 \sum_{j\epsilon\Pi_{i_1}} a_i(t) - a_j(t) + (1-\varepsilon_i)k_2 \sum_{j\epsilon\Pi_{i_2}} a_i(t) - a_j(t)] \; [a_i(t) + (1+\varepsilon_i)k_1$$
$$\sum_{j\epsilon\Pi_{i_1}} p_i(t) - p_j(t) - d_{ij} + (1-\varepsilon_i)k_1 \sum_{j\epsilon\Pi_{i_2}} p_i(t) - p_j(t) - d_{ij} + (1+\varepsilon_i)k_2$$
$$\sum_{j\epsilon\Pi_{i_1}} v_i(t) - v_j(t) + (1-\varepsilon_i)k_2 \sum_{j\epsilon\Pi_{i_2}} v_i(t) - v_j(t)]$$
$$= -\gamma s_i(t)^2$$

(4.68)

Since $\gamma > 0$, $\dot{V}_i(t)$ is a negative definite. Thus $u_i(t)$ will satisfy the approaching and sliding condition $s_i(t)\dot{s}_i(t) < 0$, which guarantees that the trajectory reaches the sliding mode in a finite

time and stay there after, therefore the condition for Lyapunov stability is satisfied. The proof of *Theorem 4.3* is completed.

This section then implements the Riccati inequality and Lyapunov analysis to solve the controllers' gain, after which the closed-loop error dynamic is analysed and the system is proved to be string stable.

The closed-loop error is defined as $E^T = [e_1(t)^T \dots e_N(t)^T]$, $e_i(t) = [\Delta p_i(t) \quad \Delta v_i(t)]^T$.

$$\Delta p_i(t) = p_i(t) - p_0(t) - d_{i0},$$
$$\Delta v_i(t) = v_i(t) - v_0(t) \tag{4.69}$$

The closed-loop error dynamic is:

$$\dot{E} = (I_N \otimes A)E + (I_N \otimes B)Y \tag{4.70}$$

where

$$Y = \begin{bmatrix} a_1(t) - a_0(t) \\ \cdots \\ a_N(t) - a_0(t) \end{bmatrix}, A = \begin{bmatrix} 0 & 1 \\ 0 & 0 \end{bmatrix}, B = \begin{bmatrix} 0 \\ 1 \end{bmatrix}.$$

After the platoon dynamics reach the sliding surface, combining $s_i(t) = 0$ into (4.64), $a_i(t)$ can be rewritten as:

$$a_i(t) = -(1+\varepsilon_i)k_1 \sum_{j \epsilon \Pi_{i_1}} p_i(t) - p_j(t) - d_{ij} - (1-\varepsilon_i)k_1 \sum_{j \epsilon \Pi_{i_2}} p_i(t) - p_j(t) - d_{ij}$$
$$-(1+\varepsilon_i)k_2 \sum_{j \epsilon \Pi_{i_1}} v_i(t) - v_j(t) - (1-\varepsilon_i)k_2 \sum_{j \epsilon \Pi_{i_2}} v_i(t) - v_j(t) \tag{4.71}$$

It yields that:

$$Y + (H_\varepsilon \otimes K)E = -1_N a_0(t) \tag{4.72}$$

where $1_N \in \mathbb{R}^N$, it is the vector with entries that are all one. Substituting (72) into (70), the sliding dynamics of the platoon is:

$$\dot{E} = [I_N \otimes A - H_\varepsilon \otimes (BK)]E - (1_N \otimes B)a_0(t) \tag{4.73}$$

where $a_0(t)$ is bounded, therefore can be treated as equivalent external disturbance ϖ. A maximum bound for $\varpi^T \varpi$ can be easily found. $\dot{E}$ can be written as:

$$\dot{E} = [I_N \otimes A - H_\varepsilon \otimes (BK)]E - (1_N \otimes B)\varpi \tag{4.74}$$

According to *Definition* 4.1 (4.48), *Lemma* 4.3 (4.50) in Section 4.3, and *Lemma* 4.2, the Lyapunov function is selected to be:

$$V = E^T(Q \otimes \bar{P})E > 0 \tag{4.75}$$

where $\bar{P} = P^{-1}$. According to the LMI-based method proposed in [93], the following theory can convert the problem into a standard LMI problem:

Theorem 4.4: Consider the platoon in (4.60) if there exist matrices $P^T = P > 0 \in \mathbb{R}^{2x2}$ and $Q^T = Q > 0 \in \mathbb{R}^{2x2}$ such that (4.77-4.78) hold.

$$\begin{bmatrix} AP + PA^T + \left(1 - \frac{\lambda_{min}(H_\varepsilon)}{2}\right) BB^T & P \\ P & -\frac{1}{\rho} \end{bmatrix} < 0$$

(4.76)

$$H_\varepsilon{}^T Q + QH_\varepsilon - 2\lambda_{min}(H_\varepsilon) Q > 0$$

(4.77)

where $\lambda_{min}(H_\varepsilon)$ is the minimum eigenvalue of the topological matrix defined in previous chapter, scalar $\rho > 0$. Then with the feedback gain K as defined as (4.78), the platoon is input-to-output $\mathcal{L}_2$ string stable for all nonzero $\varpi(t)$.

$$K = \frac{1}{2} B^T P^{-1}$$

(4.78)

The disturbance propagation of the platoon can be described by (4.79):

$$sup \frac{\| E \|_{\mathcal{L}_2}}{\| \varpi \|_{\mathcal{L}_2}} < \sqrt{\frac{\lambda_{max}(Q)}{\rho \lambda_{min}(Q)}}$$

(4.79)

Proof:

Taking the time derivative of V

$\dot{V} = \dot{E}^T (Q \otimes \bar{P}) E + E^T (Q \otimes \bar{P}) \dot{E}$

$= E^T [Q \otimes (A^T \bar{P}) - (H_\varepsilon{}^T Q) \otimes (BK)^T \bar{P} + Q \otimes (\bar{P} A) - (QH_\varepsilon) \otimes (\bar{P} BK)] E + \varpi^T [Q \otimes (B^T \bar{P})] E + E^T [Q \otimes (\bar{P} B)] \varpi$

(4.80)

Substitutes (4.78) into (4.80), $\dot{V}$ be rewritten as:

$$\dot{V} = -E^T [(H_\varepsilon{}^T Q) \otimes (\frac{1}{2} \bar{P} BB^T \bar{P}) + (QH_\varepsilon) \otimes (\frac{1}{2} \bar{P} BB^T \bar{P})] E + E^T [Q \otimes (A^T \bar{P}) + Q \otimes (\bar{P} A)] E + \varpi^T [Q \otimes (B^T \bar{P})] E + E^T [Q \otimes (\bar{P} B)] \varpi$$

(4.81)

It can be obtained that:

$$\varpi^T [Q \otimes (B^T \bar{P})] E + E^T [Q \otimes (\bar{P} B)] \varpi \leq E^T [Q \otimes (\bar{P} BB^T \bar{P})] E + \lambda_{max}(Q) \varpi^T \varpi$$

(4.82)

To prove (4.82) holds, it can be transformed into:

$$\begin{bmatrix} E \\ \varpi \end{bmatrix}^T \begin{bmatrix} Q \otimes (\bar{P} BB^T \bar{P}) & -Q \otimes (\bar{P} B) \\ -Q \otimes (B^T \bar{P}) & \lambda_{max}(Q) \end{bmatrix} \begin{bmatrix} E \\ \varpi \end{bmatrix} \geq 0$$

(4.83)

Using Schur complement, (4.83) is equivalent to:

$$(Q^{-1} - \frac{1}{\lambda_{max}(Q)} I_N) \otimes (\bar{P} BB^T \bar{P}) \geq 0$$

(4.84)

Given that $\lambda(Q^{-1}) = \frac{1}{\lambda(Q)}$, (4.84) holds, therefore, (4.82) holds. substituting (4.82) into (4.81), $\dot{V}$ is rewritten as:

$$\dot{V} = -E^T[({H_\varepsilon}^T Q)\otimes(\frac{1}{2}\bar{P}BB^T\bar{P}) + (QH_\varepsilon)\otimes(\frac{1}{2}\bar{P}BB^T\bar{P})]E + E^T[Q\otimes(A^T\bar{P}) + Q\otimes(\bar{P}A)]E + E^T[Q\otimes(\bar{P}BB^T\bar{P})]E + \lambda_{max}(Q)\varpi^T\varpi$$

(4.85)

For the first two terms in (4.85), given inequality (4.77), the following inequality holds:

$$E^T[-({H_\varepsilon}^T Q)\otimes(\frac{1}{2}\bar{P}BB^T\bar{P}) - (QH_\varepsilon)\otimes(\frac{1}{2}\bar{P}BB^T\bar{P}) + Q\otimes(A^T\bar{P}) + Q\otimes(\bar{P}A)]\ E$$
$$< -E^T\left[\left(QH_\varepsilon + {H_\varepsilon}^T Q - Q\right)\otimes\left(\tfrac{\lambda_{min}(H_\varepsilon)}{2}\bar{P}BB^T\bar{P}\right)\right]E + E^T[Q\otimes(A^T\bar{P} + \bar{P}A - \tfrac{\lambda_{min}(H_\varepsilon)}{2}\bar{P}BB^T\bar{P})]E$$
$$< E^T[Q\otimes(A^T\bar{P} + \bar{P}A - \frac{\lambda_{min}(H_\varepsilon)}{2}\bar{P}BB^T\bar{P})]E$$

(4.87)

Then we have:

$$\rho\lambda_{min}(Q)\left[E^TE - \frac{\lambda_{max}(Q)}{\rho\lambda_{min}(Q)}\varpi^T\varpi\right] + \dot{V} \le \rho E^T(Q\otimes I)E - \lambda_{max}(Q)\varpi^T\varpi + \dot{V}$$

(4.88)

Substitute (4.86) and (4.87) into (4.88), it can be obtained that:

$$\rho\lambda_{min}(Q)\left[E^TE - \frac{\lambda_{max}(Q)}{\rho\lambda_{min}(Q)}\varpi^T\varpi\right] + \dot{V} \le E^T[Q\otimes(A^T\bar{P} + \rho I + \bar{P}A - (1 - \frac{\lambda_{min}(H_\varepsilon)}{2})\bar{P}BB^T\bar{P})]E$$

(4.89)

Given LMI (4.77), (4.89) can be transformed into:

$$\rho\lambda_{min}(Q)\left[E^TE - \frac{\lambda_{max}(Q)}{\rho\lambda_{min}(Q)}\varpi^T\varpi\right] + \dot{V} < 0$$

(4.90)

(4.90) is equivalent to：

$$\int_{t=0}^{+\infty}[E^TE - \frac{\lambda_{max}(Q)}{\rho\lambda_{min}(Q)}\varpi^T\varpi]\,dt < \frac{1}{\rho\lambda_{min}(Q)}[V|_0^{+\infty} - \int_0^{+\infty}\dot{V}dt]$$

(4.91)

From (4.91), it can be derived that:

$$\int_{t=0}^{+\infty}\|\ E\ \|_{\mathcal{L}_2}{}^2\,dt - \frac{\lambda_{max}(Q)}{\rho\lambda_{min}(Q)}\int_{t=0}^{+\infty}\|\ \varpi\ \|_{\mathcal{L}_2}{}^2\,dt < 0$$

(4.92)

It can be observed that:

$$\|\ E\ \|_{\mathcal{L}_2}{}^2 < \frac{\lambda_{max}(Q)}{\rho\lambda_{min}(Q)}\|\ \varpi\ \|_{\mathcal{L}_2}{}^2$$

(4.93)

Given that $a_0(t)$ is bounded and treated as equivalent external disturbance ϖ, thus a maximum

bound for $\varpi^T\varpi$ can be easily found, which is equivalent to $\max(a_0(t)^2)$. $\max(\varpi^T\varpi) = 4$. Therefore, it can be obtained that:

$$\| \varpi(t) \|_{\mathcal{L}_2} < \infty \tag{4.94}$$

Therefore, the condition for input-to-output $\mathcal{L}_2$ string is satisfied, where $\gamma = \sqrt{\frac{\lambda_{max}(Q)}{\rho\lambda_{min}(Q)}}$. The proof of *Theorem 4.4* is completed.

4.3.2 NSGA-II Based Heterogeneous Asymmetric Degree Optimisation

Given that developing mathematical models for heterogeneous asymmetric degrees and platoon performance is neither feasible nor practical, NSGA-II is a good fit for this problem because it can detect data patterns without using mathematical models. Furthermore, in terms of searching for heterogeneous asymmetric degrees for each vehicle, this control problem has many independent input variables. When the platoon size increases, so does the number of inputs. Traditional methods cannot deal with large numbers of input variables. However, NSGA-II excels in this area. Overall, NSGA-II is a good fit for the control problem.

The critical point of applying NSGA-II to the process is to find optimal heterogeneous asymmetric degrees, which are then added to the topological matrix. Thus, a new matrix's minimum eigenvalue can be obtained. Furthermore, the controller's gain can be solved using the LMI approach based on the eigenvalue. Thus, the latest control input can be obtained, as well as the corresponding platoon performance indices, they are defined the same as in Chapter 3 (3.5-3.9). The following summarises NSGA-II for computing the optimal heterogeneous asymmetric degrees.

NSGA-II

Data: input: heterogeneous asymmetric degrees ε_i. N: size of the initial population; n: number of iterations, $f_1(x)$: Tracking index; $f_2(x)$: Fuel consumption; $f_3(x)$: Acceleration standard deviation.

Initialise population:

Generate random population for ε_i

Generate new topological matrix and calculate new minimum eigenvalue

Solve LMI (4.77-4.78)

Calculate the controllers' gain using (4.79)

Calculate the control input using (4.65)

Calculate the objective values: $f_1(x)$, $f_2(x)$, $f_3(x)$

Sort the initial population with size N

Calculate the rank using $f_1(x)$, $f_2(x)$, $f_3(x)$ as objectives

Assign crowding distance to the initial population

For i=1: n

Perform selection

Create a mating pool

Perform genetic operator (Crossover and Mutation)

Combine the population

Perform selection

end

4.3.3 Simulation Results

The hardware setup is the same as in Chapter 3. Both Urban Road scenario and the Highway scenario are considered in this section. the kinematic models (4.57,4.59) for the leader vehicle are the same as in Section 4.5. However, each vehicle's initial position, velocity, and the desired distance between itself and the leader vehicle are slightly different under both scenarios, they are presented in Tables 4.11 and 4.12.

Table 4.11 Initial states and desired gaps of each vehicle under urban road scenario

Vehicle	Position (m)	Velocity (m/s)	Desired gap (m)
Leader	0	10	0
Vehicle 1	-20	3	-20
Vehicle 2	-49	5	-40
Vehicle 3	-61	3.5	-60
Vehicle 4	-78	4.2	-80
Vehicle 5	-102	3.8	-100
Vehicle 6	-123	4.4	-120
Vehicle 7	-137	4.1	-140
Vehicle 8	-161	3.7	-160
Vehicle 9	-182	4.2	-180
Vehicle 10	-202	4.1	-200

Table 4.12 Initial states and desired gaps of each vehicle under highway scenario

Vehicle	Position (m)	Velocity (m/s)	Desired gap (m)
Leader	0	10	0
Vehicle 1	-51	11	-50
Vehicle 2	-99	9	-100
Vehicle 3	-152	9.5	-150
Vehicle 4	-205	8.8	-200
Vehicle 5	-251	10.6	-250
Vehicle 6	-297	11.5	-300
Vehicle 7	-345	11.3	-350
Vehicle 8	-402	10.8	-400

Vehicle 9	-449	9.3	-450
Vehicle 10	-501	10.2	-550

To investigate the impact of wireless communication and validate the effectiveness of the proposed strategy fully, this section considers three traditional topologies (TPSF, PLF, BDL) and one random topology in each case study based on its bidirectional complexity. The random topology is shown in Figure 4.5 below.

Figure 4.5 Random information flow topologies for the platoon

Taking PLF topology as an example, Figure 4.6 shows the platoon's spacing error in the Highway Case Study. Symmetric control is used first, where the asymmetric degrees are equal to zero. In contrast, Figure 4.7 depicts the platoon's spacing error using heterogeneous asymmetric control, which is the strategy proposed in the paper. The figures illustrate that spacing errors are significantly reduced, demonstrating the effectiveness of the proposed method. On highways, all platoons performed worse than on urban roads. It can be concluded that as the desired velocity and gap between vehicles increase, the control problem becomes more difficult. The most dramatic changes in both case studies occurred in the TPSF topology scenario. Spacing errors varied between $6m$ and $11m$ with symmetric control but were reduced to within $0.1m$ with both homogeneous and heterogeneous asymmetric control strategies. Furthermore, the PLF and BDL topologies outperform the others. The proposed strategy reduces the spacing errors from around $2m$ to near zero. The differences in spacing error between homogeneous asymmetric control and heterogeneous asymmetric control are relatively small, which is difficult to see from the figures solely. However, the proposed strategy is shown to reduce all spacing errors to less than $0.1m$, which is a reasonable threshold for ensuring consensus and stability. After 60 seconds, all platoons reach a consensus. It can be concluded that the proposed strategy can significantly reduce the platoon's spacing error.

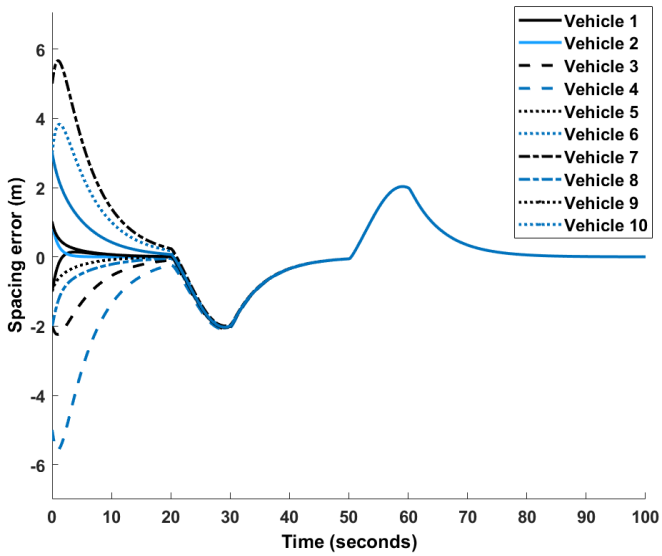

Figure 4.6 Spacing error with symmetric control under Highway Case Study with PLF topology

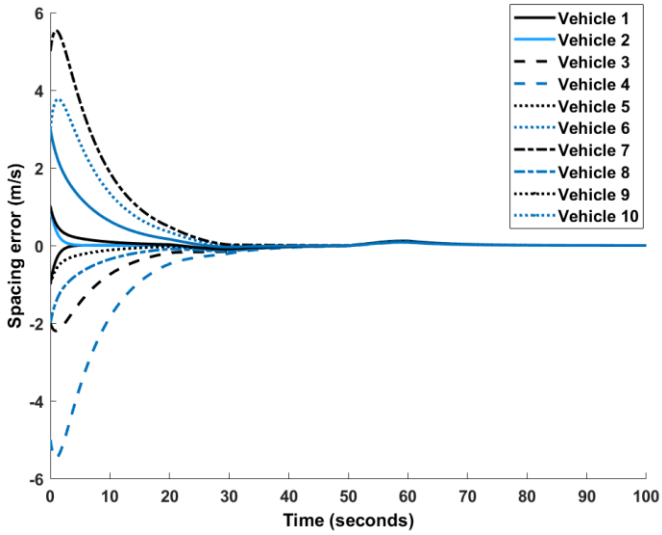

Figure 4.7 Spacing error with asymmetric control under Highway Case Study with PLF topology

Figure 4.8 depicts the platoon's velocity error for BDL topology under the Urban Road Case Study with symmetric control. The resulting velocity errors of heterogeneous asymmetric control are shown in Figure 4.9. Figures resulting from the Highway Case Study are similar. Velocity errors are significantly reduced in all cases, demonstrating the efficacy of the proposed strategy. All platoons performed better on urban roads than highways, implying that platoons' velocity consensus is more susceptible to high-velocity profiles. The proposed strategy has the most significant impact in both case studies on the TPSF and Random topology, where velocity errors were reduced to within $0.1m/s$ from $2m/s$ and $1m/s$, respectively. Moreover, BDL and PLF topology outperformed the others. The velocity error differences between homogeneous and heterogeneous asymmetric control are comparatively small. On the other hand, the proposed strategy is shown to reduce all spacing errors to less than $0.1m/s$. At 50 seconds, all platoons experienced a visible jerk in velocity errors, then achieved consensus at 60 seconds, showing that the proposed method can ensure the platoon's velocity consensus.

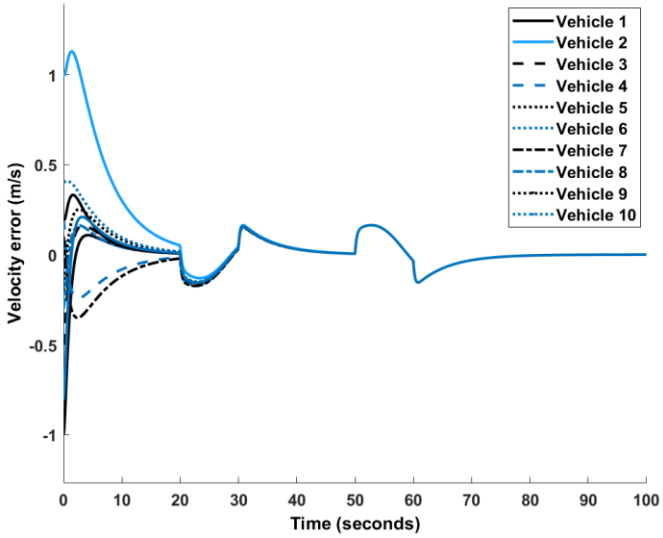

Figure 4.8 Velocity error with symmetric control under Urban Road Case Study with BDL topology

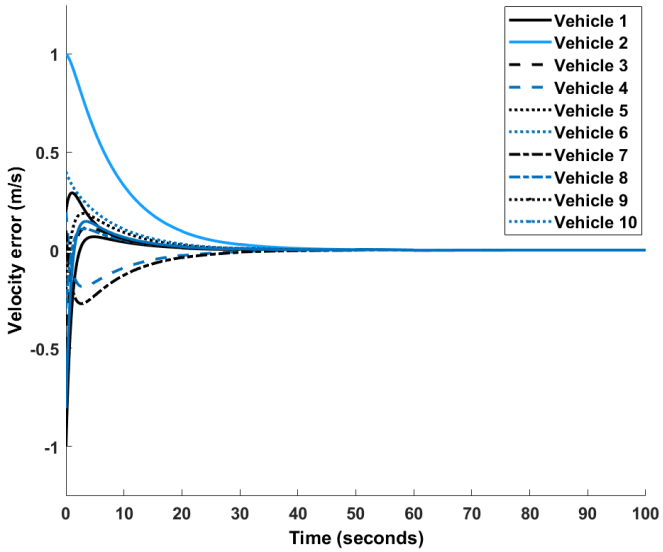

Figure 4.9 Velocity error with asymmetric control under Urban Road Case Study with BDL topology

Tables 4.13 and 4.14 display the obtained heterogeneous Pareto asymmetric degree in two case studies. For the homogeneous asymmetric control method, the Pareto optimal asymmetric degree varies between 59% and 62% for the TPSF, PLF, and BDL topology. The Pareto optimal asymmetric degree for the Random topology is about 82%. Although in both cases, all vehicles in the platoon have a different optimal asymmetric degree, no regularity is observed from the average Pareto optimal asymmetric degree. On the other hand, the controller's gains are significantly increased in all cases. With the heterogeneous asymmetric controller, the controller's gains have an average increase of 95.71% in the Urban Road Case Study and 96.16% in the Highway Case Study. Increased controller gains can significantly improve platoon performance. However, this does not imply that the higher the controller's gains, the better the platoon's performance.

Table 4.13 Heterogeneous optimal asymmetric degree for different information flow topologies under urban road scenario (%)

Vehicle Index	TPSF Topology	PLF Topology	BDL Topology	Random Topology
Vehicle 1	37.7028	4.3866	20.3393	34.4162
Vehicle 2	3.8169	12.3510	79.2367	74.5473
Vehicle 3	24.96791	61.3486	91.7491	55.2489
Vehicle 4	1.9372	36.0972	10.1663	50.1402
Vehicle 5	82.4120	30.6044	28.0382	91.4980
Vehicle 6	36.9815	73.8370	80.5722	26.4492
Vehicle 7	9.4117	30.6501	46.4649	71.1928
Vehicle 8	13.8632	57.7408	48.6109	75.8740
Vehicle 9	25.0637	44.0656	2.6883	37.4992
Vehicle 10	20.3665	28.3544	54.819	53.1265
Average	25.6523	37.9436	46.2831	56.9993

Table 4.14 Heterogeneous optimal asymmetric degree for different information flow topologies under highway scenario (%)

Vehicle Index	TPSF Topology	PLF Topology	BDL Topology	Random Topology
Vehicle 1	28.4906	4.4420	81.0039	55.2742
Vehicle 2	57.4713	13.7518	6.0768	58.6238
Vehicle 3	18.2702	46.2187	7.4281	68.8742
Vehicle 4	61.7325	86.5203	24.7905	28.6852
Vehicle 5	65.5942	30.3635	40.6708	89.7491
Vehicle 6	44.0005	26.2930	63.4554	74.4241
Vehicle 7	11.6403	7.5736	24.5636	10.9627
Vehicle 8	39.8982	5.0993	65.3486	25.7540
Vehicle 9	56.2715	54.3244	52.2687	85.9057
Vehicle 10	30.3013	78.5097	4.1552	10.3265
Average	41.3670	35.3096	36.9761	50.8580

Figure 4.10 shows the obtained Pareto fronts in the Urban Road Case Study using the proposed strategy with TPSF and Random topology. Figures resulting from the Highway Case Study are similar. Because the Pareto front varies depending on the road and topology scenario, the resemblance between graphs is negligible, implying that no linear correlations exist between the heterogeneous asymmetric degrees and the platoon's three primary performance indices. Furthermore, even though the optimal heterogeneous asymmetric degrees cannot be calculated using a traditional mathematical formula, NSGA-II is well suited to this control problem.

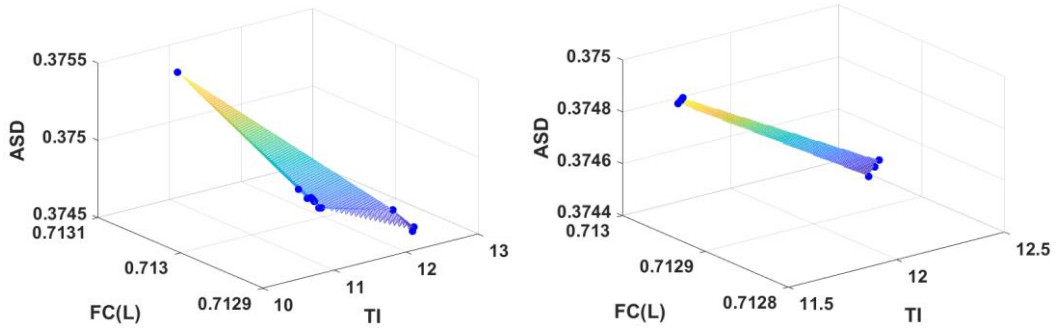

(a) (b)

Figure 4.10 Pareto front with heterogeneous asymmetric control under Urban Road Case Study. (a) TPSF; (b)Random

Tracking index, fuel consumption, and acceleration standard deviation are used to comprehensively assess the platoon's performance. The tracking index demonstrates a vehicle's ability to track the vehicles in front of it in the platoon. Since it is calculated using spacing and velocity errors, the lower the tracking index, the better the tracking ability. Table 4.15 shows the tracking index for four different topologies in the Urban Road Case Study, using Vehicles 1, 5, 10, and the platoon as examples. For homogeneous and heterogeneous asymmetric control, the platoon's tracking index improved by an average of 55.09% and 60.68%, respectively. The proposed scheme has the most considerable impact on the TPSF topology, raising its tracking index by 77.68% while only increasing the PLF topology's tracking index by 46.97%. Table 4.16 also displays the tracking index for the Highway Case Study. For homogeneous and heterogeneous asymmetric control, the platoon's tracking index improved by an average of 73.84% and 76.2%, respectively. In contrast to the Urban Road Case Study, the proposed approach improved the tracking ability of the TPSF and PLF topologies by 87.68% and 66.46%, respectively. Figure 4.11 compares the platoon's tracking index across four different topologies in both case studies to provide an intuitive view. It can be concluded that the proposed heterogeneous asymmetric control strategy outperforms the homogeneous asymmetric control strategy. The proposed approach is successful when dealing with platoons travelling at a reasonably high velocity and requiring wide inter-vehicle gaps.

Table 4.15 Tracking index for different information flow topologies under urban road scenario

Information flow topology	Control Strategy	Vehicle 1	Vehicle 5	Vehicle 10	Platoon Overall
TPSF	Symmetric	1.81	4.427	6.6901	47.71
	Homogeneous	0.4512	1.068	0.856	12.29
	Heterogeneous	**0.3872**	**0.9335**	**0.7566**	**10.65**
PLF	Symmetric	1.68	2.068	1.92	21.97
	Homogeneous	0.4986	1.155	0.9205	13.47
	Heterogeneous	**0.4827**	**1.014**	**0.8127**	**11.65**
BDL	Symmetric	1.734	2.116	1.869	22.59

	Homogeneous	0.5007	1.157	0.8956	13.4
	Heterogeneous	**0.4555**	**1.056**	**0.7543**	**12.02**
Random	Symmetric	3.211	4.136	4.158	40.4
	Homogeneous	0.4985	1.157	0.925	13.44
	Heterogeneous	**0.4549**	**1.017**	**0.8229**	**11.61**

Table 4.16 Tracking index for different information flow topologies under highway scenario

Information flow topology	Control Strategy	Vehicle 1	Vehicle 5	Vehicle 10	Platoon Overall
TPSF	Symmetric	3.065	7.632	13.28	87.4
	Homogeneous	0.1052	0.3094	1.032	11.7
	Heterogeneous	**0.1026**	**0.2839**	**0.9497**	**10.77**
PLF	Symmetric	2.673	2.753	3.314	34.11
	Homogeneous	0.0970	0.278	1.17	12.65
	Heterogeneous	**0.2365**	**0.3411**	**1.026**	**11.44**
BDL	Symmetric	2.638	2.730	3.116	34.23
	Homogeneous	0.102	0.2827	1.089	12.56
	Heterogeneous	**0.0939**	**0.2635**	**0.9765**	**11.47**
Random	Symmetric	5.863	6.949	7.871	71.8
	Homogeneous	0.1009	0.29	1.166	12.54
	Heterogeneous	**0.1868**	**0.3618**	**1.064**	**11.36**

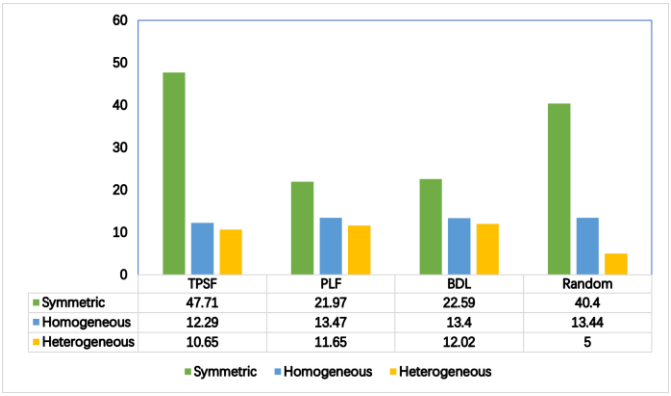

(a)

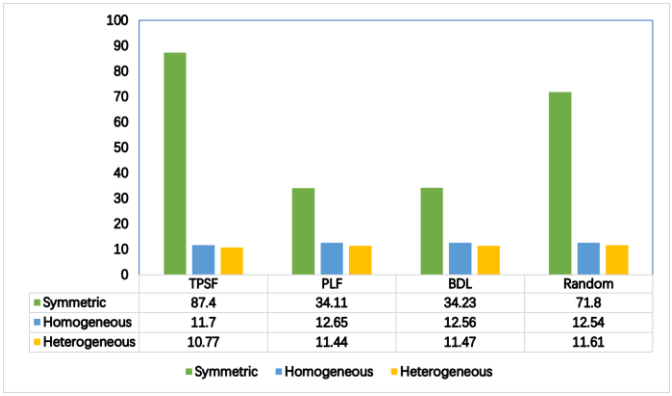

(b)

Figure 4.11 Tacking index comparison. (a) Urban Road; (b) Highway

Fuel economy is another essential platoon property measured in terms of fuel consumption. The vehicle's fuel efficiency increases as the amount of fuel used decreases. Tables 4.17 and 4.18 demonstrate the fuel consumption for various topologies in the Urban Road and Highway Case Study. The tables show that the proposed approach reduces the fuel consumption of all vehicles, and the platoon consumes more fuel on the highway than on the urban road in general. On the other hand, changes in fuel consumption are less vulnerable to control strategy changes. Fuel

economy is still improved by an average of 0.4633% and 0.4494% with the homogeneous and heterogeneous asymmetric control, respectively, in the Urban Road Case Study. Fuel economy is improved by an average of 3.5324% for all asymmetric control methods in the Highway Case Study. Figure 4.12 compares platoon fuel consumption over four different topologies in both case studies to provide a clear overview. Both asymmetric control methods boost platoon fuel economy to nearly the same extent, particularly on highways. Furthermore, the proposed approach significantly impacts the TPSF topology's fuel efficiency, improving it by 0.8619% and 6.5076% under the Urban Road and Highway Case Studies, respectively.

Table 4.17 Fuel consumption for different information flow topologies under urban road scenario (L)

Information flow topology	Control Strategy	Vehicle 1	Vehicle 5	Vehicle 10	Platoon Overall
TPSF	Symmetric	0.0643	0.0664	0.0661	0.7193
	Homogeneous	0.0642	0.0657	0.0649	0.7129
	Heterogeneous	**0.0642**	**0.0657**	**0.0650**	**0.7131**
PLF	Symmetric	0.0643	0.0659	0.0651	0.7142
	Homogeneous	0.0642	0.0657	0.0649	0.7129
	Heterogeneous	**0.0642**	**0.0657**	**0.0649**	**0.7130**
BDL	Symmetric	0.0643	0.0659	0.0651	0.7142
	Homogeneous	0.0642	0.0657	0.0649	0.7129
	Heterogeneous	**0.0642**	**0.0657**	**0.0649**	**0.7129**
Random	Symmetric	0.0644	0.0663	0.0654	0.7172
	Homogeneous	0.0642	0.0657	0.0649	0.7129
	Heterogeneous	**0.0642**	**0.0657**	**0.0649**	**0.7130**

Table 4.18 Fuel consumption for different information flow topologies under highway scenario (L)

Information flow topology	Control Strategy	Vehicle 1	Vehicle 5	Vehicle 10	Platoon Overall
TPSF	Symmetric	0.1089	0.1394	0.1342	1.383
	Homogeneous	0.1068	0.1296	0.1179	1.293
	Heterogeneous	**0.1068**	**0.1296**	**0.1179**	**1.293**
PLF	Symmetric	0.1083	0.1320	0.1198	1.313
	Homogeneous	0.1068	0.1295	0.1178	1.293
	Heterogeneous	**0.1069**	**0.1269**	**0.1179**	**1.293**
BDL	Symmetric	0.1083	0.1320	0.1197	1.313
	Homogeneous	0.1068	0.1295	0.1178	1.293

	Heterogeneous	**0.1068**	**0.1295**	**0.1178**	**1.293**
Random	Symmetric	0.1108	0.1378	0.1247	1.355
	Homogeneous	0.1068	0.1295	0.1178	1.293
	Heterogeneous	**0.1069**	**0.1296**	**0.1179**	**1.293**

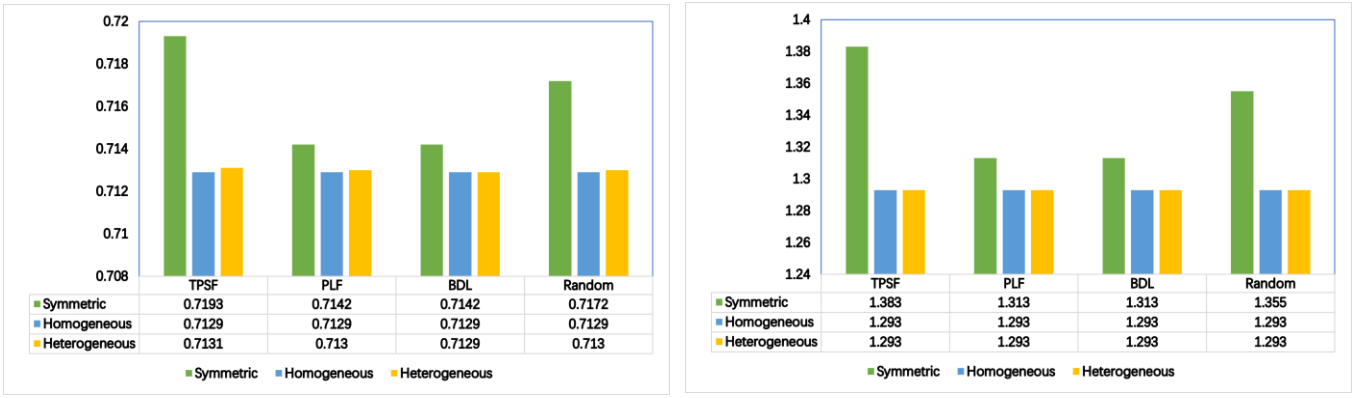

(a) (b)

Figure 4.12 Fuel consumption (L) Comparison. (a) Urban Road; (b) Highway

Because it reflects the smoothness of the profile, the acceleration standard deviation (ASD) is used to measure the platoon's driving comfort. Smooth and comfortable driving has long been recognised as an essential role of the intelligent vehicle system. The smaller the ASD, the better the driving experience. Tables 4.19 and 4.20 show the ASD for four different topologies in the Urban Road and Highway Case Study. The tables show that the suggested approach reduces the ASD of all vehicles, and the platoon has more driving comfort on the urban road than on the highway in general. Driving comfort is increased by an average of 3.6513% and 3.5237% with the homogeneous and heterogeneous asymmetric control, respectively, in the Urban Road Case Study. In the Highway Case Study, homogeneous and heterogeneous asymmetric control increase driving comfort by an average of 3.5882% and 3.5237%, respectively. Figure 4.13 shows the platoon's acceleration standard deviation over four different topologies in both case studies to present a good overview. Both asymmetric control methods enhance the platoon's driving comfort nearly the same amount, particularly on urban roads. Moreover, the proposed approach significantly impacts the TPSF topology's fuel efficiency, improving it by 6.5163% and 6.4914% under the Urban Road and Highway Case Study, respectively.

Table 4.19 Acceleration standard deviation for different information flow topologies under urban road scenario

Information flow topology	Control Strategy	Vehicle 1	Vehicle 5	Vehicle 10	Platoon Overall
TPSF	Symmetric	0.3879	0.3967	0.4236	0.4012
	Homogeneous	0.3803	0.3735	0.3791	0.3747
	Heterogeneous	**0.3808**	**0.3742**	**0.3810**	**0.3755**

PLF	Symmetric	0.3854	0.3798	0.3849	0.3808
	Homogeneous	0.3801	0.3732	0.3784	0.3744
	Heterogeneous	**0.3806**	**0.3737**	**0.3791**	**0.3748**
BDL	Symmetric	0.3860	0.3800	0.3856	0.3810
	Homogeneous	0.3801	0.3732	0.3786	0.3744
	Heterogeneous	**0.3803**	**0.3734**	**0.3796**	**0.3747**
Random	Symmetric	0.3943	0.3924	0.3981	0.3924
	Homogeneous	0.3801	0.3732	0.3784	0.3744
	Heterogeneous	**0.3806**	**0.3738**	**0.3791**	**0.3749**

Table 4.20 Acceleration standard deviation for different information flow topologies under highway scenario

Information flow topology	Control Strategy	Vehicle 1	Vehicle 5	Vehicle 10	Platoon Overall
TPSF	Symmetric	0.7641	0.7920	0.8365	0.8026
	Homogeneous	0.7481	0.7460	0.7469	0.7503
	Heterogeneous	**0.7481**	**0.7460**	**0.7467**	**0.7505**
PLF	Symmetric	0.7595	0.7580	0.7581	0.7625
	Homogeneous	0.7481	0.7458	0.7468	0.7499
	Heterogeneous	**0.7486**	**0.7461**	**0.7469**	**0.7507**
BDL	Symmetric	0.7599	0.7576	0.7576	0.7623
	Homogeneous	0.7481	0.7458	0.7466	0.7498
	Heterogeneous	**0.7481**	**0.7458**	**0.7464**	**0.7500**
Random	Symmetric	0.7774	0.7830	0.7861	0.7856
	Homogeneous	0.7481	0.7458	0.7468	0.7499
	Heterogeneous	**0.7484**	**0.7462**	**0.7471**	**0.7507**

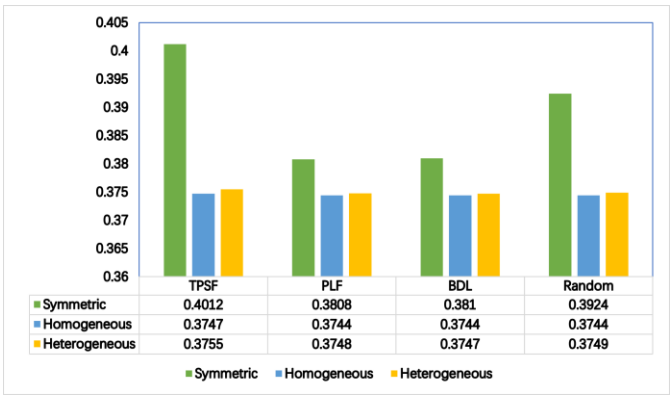

(a)

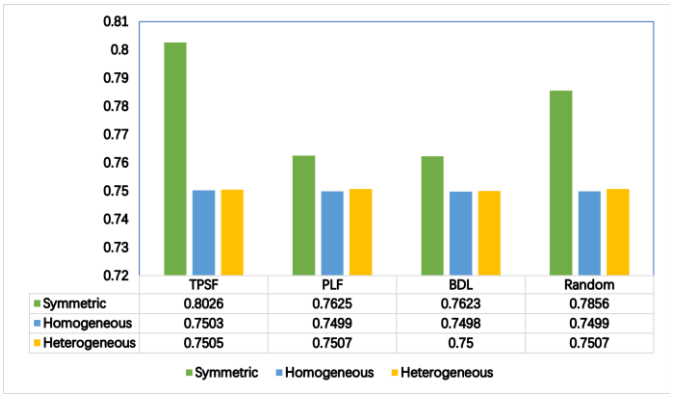

(b)

Figure 4.13 Acceleration Standard Deviation comparison. (a) Urban Road; (b) Highway

4.4 Conclusion

This Section consists of two parts. The first part studies the homogeneous optimal asymmetric topology based on a linearised third-order vehicle dynamic model with time delay. The second part investigates the heterogeneous optimal asymmetric topology based on a nonlinear third-order vehicle dynamic model. By incorporating asymmetric degrees into the control mechanism, the topological matrix changes. Sliding mode controllers incorporate Riccati inequality and Lyapunov analysis to obtain the controller's gains, ensuring the stability and string stability of the platoon. NSGA-II is then used to find the Pareto optimal asymmetric degrees using three platoon performance indices: tracking index, fuel consumption, and acceleration standard deviation. A platoon of eleven vehicles of different vehicle dynamics is studied. The simulation employs symmetric control, homogeneous asymmetric control, and heterogeneous asymmetric control to demonstrate the superiority of the proposed technique. The urban road and highway case study includes four topologies: the TPSF, PLF, BDL, and Random topology. The results show that the proposed approach can significantly reduce spacing and velocity errors. In addition, the platoon's overall performance improves as stability is achieved. Compared to symmetric control, the proposed heterogeneous asymmetric control significantly improves tracking ability, fuel economy, and driving comfort. Compared to homogeneous asymmetric control, heterogeneous asymmetric control improves tracking ability while remaining mostly unchanged regarding fuel consumption and driving comfort. The next Chapter studies switching information flow topology and proposes a two-step optimal topology searching framework.

Chapter 5

Switching Information Flow Topology

5.1 Introduction

The previous chapter introduces the concept of optimal asymmetric information flow topology. It investigates in Pareto optimal homogeneous asymmetric degree in the platoon with time delay. It further studies Pareto optimal heterogeneous asymmetric degrees in a nonlinear platoon. The strategy takes full advantage of asymmetric information flow topology, and extensive simulation proves its effectiveness. This chapter introduces a two-step information flow topology switching framework, and two studies are presented. The first one deals with the platoon with actuator fault. The second one handles the platoon with packet loss.

Most research [98-101] studied fixed information flow topology. However, the external environment directly impacts communication quality [47]. If the controller is solely designed based on fixed topologies, the platoon can quickly lose its stability over poor communication, which is neither feasible nor efficient for practical problems. As a result, switching information flow topology research has grown in popularity in recent years [44-45,102-105]. Wen *et al.* [102] proposed a switching topology sampled-data control strategy to deal with communication delays and external disturbances. Tracking errors are stabilised with the Markovian jumping system theory. Li et al. [44] examined the stability of a platoon with a switching information flow topology, deriving a sufficient condition for stability utilising the Hurwitz criteria and the Riccati inequality. Chehardoli *et al.* [45] presented an adaptive control strategy incorporating parameter uncertainties to deal with a complex platoon structure, where the information flow topology switched between several traditional topologies. Asymptotic stability is also established. Salvi *et al.* [103] proposed an LMI-based approach for estimating delay margin and decay rate while achieving string stability in a switching information flow topology scenario. The results demonstrated that the proposed approach effectively deals with the platoon's external disturbances and communication impairment.

However, previous studies on switching topology have two limitations. For starters, most studies only considered switching between traditional topologies. The proposed control methods are just a framework supporting only a few types of conventional topologies [44-45], which limits the platoon's performance and lacks ability when dealing with imperfect communication scenarios. Second, almost all topology switching processes are predefined manually and entirely offline with no online automatic motion [104-105]. Because the switching process is entirely offline, these studies cannot deal with imperfect communication scenarios in real time and thus cannot solve the platoon's practical communication failure problems. It needs to utilise the advantages of switching topology fully. As a result, this chapter aims to bridge the gap by proposing a two-step topology switching framework in which the Pareto optimal topology is first searched offline. Superior topologies are selected as candidates. The optimal topology can then be selected and switched online from the candidates while facing various types of communication failure in real time. The

proposed framework requires very little computation time and energy in real time.

The platoon's performance evaluation is another essential aspect of the platoon's control objectives. Previous studies have widely used MPC to deal with multiple control objectives. It can optimise the platoon's trajectories by solving constrained optimisation problems [8]. The weighted sum method is widely used in the optimisation function's construction. Fixed weighting coefficients are preferred in some studies. For instance, Wang *et al.* [55] designed a centralised cooperative MPC controller for the platoon's signalised isolated intersections. Three optimisation objectives are considered: intersection throughput, fuel consumption and safety. As a result, the linear quadratic control problems are effectively solved. Yang *et al.* [56] proposed an eco-driving control framework for the platoon based on optimising travel time, fuel consumption, and safety. The proposed strategy, which uses two-stage control logic and an embedded traffic flow model, can reduce freeway congestion while lowering fuel consumption. It also recognises that the choice of weighting coefficients represents a trade-off between multiple objectives, and the optimisation solutions could be more practically desirable with limited options of weighting coefficients. Using fixed weighting coefficients has its drawbacks [60], because not only the optimal solution usually obtained is the corner solution on the Pareto front, but it also varies significantly when the weighting coefficients change slightly. Some studies developed a weighting coefficient tuning strategy to overcome these limitations. Yu *et al.* [61], for example, proposed a dynamic weight tuning optimisation technique in the study to improve ride comfort and reduce tracking errors using an MPC controller. The results demonstrated its superiority over the conventional strategy. Zhao *et al.* [57] also proposed a similar real-time weight-tuning method. In both studies, because the weighting coefficients are heavily reliant on the inter-vehicle states, any feedback delay can compromise the platoon's stability to a large extent. To avoid the drawbacks, control strategies that are not based on weighted sum optimisation have also been suggested. For example, He *et al.* [63] proposed an innovative predictive cruise control method to optimise platoon fuel consumption, tracking ability and safety. The optimisation is weight-free because the utopia point is implemented using a sequential quadratic programming algorithm. However, since the utopia point cannot be reached with conflicting objectives, a compromise solution must be introduced. The proposed strategy's complexity is also questionable because quadratically constrained problems are computationally expensive [60]. This chapter proposes a modified MOEA/D to optimise multiple aspects of the platoon's performance to address the gaps identified in state-of-the-art. MOEA/D can preserve a set of superior Pareto optimal solutions while avoiding all the shortcomings.

The main contributions of this chapter are listed below:

1) Within the scope of switching topology, some previous studies focused solely on switching among a few traditional topologies with random switching signals, which compromise the platoon's performance and pose unnecessary risks to its stability. Other studies conduct the topology switching process entirely offline, reducing its practicality while proving energy-consuming. This research proposed a two-step framework to balance the trade-off between online and offline searching. When both searching processes are combined, superior topology solutions

are preserved with offline searching first. Computation time and energy are significantly reduced with online searching. The proposed framework can quickly deal with predictable imperfect communication scenarios in real time while providing a satisfying topology switching solution. It is suitable for road segments where traffic and weather conditions are predictable over a specific period.

2) The state-of-the-art has several drawbacks in the context of the platoon's multi-objective optimisation. This chapter proposes MOEA/D and fills in the gaps. First, it overcomes the sensitivity and optimality shortcomings caused by the limited number of fixed weighting coefficient options. Second, the system will not be compromised with information feedback delay since it does not rely on inter-vehicle states to adjust weighting coefficients. Finally, rather than using normalisation in optimisation problems, such as the utopia point, to obtain a single optimal solution, this chapter can obtain the entire Pareto front with multiple Pareto optimal solutions. It can better balance the trade-off and provide flexible optimal solutions that can adjust to the platoon's priority in different scenarios.

3) The latest research on the platoon's packet loss was based primarily on a third-order linearised vehicle dynamic model that only addressed powertrain time lag. On the other hand, this research proposes a discrete sliding mode controller based on a nonlinear vehicle dynamic model to deal with packet loss. Therefore, it is more practical and suitable for platoons in real-world applications.

5.2 Switching Information Flow Topology with Actuator Faults

This section proposes a real-time switching topology strategy to improve the platoon's performance under poor communication conditions. First, a sliding mode controller with an adaptive mechanism is developed for a nonlinear heterogeneous platoon with actuator faults. Then, the Lyapunov approach is applied to the platoon's tracking error dynamics, ensuring uniformly ultimately bounded stability and string stability. Finally, a two-step switching topology framework is introduced. In the first step, an offline Pareto optimal topology search with some imperfect communication scenarios predicted is applied, where the platoon's tracking ability, fuel consumption, and driving comfort are optimised using MOEA/D. In the second step, the optimal topology is switched and selected from among the previously obtained Pareto optimal topology candidates in real-time to minimise the control cost of targeting external disturbance and losing connection with the leader. Finally, numerical simulations are applied to validate the proposed approach.

5.2.1 Vehicle Dynamic Model

The vehicle dynamic model of the leader is the same as (3.1) in Chapter 3. A third-order nonlinear model is used to express the dynamic properties of vehicle i, it is mostly the same as (2.6) in Chapter 2, but actuator faults are introduced to the vehicle's dynamic, it is expressed as:

$$\dot{p}_i(t) = v_i(t)$$

$$\dot{v}_i(t) = a_i(t)$$
$$\dot{a}_i(t) = \frac{u_{oi}(t)}{m_i\tau_i} + f(v_i(t), a_i(t))$$
$$u_{oi}(t) = \big(1 - \rho_i(t)\big)u_i(t) + r_i(t)$$
$$f\big(v_i(t), a_i(t)\big) = -\frac{a_i(t)}{\tau_i} - \frac{2K_{di}v_i(t)a_i(t)}{m_i} - \frac{K_{di}v_i(t)^2}{m_i\tau_i} - \frac{d_{mi}}{m_i\tau_i} - w_i(t)$$

(5.1)

where $u_{oi}(t)$ is vehicle i's actuator output, $\rho_i(t)$ is the partial loss of effectiveness faulty severity, $r_i(t)$ is the biased faulty severity of vehicle i. It is assumed that the partial loss of effectiveness faulty severity and the biased faulty severity are bounded in the platoon, there exist positive constants $\tilde{\rho}$ and $\tilde{r}$ such that $0 \leq \rho_i(t) < \tilde{\rho}$, and $\| r_i(t) \| < \tilde{r}$, where $\tilde{\rho}$ is a positive constant with a value less than 1.

The information flow topology model is the same as in Chapter 3. However, it is assumed that the adjacency matrix T in the study can be reduced to a lower triangular matrix, which indicates that a CAV can only receive information from CAVs ahead of it in the platoon. The following is the adjacency matrix T:

$$T = \begin{bmatrix} 0 & \cdots & \cdots & \cdots & 0 \\ \vdots & \ddots & \ddots & \ddots & \vdots \\ t_{i-2,1} & t_{i-2,2} & \ddots & \ddots & \vdots \\ t_{i-1,1} & t_{i-1,2} & t_{i-1,3} & \ddots & \vdots \\ t_{i,1} & t_{i,2} & t_{i,3} & \cdots & 0 \end{bmatrix}$$

5.2.2 Platoon's Error Dynamics

The main goal of platoon control is to ensure convergence, which can be interpreted as ensuring that all of the followers' position, velocity, and acceleration profiles converge to the leader's profile. The platoon's stability is equivalent to the convergence of the platoon's tracking errors. To simplify the expression, this section defines tracking errors, lumped tracking error measurements, and their compacted forms. The relationship between tracking errors and vehicle dynamics is also presented. The tracking errors are defined as:

$$\Delta p_i(t) = p_i(t) - p_0(t) - d_{i0}$$
$$\Delta v_i(t) = v_i(t) - v_0(t)$$
$$\Delta a_i(t) = a_i(t) - a_0(t)$$

(5.2)

where d_{i0} is the desired spacing between vehicle i and the leader. Let $\tilde{p}(t) = [\Delta p_1(t), \Delta p_2(t), \cdots, \Delta p_N(t)]^T$, $\tilde{v}(t) = [\Delta v_1(t), \Delta v_2(t), \cdots \Delta v_N(t)]^T$, $\tilde{a}(t) = [\Delta a_1(t), \Delta a_2(t), \cdots, \Delta a_N(t)]^T$. The lumped tracking error measurements are defined as:

$$ep_i(t) = \sum_{j \in \Pi_i} p_i(t) - p_j(t) - d_{ij}$$
$$ev_i(t) = \sum_{j \in \Pi_i} v_i(t) - v_j(t)$$

$$ea_i(t) = \sum_{j \epsilon \Pi_i} a_i(t) - a_j(t)$$

(5.3)

where d_{ij} is the required distance between vehicles i and j. Let $E_p(t) = [ep_1(t), ep_2(t), \cdots, ep_N(t)]^T$, $E_v(t) = [\ ev_1(t), ev_2(t), \cdots, ev_N(t)]^T, E_a(t) = [ea_1(t), ea_2(t), \cdots, ea_N(t)]^T$. The compact form of the lumped tracking error measurements is as follows:

$$E_p(t) = H\tilde{p}(t)$$
$$E_v(t) = H\tilde{v}(t)$$
$$E_a(t) = H\tilde{a}(t)$$

(5.4)

where H is the overall topological matrix. Combining (5.5) with the vehicle dynamic model (5.1), the relationship between tracking error measurements and vehicle dynamics can be written as:

$$\dot{E_p}(t) = E_v(t)$$
$$\dot{E_v}(t) = E_a(t)$$
$$\dot{E_a}(t) = H(F - 1_N a_0\dot{(t)} + U(t))$$

(5.5)

where $F = [f(v_1(t), a_1(t)), f(v_2(t), a_2(t)), \cdots, f(v_N(t), a_N(t))]^T$, and $U(t) = [\frac{u_{o1}(t)}{m_1\tau_1}, \frac{u_{o2}(t)}{m_2\tau_2}, \cdots, \frac{u_{oN}(t)}{m_N\tau_N}]^T$. It is assumed that there exit constants $\theta_1, \theta_2, \theta_3 > 0$ such that: $\| f(v_i(t), a_i(t)) - a_0\dot{(t)} \| \leq \theta_1 \| \Delta p_i(t) \| + \theta_2 \| \Delta v_i(t) \| + \theta_3 \| \Delta a_i(t) \|$ for $i = 1,2, \cdots, N$, and $f(0,0) = 0$.

5.2.3 Sliding Mode Controller Design

The controller is designed based on the core principle of UUB cooperative tracking. An adaptive sliding mode tracking strategy inspired by [106] is proposed to achieve the platoon's cooperative tracking. The sliding surface is selected to be:

$$s_i(t) = k_1 ep_i(t) + k_2 ev_i(t) + ea_i(t)$$

(5.6)

where $k_1, k_2 > 0$, and they are controller's gains. Let $S(t) = [s_1(t), s_2(t), \cdots, s_N(t)]^T$.Therefore, the compacted form of the sliding surface $S(t)$ can be expressed as:

$$S(t) = k_1 E_p(t) + k_2 E_v(t) + E_a(t)$$

(5.7)

If the trajectory of the lumped tracking error measurements system (6) is kept on the sliding surface $s = 0$, then the asymptotical stability of the platoon can be achieved. The time derivative can be formulated as:

$$S\dot{(t)} = k_1 \dot{E_p}(t) + k_2 \dot{E_v}(t) + \dot{E_a}(t)$$

(5.8)

To ensure cooperative tracking, an interim control input term $\hat{u}_i(t)$ is used, let $\hat{U}(t) = [\hat{u}_1(t), \hat{u}_2(t), \cdots, \hat{u}_N(t)]^T$. Therefore, the compacted form of the interim control input is designed as:

$$\hat{U}(t) = H^{-1}(G(s) - k_1 E_v(t) - k_2 E_a(t))$$

(5.9)

where $G(s) = [g_1(s), g_2(s), \cdots, g_N(s)]^T$, $g_i(s)$ is designed as:

$$g_i(s) = -\beta_i(t) sgn(s_i(t))$$

(5.10)

To reduce the chattering problem, $sgn(s_i(t)) = \frac{s_i(t)}{\|s_i(t)\| + \epsilon}$, where $\epsilon > 0$. $\beta_i(t)$ is designed using an adaptive mechanism to reduce the chattering in the control system and increase the control accuracy:

$$\dot{\beta}_i(t) = \alpha(\| s_i(t) \| - \gamma \beta_i(t))$$

(5.11)

where $\beta_i(0) = 1.5$, α and γ are positive parameters. $\beta_i(t)$ also satisfy $\beta_i(t) \leq \frac{1}{2}\bar{\beta}$, where $\bar{\beta}$ is the upper bound of $\beta_i(t)$, it is selected to be 600 in this section. The adaptive mechanism used is a first-order approximation filter for the sliding mode controller, it also prevents unlimited growth of the switching gain. The final control input is designed as:

$$u_i(t) = m_i \tau_i \hat{u}_i(t)$$

(5.12)

The Lyapunov stability analysis technique is used to prove the platoon's UB and UUB stability. String stability is proved using Gronwall's inequality. LMIs are presented to regulate the controller's gains and topology.

Definition 5.1 [107]: (UB) State $\eth(t)$ is said to be uniformly bounded if given any $\eta > 0$, there exists a $\hbar(\eta) < \infty$ such that if $\| \eth(t_0) \| \leq \eta$, then $\| \eth(t) \| \leq \hbar(\eta)$ for all $t \geq t_0$.

Definition 5.2 [107]: (UUB) State $\eth(t)$ is said to be uniformly ultimately bounded if given any $\eta > 0$, with $\| \eth(t_0) \| \leq \eta$, there exists a $\underline{\hbar} < 0$ such that $\| \eth(t) \| \leq \overline{\hbar}$ for any $\overline{\hbar} > \underline{\hbar}$ as $t \geq t_0 + T(\overline{\hbar}, \eta)$, where $T(\overline{\hbar}, \eta) < \infty$.

Definition 5.3 [107]: (String Stability) The equilibrium $E_p(t) = 0$ of a platoon is said to be string stable if given any $\hbar > 0$, there exits $\eta > 0$, such that if $\| E_p(t_0) \|_\infty < \eta$, then $sup \| E_p(t) \|_\infty < \hbar$ for all $t > t_0$.

Theorem 5.1: Let $\eth(t) = S(t)$. If all assumptions are valid with known Lipschitz parameters $\theta_1, \theta_2, \theta_3, \bar{\beta}$, and the following inequalities (5.13-5.14) hold, then the platoon system renders the UB and UUB performances of $\eth(t)$ under the proposed controller (5.9):

$$\varpi = 1 - \lambda_{max}\left(\frac{H_\rho + H_\rho{}^T}{2}\right) > 0$$

(5.13)

$$\| H_\rho[k_1 E_v(t) + k_2 E_a(t)] \| + \| H \| \sqrt{N}\, \bar{r} < \varpi\bar{\beta} - \| H \| \| H^{-1} \| [\theta_1 \| E_p(t) \| + \theta_2 \| E_v(t) \| + \theta_3 \| E_a(t) \|]$$

(5.14)

where $H_\rho = H\Theta H^{-1}, \Theta = \mathrm{diag}\{\rho_1(t), \rho_2(t), \cdots, \rho_N(t)\}$.

Proof: The Lyapunov function candidate is selected as:

$$V(t) = \frac{1}{2} S(t)^T S(t) + \frac{\varpi}{2\alpha} \sum_{i=1}^{N} (\beta_i(t) - \bar{\beta})^2$$

(5.15)

The time derivative of the Lyapunov function is stated as follows:

$$\dot{V(t)} = S(t)^T \dot{S(t)} + \frac{\varpi}{\alpha} \sum_{i=1}^{N} [\beta_i(t) - \bar{\beta}] \dot{\beta}_i(t)$$

(5.16)

Substituting (5.8) and (5.11) into (5.16), $\dot{V}(t)$ can be obtained as:

$$\dot{V}(t) = S(t)^T \left(k_1 E_v(t) + k_2 E_a(t) + \dot{E_a}(t) \right) + \varpi \sum_{i=1}^{N} (\beta_i(t) - \bar{\beta}) [\| s_i(t) \| - \gamma \beta_i(t)]$$

(5.17)

Substituting (5.5), (5.1) and (5.9) into (5.17), $\dot{V}(t)$ can be written as:

$$\dot{V}(t) = S(t)^T \left[k_1 E_v(t) + k_2 E_a(t) + H \left(F - 1_N \dot{a_0}(t) + U(t) \right) \right] + \varpi \sum_{i=1}^{N} (\beta_i(t) - \bar{\beta}) [\| s_i(t) \| - \gamma \beta_i(t)]$$

$$= S(t)^T [k_1 E_v(t) + k_2 E_a(t) + H(F - 1_N \dot{a_0}(t) + (I_N - \Theta)\hat{U}(t) + 1_N r_i(t))] + \varpi \sum_{i=1}^{N} (\beta_i(t) - \bar{\beta}) [\| s_i(t) \| - \gamma \beta_i(t)]$$

$$= S(t)^T [k_1 E_v(t) + k_2 E_a(t) + H(F - 1_N \dot{a_0}(t) + 1_N r_i(t)) + H(I_N - \Theta) H^{-1} (G(s) - k_1 E_v(t) - k_2 E_a(t))] + \varpi \sum_{i=1}^{N} (\beta_i(t) - \bar{\beta}) [\| s_i(t) \| - \gamma \beta_i(t)]$$

(5.18)

Rearranging (5.18), $\dot{V}(t)$ can be expressed as:

$$\dot{V}(t) = S(t)^T [G(s) + H(F - 1_N \dot{a_0}(t) + 1_N r_i(t)) + H_\rho \left(k_1 E_v(t) + k_2 E_a(t) - G(s) \right)] + \varpi \sum_{i=1}^{N} (\beta_i(t) - \bar{\beta}) [\| s_i(t) \| - \gamma \beta_i(t)]$$

(5.19)

Based on the previous assumptions, it can be derived that:

$$\| F - 1_N \dot{a_0}(t) \| \leq \| [\theta_1 \| \Delta p_i(t) \| + \theta_2 \| \Delta v_i(t) \| + \theta_3 \| \Delta a_i(t) \|, \cdots, \theta_1 \| \Delta p_N(t) \| + \theta_2 \| \Delta v_N(t) \| + \theta_3 \| \Delta a_N \|]^T \| \leq \theta_1 \| \tilde{p}(t) \| + \theta_2 \| \tilde{v}(t) \| + \theta_3 \| \tilde{a}(t) \|$$

(5.20)

Therefore, it can be computed that:

$$\| H\left(F - 1_N a_0\dot{(t)}\right) \| \leq \| H \| (\theta_1 \| \tilde{p}(t) \| + \theta_2 \| \tilde{v}(t) \| + \theta_3 \| \tilde{a}(t) \|) \leq \| H \| \| H^{-1} \| (\theta_1 \| E_p(t) \| + \theta_2 \| E_v(t) \| + \theta_3 \| E_a(t) \|)$$

(5.21)

Given inequality (5.13), it can be obtained that:

$$S(t)^T H_\rho G(s) \geq \lambda_{max}\left(\frac{H_\rho + H_\rho{}^T}{2}\right) S(t)^T G(s)$$

(5.22)

Therefore, $V\dot{(t)}$ can be simplified as:

$$V\dot{(t)} \leq [\| H \| \| H^{-1} \| \left(\theta_1 \| E_p(t) \| + \theta_2 \| E_v(t) \| + \theta_3 \| E_a(t) \|\right) + \| H \| \sqrt{N}\, \bar{r} + \| H_\rho(k_1 E_v(t) + k_2 E_a(t)) \|] \| S(t) \| + \varpi S(t)^T G(s) + \varpi \sum_{i=1}^{N} (\beta_i(t) - \bar{\beta})[\| s_i(t) \| - \gamma \beta_i(t)]$$

(5.23)

Substituting (5.10) into (5.23), the following inequality holds:

$$\dot{V}(t) \leq \Gamma \| S(t) \| - \varpi \sum_{i=1}^{N} \bar{\beta}(t) \| s_i(t) \| + \varpi \sum_{i=1}^{N} -\gamma \beta_i(t)[\beta_i(t) - \bar{\beta}]$$

(5.24)

where $\Gamma = \| H \| \| H^{-1} \| (\theta_1 \| E_p(t) \| + \theta_2 \| E_v(t) \| + \theta_3 \| E_a(t) \|) + \| H \| \sqrt{N}\, \bar{r} + \| H_\rho[k_1 E_v(t) + k_2 E_a(t)] \|$.

According to the definition,max $(-\beta_i(t)(\beta_i(t) - \bar{\beta})) = \frac{1}{4}\bar{\beta}^2$, $V\dot{(t)}$ satisfy:

$$V\dot{(t)} \leq -(\varpi\bar{\beta} - \Gamma) \| S(t) \| + \frac{\gamma N \varpi}{4}\bar{\beta}^2$$

(5.25)

Since $\varpi, \gamma, N, \bar{\beta}$ are all positive values, (5.25) indicates that $V\dot{(t)}$ is negative definite for all $\| S(t) \| \geq \frac{\gamma N \varpi \bar{\beta}^2}{4(\varpi\bar{\beta} - \Gamma)}$, if the following inequality holds:

$$\varpi\bar{\beta} - \Gamma > 0$$

(5.26)

(5.25) is equivalent to inequality (5.14). Therefore, referring to the standard arguments in [67], the system renders UB and UUB performance of $S(t)$. The uniform boundness is:

$$R = \frac{\gamma N \varpi \bar{\beta}^2}{4(\varpi\bar{\beta} - \Gamma)}$$

(5.27)

$$\hbar(\eta) = \begin{cases} R & if\ \eta \leq R \\ \eta & Otherwise \end{cases}$$

(5.28)

The uniform ultimate boundness is:

$$\underline{\hbar} = R$$

(5.29)

$$T(\overline{\hbar},\eta)=\begin{cases}0 & if\ \eta \le R\\ \dfrac{\eta^2-\overline{\hbar}^2}{\overline{\hbar}^2-R^2} & Otherwise\end{cases}$$

(5.30)

Thus, the proposed controller (5.9) can render the UB and UUB performance of $S(t)$. The proof of *Theorem 5.1* is completed.

Theorem 5.2 : If all assumptions are valid with known Lipschitz parameters $\theta_1,\theta_2,\theta_3$, $\bar{\beta}$, inequalities (4.13-5.14), and the following inequality (5.31) holds, then the platoon system is string stable under the proposed controller (5.9).

$$k_2{}^2-4k_1\ge 0$$

(5.31)

Proof: Since the controller proposed (10) renders the UUB performance of $S(t)$, $S(t)$ can converge to a small range $(-\overline{\hbar},\overline{\hbar})$ in finite time $T(\overline{\hbar},\eta)$. It can be derived that:

$$-\overline{\hbar}<S(t)<\overline{\hbar}$$

(5.32)

(5.32) is equivalent to:

$$-\overline{\hbar}<k_1E_p+k_2\dot{E_p}+\ddot{E_p}<\overline{\hbar}$$

(5.33)

By solving (5.33), it can be obtained that:

$$\dot{E_p}(t)+\varrho_1E_p(t)\le\varrho_1\frac{\overline{\hbar}}{k_1}+\left[\dot{E_p}(T)+\varrho_1E_p(T)-\varrho_1\frac{\overline{\hbar}}{k_1}\right]exp^{-\frac{k_1}{\varrho_1}(t-T)}$$

$$\dot{E_p}(t)+\varrho_1E_p(t)\ge-\varrho_1\frac{\overline{\hbar}}{k_1}+\left[\dot{E_p}(T)+\varrho_1E_p(T)+\varrho_1\frac{\overline{\hbar}}{k_1}\right]exp^{-\frac{k_1}{\varrho_1}(t-T)}$$

(5.34)

where $t>T$ and $\varrho_1=\frac{2k_1}{k_2-\sqrt{k_2{}^2-4k_1}}$, noted that ϱ_1 is only a real number if inequality (32) holds.

According to Gronwall's inequality, (5.34) can be further reduced to:

$$E_p(t)\le\frac{\varrho_2}{\varrho_1}+(E_p(T)-\frac{\varrho_2}{\varrho_1})exp^{-\varrho_1(t-T)}$$

$$E_p(t)\ge-\frac{\varrho_3}{\varrho_1}+(E_p(T)-\frac{\varrho_3}{\varrho_1})exp^{-\varrho_1(t-T)}$$

(5.35)

where

$$\varrho_2=\varrho_1\frac{\overline{\hbar}}{k_1}+\left[\dot{E_p}(T)+\varrho_1E_p(T)-\varrho_1\frac{\overline{\hbar}}{k_1}\right]exp^{-\frac{k_1}{\varrho_1}(t-T)}$$

$$\varrho_3=-\varrho_1\frac{\overline{\hbar}}{k_1}+\left[\dot{E_p}(T)+\varrho_1E_p(T)+\varrho_1\frac{\overline{\hbar}}{k_1}\right]exp^{-\frac{k_1}{\varrho_1}(t-T)}$$

(5.36)

It indicates that $E_p(t)$ is also uniformly ultimate bounded, where the time of boundness t_0 is

given by T. Considering *Definition 5.3*, the string stability of the platoon is proved.

Configurable parameters ϵ, α, γ,k_1 and k_2 are yet to be specified, the final values selected after tuning are shown in Table 5.1. Here are some remarks on the parameters.

Remark 1: γ depicts the trade-off between control precision and chattering. With smaller ϵ, the control accuracy is higher, but the chattering is worse.

Remark 2: ϵ is intended to reduce chattering and smooth the sign function. ϵ , like γ, faces trade-off between control accuracy and chattering as well. However, it is discovered during parameter turning that the overall control accuracy and chattering reduction are better with smaller γ and larger ϵ.

Remark 3: α, k_1 and k_2 have an influence on the adaptive gain and the controller's gains, they all display the trade-off between control accuracy and energy consumption. The control accuracy is higher with larger α, k_1 and k_2, but more energy is required. k_1 and k_2 are chosen based on inequality (5.31) to ensure the platoon's string stability.

Table 5.1 Controller's parameters

ϵ	α	γ	k_1	k_2	$\theta_1/\theta_2/\theta_3$
10	2.5	0.001	2	10	300

5.2.4 Two-step Topology Switching Framework

The platoon's performance optimisation considers tracking ability, fuel economy, and driving comfort, which are the same as (3.5-3.9) in Chapter 3. In this section, an overall control objective is proposed to take all three components into account. For the online process, the platoon's objective function is defined as:

$$J = \sum_{i=0}^{N} \begin{bmatrix} TI \\ FC \\ ASD \end{bmatrix}^T \mathbb{Q} \begin{bmatrix} TI \\ FC \\ ASD \end{bmatrix} \tag{5.37}$$

J is regarded as the control cost. $\mathbb{Q}$ >0 is a weighting matrix, it is expressed as $\mathbb{Q} = diag(Q_{TI}, Q_{FC,} Q_{ASD})$, the three elements correspond to the above-mentioned performance evaluation standards. It should be noted that a simple weighted sum method is used here for the online process to save consumption energy, aiming at finding the optimal topology in real-time more efficiently.

During offline topology optimisation, common communication failure scenarios are anticipated, such as vehicles experiencing unexpected external disturbances or abruptly losing connections with the leader. Then, the system performs offline Pareto optimal topology searching based on the predicted scenarios. Finally, for each scenario, a Pareto optimal topology is obtained, which will be used as candidates for online searching in the following step.

In terms of offline searching, 0 or 1 indicates the presence or absence of the communication link. Initially, a set of uniformly distributed weight vectors is generated using MOEA/D. The neighbourhood of each weight vector is then defined based on its Euclidean distance from other

vectors. The genetic operator is used in each iteration to include a new solution. The neighbourhood solutions are updated after the solution has been improved and updated based on the fitness value. The last step is to update the external population. Populations are verified using inequalities (5.13-5.14) to ensure the platoon's UUB and string stability. Unqualified populations are eliminated. The iteration will continue until the stopping criteria are met. Following that, a collection of Pareto optimum solutions can be obtained. As a result, the Pareto optimal topology for each communication scenario can be determined.

This section explains the topology switching process in the second step. A two-step topology switching framework is proposed. Both the online and offline optimisation processes in the platoon have limitations. The process can be highly time and energy-consuming when using online multi-objective optimisation. As a result, finding a satisfying solution in real-time is challenging when the system needs more capacity. On the other hand, offline multi-objective optimisation can produce numerically superior solutions with a large amount of offline calculation. However, the limitation occurs when the real-time communication scenario becomes unpredictable. As a result, this section proposes a two-step framework that combines the online and offline processes while taking full advantage of both methods.

Several common communication scenarios are anticipated first. The system then performs offline Pareto optimal topology searching using MOEA/D on the predicted scenarios, yielding a set of superior Pareto optimal topology candidates for each scenario. Finally, when the platoon operates in real-time, the system performs online optimal topology searching within the Pareto optimal topology candidates. Online searching is solely based on the weighted sum method described in (5.37) to find the optimal topology with the lowest control cost.

The proposed strategy can select and switch optimal topology in real-time with less energy required, providing a satisfying solution simultaneously. The proposed two-step framework is summarised below:

Two-step Topology Switching Framework

1.OFFLINE SEARCHING:

Initialize: Predict communication failure scenarios $ב_m$. Initiate a uniform spread of N weights vectors. Define N weights vectors' neighbourhood. Initiate a population: p_i and t_{ij} in information flow topology model as input variables. Initiate external population. Define the three control objectives: $f(1), f(2), f(3)$. Define the maximum iteration number: n. Calculate initial population's fitness value.

For $i = 1: m$

For $j = 1: n$

Reproduction: Create a new solution using generic operators

Improvement: Apply a problem-specific repair

Update: Population's fitness value using (3.5-3.9)

Neighbourhood's solution

External population

Eliminating unqualified populations using inequalities (5.13-5.14)

End

Obtain A set of Pareto optimal topologies

Select one Pareto optimal topology $\mho_i$ as the candidate

End

2.ONLINE SWITCHING:

Initialize: Find the number of time interval. Obtain weighting matrix $\mathbb{Q}$.

For $i = 1: T - 1$

Define time interval as $[t_i, t_{i+1})$

For $j = 1: m$

Apply $\mho_j$ to the system

Calculate the control cost J_j using (5.37)

End

Find $\min(J)$ and the corresponding index c_i

If $i \geq 2$ && $c_i\sim = c_{i-1}$

SWITCH: Apply $\mho_{c_i}$ to time interval $[t_i, t_{i+1})$

Else

STAY: Keep $\mho_{c_{i-1}}$ to time interval $[t_i, t_{i+1})$

End

End

5.2.5 Simulation Results

The hardware setup is the same as in Chapter 3. To show the influence of information flow topology and the effectiveness of the proposed approach, a platoon of eleven heterogeneous vehicles is constructed, with the fixed topology being tested first, followed by the switching topology. Consider the urban road traffic scenario, the kinematic profile for the leader is designed as:

$$a_0(t) = \begin{cases} 0 & 0 < t \leq 250s \\ 0.1m/s & 250 < t \leq 300s \\ 0 & 300 < t \leq 550s \\ -0.1m/s & 550 < t \leq 600s \\ 0 & 600 < t \leq 1000s \end{cases} \tag{5.38}$$

Table 5.2 displays the starting location, velocity, and required distance between each vehicle and the leading vehicle.

Table 5. Initial states and desired gaps of each vehicle

Vehicle	Position (m)	Velocity (m/s)	Desired gap (m)
Leader	0	4	0

Vehicle 1	-21	3	-20
Vehicle 2	-49	5	-40
Vehicle 3	-61	3.5	-60
Vehicle 4	-78	4.2	-80
Vehicle 5	-102	3.8	-100
Vehicle 6	-123	4.4	-120
Vehicle 7	-137	4.1	-140
Vehicle 8	-161	3.7	-160
Vehicle 9	-182	4.2	-180
Vehicle 10	-199	4.1	-200

To fully investigate the effectiveness of the proposed method, different communication scenarios are taken into consideration to describe the uncertainty of communication among CAVs in the platoon. As experiencing external disturbances and losing connection with the leader vehicle are very common in reality, the communication scenarios are designed to account for these events. To begin with, the communication remains normal in the platoon from the beginning to $250s$. Then, we assume that Vehicle 3 encounters external disturbance from $250s$ to $400s$, similarly Vehicle 6 encounters external disturbance from $400s$ to $500s$. The disturbance is described in (5.39). Moreover, both Vehicle 3 and Vehicle 4 loss connection from the leader vehicle at $t = 500s$, then the communication is recovered at $t = 600s$. All communication links are back to normal till $t = 1000s$.

$$w_i(t) = A_w + 0.5\sin\left(\frac{\pi}{10}t\right) \tag{5.39}$$

where A_w is a positive constant, represents the magnitude of the external disturbances.

The time interval in this section is naturally divided into five sections, which are $[0,250)s$, $[250,400)s$, $[400,500)s$, $[500,600)s$ and $[600,1000]s$.The weighting matrix is selected to be $\mathbb{Q} = diag(0.8,0.1,0.1)$. Because the proposed framework is based on time intervals that have been pre-defined. It should be noted that the proposed strategy is appropriate for road segments where traffic and weather conditions are predictable and show regularity over a specific period.

As for fixed topology, the fixed topology evaluated in this research is the Predecessor following topology (PF), which is generally employed in most studies due to its high performance. As for switching topology, the Pareto optimal topology in each time interval based on the predicted communication scenario is obtained using MOEA/D, which takes three performance indices into account. $\mho = T + P$ is used to display the resulting Pareto optimal topology. The results in each time interval are listed in Table 5.3. Because communication scenarios are not jeopardized in the first and the last time intervals. It is possible to conclude that $\mho_5 = \mho_1$. It should be noted that $\mho$ differs from the overall topological matrix H in terms of mathematical expressions. $T + P$ is chosen specifically here to display the topology due to its intuitiveness.

Table 5.3 Pareto optimal information flow topology $\mho$ obtained offline

$$\begin{bmatrix} 1 & 0 & 0 & 0 & 0 & 0 & 0 & 0 & 0 & 0 \\ 1 & 0 & 0 & 0 & 0 & 0 & 0 & 0 & 0 & 0 \\ 1 & 1 & 1 & 0 & 0 & 0 & 0 & 0 & 0 & 0 \\ 0 & 1 & 0 & 1 & 0 & 0 & 0 & 0 & 0 & 0 \\ 1 & 0 & 1 & 0 & 0 & 0 & 0 & 0 & 0 & 0 \\ 1 & 0 & 0 & 1 & 1 & 1 & 0 & 0 & 0 & 0 \\ 0 & 1 & 0 & 0 & 0 & 0 & 0 & 0 & 0 & 0 \\ 1 & 1 & 0 & 1 & 0 & 0 & 0 & 1 & 0 & 0 \\ 1 & 0 & 1 & 0 & 1 & 0 & 0 & 0 & 1 & 0 \\ 1 & 1 & 1 & 1 & 1 & 1 & 0 & 0 & 0 & 1 \end{bmatrix} \quad \mathcal{U}_1$$

$$\begin{bmatrix} 1 & 0 & 0 & 0 & 0 & 0 & 0 & 0 & 0 & 0 \\ 1 & 0 & 0 & 0 & 0 & 0 & 0 & 0 & 0 & 0 \\ 1 & 1 & 0 & 0 & 0 & 0 & 0 & 0 & 0 & 0 \\ 1 & 1 & 0 & 1 & 0 & 0 & 0 & 0 & 0 & 0 \\ 1 & 1 & 1 & 0 & 0 & 0 & 0 & 0 & 0 & 0 \\ 0 & 1 & 1 & 1 & 1 & 0 & 0 & 0 & 0 & 0 \\ 0 & 1 & 0 & 0 & 0 & 0 & 1 & 0 & 0 & 0 \\ 0 & 1 & 1 & 1 & 1 & 1 & 0 & 1 & 0 & 0 \\ 1 & 1 & 1 & 1 & 1 & 1 & 1 & 0 & 0 & 0 \\ 1 & 1 & 1 & 0 & 1 & 0 & 0 & 1 & 0 & 0 \end{bmatrix} \quad \mathcal{U}_2$$

$$\begin{bmatrix} 1 & 0 & 0 & 0 & 0 & 0 & 0 & 0 & 0 & 0 \\ 1 & 1 & 0 & 0 & 0 & 0 & 0 & 0 & 0 & 0 \\ 1 & 0 & 1 & 0 & 0 & 0 & 0 & 0 & 0 & 0 \\ 0 & 1 & 0 & 1 & 0 & 0 & 0 & 0 & 0 & 0 \\ 1 & 1 & 1 & 1 & 0 & 0 & 0 & 0 & 0 & 0 \\ 1 & 1 & 1 & 1 & 1 & 1 & 0 & 0 & 0 & 0 \\ 0 & 1 & 1 & 1 & 0 & 0 & 0 & 0 & 0 & 0 \\ 1 & 1 & 1 & 1 & 1 & 1 & 1 & 1 & 0 & 0 \\ 1 & 1 & 1 & 1 & 1 & 1 & 1 & 1 & 1 & 0 \\ 0 & 1 & 0 & 0 & 0 & 0 & 1 & 0 & 0 & 0 \end{bmatrix} \quad \mathcal{U}_3$$

$$\begin{bmatrix} 1 & 0 & 0 & 0 & 0 & 0 & 0 & 0 & 0 & 0 \\ 1 & 0 & 0 & 0 & 0 & 0 & 0 & 0 & 0 & 0 \\ 1 & 1 & 1 & 0 & 0 & 0 & 0 & 0 & 0 & 0 \\ 0 & 1 & 0 & 0 & 0 & 0 & 0 & 0 & 0 & 0 \\ 1 & 1 & 1 & 0 & 0 & 0 & 0 & 0 & 0 & 0 \\ 1 & 1 & 0 & 1 & 1 & 0 & 0 & 0 & 0 & 0 \\ 0 & 1 & 0 & 1 & 0 & 0 & 0 & 0 & 0 & 0 \\ 1 & 0 & 0 & 1 & 1 & 1 & 0 & 1 & 0 & 0 \\ 1 & 1 & 1 & 0 & 1 & 1 & 0 & 1 & 1 & 0 \\ 1 & 1 & 0 & 0 & 1 & 1 & 1 & 1 & 0 & 1 \end{bmatrix} \quad \mathcal{U}_4$$

The platoon's spacing error for fixed topology and switching topology are illustrated in Figure 5.1. It shows that the spacing errors are primarily reduced, especially from $250s$ to $500s$ The spacing errors under fixed topology fluctuate around $1.3\,m$, whereas the spacing errors under switching topology are all within 1m. Vehicles 3 and 6 are underperforming due to the external disturbances they encountered. The influence of Vehicles 3 and 6 on the rest of the platoon is significantly reduced by switching topology. Figure 5.2 illustrates the error in the platoon's velocity for both fixed and switching topologies. The proposed strategy results in minor velocity errors, demonstrating its efficacy. Switching topology reduces velocity error the most at $t = 250s$ and $t = 400s$. The velocity error is reduced from $-0.4m$ to $-0.1m$ at $t = 400s$. After $600s$, the velocity achieved consistency, suggesting that the proposed technique can achieve the platoon's velocity consensus. The proposed sliding mode control approach achieves stability effectively. The switching topology method can reduce the platoon's tracking errors. It is especially effective when working with external disturbances.

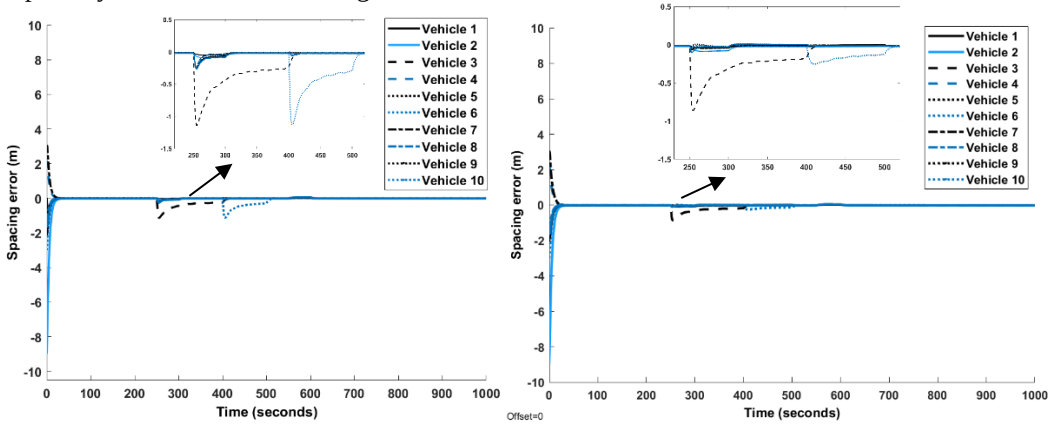

(a) (b)

Figure 5.1 Spacing errors. (a) Fixed topology; (b) Switching topology

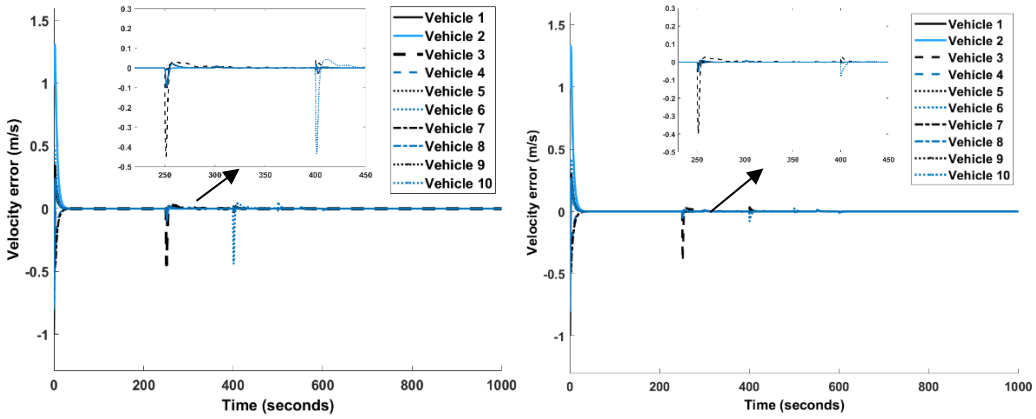

(a) (b)

Figure 5.2 Velocity errors. (a) Fixed topology; (b) Switching topology

Figure 5.3 depicts the online topology switching results during the simulation time. When different communication scenarios are applied to each time interval, the topology chosen online differs. All of the topologies selected are consistent with the Pareto optimal topology candidates found during offline searching with MOEA/D. Finally, the effectiveness and precision of the two-step framework are proved.

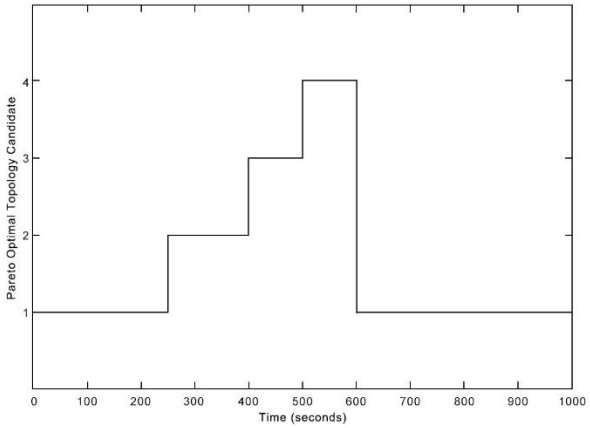

Figure 5.3 Online Topology switching

Table 5.4 compares all performance indices between fixed and switching topology, using vehicles 1, 5, and 10 as examples. Table 5.5 shows the platoon's performance with the switching topology method in each time interval.

Table 5.4 Performance comparison for different information flow topologies

Performance Index	Information flow topology	Vehicle 1	Vehicle 5	Vehicle 10	Platoon Overall
TI	Fixed	1.137	1.458	2.001	24.99
	Switching	**1.42**	**1.29**	**1.263**	**19.68**
FC	Fixed	0.6034	0.6035	0.6035	6.639
	Switching	**0.6034**	**0.6031**	**0.6035**	**6.638**
ASD	Fixed	0.0407	0.0341	0.0396	0.0363

	Switching	**0.0415**	**0.0349**	**0.0318**	**0.0361**
Control Cost	Fixed	1.0708	1.7371	3.2398	504.01
	Switching	**1.6497**	**1.3678**	**1.3127**	**314.25**

Table 5.5 Performance under switching topology in each time interval

Time / Criterion	0-250 (s)	250-400 (s)	400-500 (s)	500-600 (s)	600-1000 (s)
TI	10.3377	12.0870	10.4949	9.6127	11.5793
FC	1.6524	1.0132	0.6616	0.6613	2.6434
ASD	0.0299	0.0652	0.0566	0.0718	0.0236
Cost	**85.7673**	**116.9793**	**88.1577**	**79.9670**	**107.9630**

Table 5.4 shows that with switching topology, Vehicle 5 and the platoon consume less fuel than with fixed topology, and that Vehicles 5, 10, and the platoon have a lower acceleration standard deviation value as well, indicating that both fuel economy and driving comfort are improved. Although fuel consumption and acceleration standard deviation may be insensitive to changes in information flow topology, Table 5.4 shows that the switching topology strategy can improve driving comfort and fuel economy in a limited way. Furthermore, the tracking index, regarded as the most crucial performance evaluation in most studies, changes radically. The proposed switching topology approach improved tracking ability by 26.98 % and control cost by 60.3 9%, proving the effectiveness of the proposed framework.

Table 5.5 details the platoon's performance at each time interval. The tracking ability and fuel consumption are superior and consistent with switching topology. Moreover, it can be seen that when communication is regular, driving comfort is at its best. External disturbances and losing contact with the leader reduced vehicles' driving comfort to some extent.

5.3 Discrete Switching Information Flow Topology with Packet Loss

This section provides a real-time switching topology technique for improving the platoon's performance under poor communication. First, a discrete sliding mode controller with a double power reaching law is designed for a platoon with packet loss. Then, Lyapunov analysis is applied to ensure the platoon's stability and string stability. Finally, a two-step switching topology framework with modified MOEA/D is introduced. The proposed method maximises the advantages of information flow topology. It deals with poor communication, improves the platoon's performance, and ensures stability.

The vehicle dynamic model of the leader is the same as (3.1) in Chapter 3. A third-order nonlinear model is used to express the dynamic properties of vehicle i, it is the same as (2.6) in Chapter 2. The packet loss model is the same as (3.19) in Section 3.6.2. Instead of p, the packet dropout rate from vehicle j to vehicle i is denoted by θ_{ij}. θ_{ij} has a positive upper bound ∂ for $i = 1,2 \dots N$, and $j = 1,2 \dots N$.

The information flow topology model is the same as in Section 5.2. Considering the packet loss model defined previously, two additional topological matrices H_1 and H_2 are defined to predict packet dropout rates. H_1 is the possibility of normal communication. The adjacency matrix $T_1 = [t_{ij} \times (1 - \theta_{ij})]$, The in-degree of node i is defined as $\bar{d}_i = \sum_{j=1}^{N} t_{ij} \times (1 - \theta_{ij})$. Denote $D_1 = diag(\bar{d}_1, \bar{d}_2 \dots \bar{d}_N)$. The Laplacian matrix L is defined as $L_1 = D_1 - T_1$. The linked matrix $P_1 = diag(p_1 \times (1 - \theta_{10}), p_2 \times (1 - \theta_{20}) \dots p_N \times (1 - \theta_{N0}))$. The topological matrix $H_1 = L_1 + P_1$. Similarly, H_2 implies the possibility of communication failure. $T_2 = [t_{ij} \times \theta_{ij}]$, The in-degree of node i is defined as $\underline{d}_i = \sum_{j=1}^{N} t_{ij} \times \theta_{ij}$. $D_2 = diag(\underline{d}_1, \underline{d}_2 \dots \underline{d}_N)$. L is defined as $L_2 = D_2 - T_2$. $P_2 = diag(p_1 \times \theta_{10}, p_2 \times \theta_{20} \dots p_N \times \theta_{N0})$. $H_2 = L_2 + P_2$. H_1 and H_2 are used in the controller design in the following section.

5.3.1 Platoon's Error Dynamics

The tracking errors are defined the same as (5.2) in Section 5.2. The error dynamics of the platoon can be written as:

$$\begin{aligned} \Delta\dot{p}_i(t) &= \Delta v_i(t) \\ \Delta\dot{v}_i(t) &= \Delta a_i(t) \\ \Delta\dot{a}_i(t) &= \frac{u_i(t)}{m_i\tau_i} + f\big(v_i(t), a_i(t)\big) - \dot{a}_0(t) \end{aligned} \tag{5.40}$$

The error dynamics can be expressed as:

$$\dot{e}_i(t) = Ae_i(t) + B\left(u_i(t) + g\big(v_i(t), a_i(t)\big)\right) + C[w_i(t) - \dot{a}_0(t)] \tag{5.41}$$

where

$$A = \begin{bmatrix} 0 & 1 & 0 \\ 0 & 0 & 1 \\ 0 & 0 & -\frac{1}{\tau_i} \end{bmatrix}, B = \begin{bmatrix} 0 \\ 0 \\ \frac{1}{m_i\tau_i} \end{bmatrix}, C = \begin{bmatrix} 0 \\ 0 \\ 1 \end{bmatrix}$$

$$e_i(t) = [\Delta p_i(t), \Delta v_i(t), \Delta a_i(t)]^T$$

$$g\big(v_i(t), a_i(t)\big) = -2K_{di}v_i(t)a_i(t)\tau_i - K_{di}v_i(t)^2 - d_{mi}$$

5.3.2 Discrete Sliding Mode Controller Design

This section provides the design of the discrete sliding mode controller. Firstly, it describes the discretisation model of the platoon. Then, it proposes the construction of the discrete sliding mode controller. Finally, it investigates the asymptotic and string stability of the platoon.

Considering the state of the platoon's leader as $x_0(t) = [p_0(t), v_0(t), a_0(t)]^T$, it can be obtained from the leader's dynamic model that:

$$\dot{x}_0(t) = A_0x_0(t) + B_0\dot{a}_0(t) \tag{5.42}$$

where

$$A_0 = \begin{bmatrix} 0 & 1 & 0 \\ 0 & 0 & 1 \\ 0 & 0 & 0 \end{bmatrix}, B_0 = \begin{bmatrix} 0 \\ 0 \\ 1 \end{bmatrix}$$

The discretisation of the leader vehicle is [108]:

$$x_0(k+1) = A_{d0}x_0(k) + B_{d0}u_0(k) \tag{5.43}$$

where

$$A_{d0} = e^{A_0\mathcal{T}}, B_{d0} = \int_0^{\mathcal{T}} e^{A_0\sigma}B_0 d\sigma$$

k counts the number of discrete signals starting from the initial time 0. $\mathcal{T}$ represents the sampling period. The fourth-order Runge-Kutta method [109] is employed to find the discretisation of the error dynamics (5.41) as follows:

$$\begin{gathered} k_1 = \dot{e}_i(k) \\ k_2 = \dot{e}_i\left(k + k_1\frac{\mathcal{T}}{2}\right) \\ k_3 = \dot{e}_i\left(k + k_2\frac{\mathcal{T}}{2}\right) \\ k_4 = \dot{e}_i(k + k_3\mathcal{T}) \\ e_i(k+1) = e_i(k) + \frac{\mathcal{T}}{6}(k_1 + 2k_2 + 2k_3 + k_4) \end{gathered} \tag{5.44}$$

Ignoring all terms with coefficients less than 10^{-5}, a linear discretisation model can be obtained here:

$$e_i(k+1) = A_d e_i(k) + B_d \tilde{u}_i(k) \tag{5.45}$$

where

$$\tilde{u}_i(k) = [u_i(k), w_i(k) - \dot{a}_0(k), 1]$$
$$B_d = [B_{d1}, B_{d2}, B_{d3}]$$

Defining the global error dynamic system as $E(k) = [e_1(k), e_2(k) \cdots e_N(k)]^T$, the global control input as $U(k) = [u_1(k), u_2(k) \cdots u_N(k)]^T$, and the global external disturbance as $W(k) = [w_1(k) - \dot{a}_0(k), w_2(k) - \dot{a}_0(k) \cdots w_N(k) - \dot{a}_0(k)]^T$, the discretisation of the global error dynamic system can be written as:

$$E(k+1) = A_D E(k) + B_{D1}U(k) + B_{D2}W(k) + B_{D3}1_N \tag{5.46}$$

where

$$A_D = I_N \otimes A_d, B_{D1} = I_N \otimes B_{d1}$$
$$B_{D2} = I_N \otimes B_{d2}, B_{D3} = I_N \otimes B_{d3}$$

The system's output error dynamics $Y(k)$ is defined to measure the spacing tracking performance:

$$Y(k) = B_{D4}E(k) \tag{5.47}$$

where $B_{D4} = I_N \otimes [1 \quad 0 \quad 0]$.

Inspired by [12], the lumped tracking error prediction $et_i(k)$ is defined as $et_i(k) = [ep_i(k), ev_i(k), ea_i(k)]^T$. Each term is defined as follows:

$$ep_i(k) = \left(1-\theta_{ij}\right)\sum_{j\epsilon\Pi_i} p_i(k) - p_j(k) - d_{ij} + \theta_{ij}\sum_{j\epsilon\Pi_i} p_i(k-1) - p_j(k-1) - d_{ij} \tag{5.48}$$

$$ev_i(k) = \left(1-\theta_{ij}\right)\sum_{j\epsilon\Pi_i} v_i(k) - v_j(k) + \theta_{ij}\sum_{j\epsilon\Pi_i} v_i(k-1) - v_j(k-1) \tag{5.49}$$

$$ea_i(k) = \left(1-\theta_{ij}\right)\sum_{j\epsilon\Pi_i} a_i(k) - a_j(k) + \theta_{ij}\sum_{j\epsilon\Pi_i} a_i(k-1) - a_j(k-1) \tag{5.50}$$

The global consensus error prediction $\xi(k)$ is defined as $\xi(k) = [et_1(k), et_2(k), \cdots, et_N(k)]^T$. It can be written as:

$$\xi(k) = \gamma_1 E(k) + \gamma_2 E(k-1) \tag{5.51}$$

where $\gamma_1 = H_1 \otimes I_3$, $\gamma_2 = H_2 \otimes I_3$. Then we can get:

$$\xi(k+1) = \gamma_1[A_D E(k) + B_{D1}U(k) + B_{D2}W(k) + B_{D3}1_N] + \gamma_2 E(k) \tag{5.52}$$

The sliding surface $s_i(k)$ for the following vehicles is selected as:

$$s_i(k) = Ket_i(k) \tag{5.53}$$

where $K = [K_1, K_2, K_3]$. They are the negative sliding gains to be determined. The sliding surface in the global form $S(k)$ can be written as:

$$S(k) = K_D\,[\gamma_1 E(k) + \gamma_2 E(k-1)] \tag{5.54}$$

where $S(k) = [s_1(k), s_2(k), \cdots, s_N(k)]^T$, $K_D = I_N \otimes K$. We can have:

$$S(k+1) = K_D\,[\gamma_1 E(k+1) + \gamma_2 E(k)] \tag{5.55}$$

Substituting (5.46) into (5.55), $S(k+1)$ can be expressed as:

$$S(k+1) = K_D\gamma_1[A_D E(k) + B_{D1}U(k) + B_{D2}W(k) + B_{D3}1_N] + K_D\gamma_2 E(k) \tag{5.56}$$

Inspired by the reaching law designed in [110], the global consensus double power reaching law is defined as follows:

$$S(k+1) = (I_N - Q\mathcal{T})S(k) - \Xi\mathcal{T}sign(S(k)) \tag{5.57}$$

where $Q = diag[q_1, q_2 \ldots q_N]$ >0, $\Xi = diag[\epsilon_1, \epsilon_2 \ldots \epsilon_N]$ >0. $1 > 1 - q_i\mathcal{T} > 0$. To reduce chattering in the discrete sliding mode controller, $sign(s_i(k))$ is defined as:

$$sign\left(s_i(k)\right) = \frac{s_i(k)}{\| s_i(k) \| + \sigma} \tag{5.58}$$

where $\sigma > 0$.

Substituting (5.55) into (5.57), it can be derived that:

$$K_D\gamma_1[A_D E(k) + B_{D1}U(k) + B_{D2}W(k) + B_{D3}1_N + K_D\gamma_2 E(k) = (I_N - Q\mathcal{T})S(k) - \Xi\mathcal{T} sign(S(k))$$

(5.59)

Rearranging (5.59), the global control input $U(k)$ can be computed as below:

$$U(k) = -(K_D\gamma_1 B_{D1})^{-1}[(K_D\gamma_1 A_D + K_D\gamma_2)E(k) + K_D\gamma_1 B_{D2}W(k) + K_D\gamma_1 B_{D3}1_N - (I_N - Q\mathcal{T})S(k) + \Xi\mathcal{T}sign\big(S(k)\big)]$$

(5.60)

The asymptotic stability of the platoon is proved firstly. Then the string stability is analysed using Lyapunov analysis and Riccati inequality. LMIs are computed subsequently.

The Lyapunov function is selected as:

$$\mathcal{V}_i(k) = s_i(k)^2$$

(5.61)

Therefore, the forward derivative function can be obtained:

$$\begin{aligned}\Delta\mathcal{V}_i(k) &= \mathcal{V}_i(k+1) - \mathcal{V}_i(k)\\ &= s_i(k+1)^2 - s_i(k)^2\\ &= (s_i(k+1) - s_i(k))(s_i(k+1) + s_i(k))\end{aligned}$$

(5.62)

For the platoon's asymptotical stability, it is required to ensure $\Delta\mathcal{V}_i(k) < 0$, which is equivalent to proving the following two inequalities:

$$\begin{aligned}s_i(k+1) + s_i(k) > 0\\ s_i(k+1) - s_i(k) < 0\end{aligned}$$

(5.63)

According to (5.57), the following holds:

$$\begin{aligned}s_i(k+1) - s_i(k) &= (1 - q_i\mathcal{T})s_i(k) + \epsilon_i\mathcal{T}sign\big(s_i(k)\big) - s_i(k)\\ s_i(k+1) + s_i(k) &= (1 - q_i\mathcal{T})s_i(k) + \epsilon_i\mathcal{T}sign\big(s_i(k)\big) + s_i(k)\end{aligned}$$

(5.64)

Substituting (5.64) into (5.63), it can be obtained that:

$$\begin{aligned}&q_i\mathcal{T}s_i(k) + \epsilon_i\mathcal{T}sign\big(s_i(k)\big) > 0 \qquad \text{for } i = 1,2 \dots N\\ &2 - q_i\mathcal{T}s_i(k) - \epsilon_i\mathcal{T}sign\big(s_i(k)\big) > 0 \qquad \text{for } i = 1,2 \dots N\end{aligned}$$

(5.65)

Therefore, the sufficient condition for achieving stability is described by (5.65). By tuning q_i and ϵ_i, the stability of the platoon can be established. The string stability is analysed as follows:

Lemma 5.1 [12],[96]: The platoon system is input-to-output $\mathcal{L}_2$ string stable if all inputs belong to $\mathcal{L}_2$ space, and the output error dynamics $Y(k)$ are once again in the $\mathcal{L}_2$ space for any platoon length $m \in \mathbb{N}$, with the $\mathcal{L}_2$ gain bounded by γ^2, as shown in below:

$$\sum_{k=0}^{\infty}\mathbb{E}\{\| Y(k) \|_{\mathcal{L}_2}\} \leq \gamma^2 \sum_{k=0}^{\infty}\mathbb{E}\{\| \widetilde{W}(k) \|_{\mathcal{L}_2}\}$$

(5.66)

The Lyapunov function is selected as:

$$V(k) = E^T(k)PE(k) + E^T(k-1)RE(k-1)$$

(5.67)

where P and R are positive definite matrices with appropriate dimensions. Substituting (5.60) into (5.46), it can be obtained that:

$$\begin{aligned} E(k+1) &= A_D E(k) + B_{D1}U(k) + B_{D2}W(k) + B_{D3}1_N \\ &= A_D E(k) - B_{D1}(K_D\gamma_1 B_{D1})^{-1}[(K_D\gamma_1 A_D + K_D\gamma_2)E(k) + K_D\gamma_1 B_{D2}W(k) + \\ &\quad K_D\gamma_1 B_{D3}1_N - (I_N - Q\mathcal{T})K_D\big(\gamma_1 E(k) + \gamma_2 E(k-1)\big) + \Xi\mathcal{T}sign(S(k))] \end{aligned}$$

(5.68)

(5.68) can be rearranged into:

$$\begin{aligned} E(k+1) = {} & [A_D - B_{D1}(K_D\gamma_1 B_{D1})^{-1}(K_D\gamma_1 A_D + K_D\gamma_2 - (I_N - Q\mathcal{T})K_D\gamma_1)]E(k) \\ & + [B_{D1}(K_D\gamma_1 B_{D1})^{-1}(I_N - Q\mathcal{T})K_D\,\gamma_2]E(k-1) \\ & + [-B_{D1}(K_D\gamma_1 B_{D1})^{-1}, -B_{D1}(K_D\gamma_1 B_{D1})^{-1}K_D\gamma_1 B_{D2} \\ & + B_{D2}\,, -B_{D1}(K_D\gamma_1 B_{D1})^{-1}K_D\gamma_1 B_{D3} + B_{D3}]\widetilde{W}(k) \end{aligned}$$

(5.69)

where $\widetilde{W}(k) = [\Xi Tsign\big(S(k)\big), W(k), 1_N]^T$. Reorganising (5.69), $E(k+1)$ can be written as:

$$E(k+1) = \mathrm{Z}_1 E(k) + \mathrm{Z}_2 E(k-1) + \mathrm{Z}_3\widetilde{W}(k)$$

(5.70)

where

$$\begin{aligned} \mathrm{Z}_1 &= A_D - B_{D1}(K_D\gamma_1 B_{D1})^{-1}[K_D\gamma_1 A_D + K_D\gamma_2 \\ &\qquad -(I_N - Q\mathcal{T})K_D\gamma_1] \\ \mathrm{Z}_2 &= B_{D1}(K_D\gamma_1 B_{D1})^{-1}(I_N - Q\mathcal{T})K_D\,\gamma_2 \\ \mathrm{Z}_3 &= [-B_{D1}(K_D\gamma_1 B_{D1})^{-1}, -B_{D1}(K_D\gamma_1 B_{D1})^{-1}K_D\gamma_1 B_{D2} \\ &\quad +B_{D2}\,, -B_{D1}(K_D\gamma_1 B_{D1})^{-1}K_D\gamma_1 B_{D3} + B_{D3}] \end{aligned}$$

(5.71)

The forward derivative function of the Lyapunov candidate can be obtained as:

$$\begin{aligned} \Delta V(k) = {} & V(k+1) - V(k) \\ & = E^T(k+1)PE(k+1) + E^T(k)RE(k) - E^T(k)PE(k) - E^T(k-1)RE(k-1) \end{aligned}$$

(5.72)

The upper bound of packet dropout rates ∂ is employed here instead of heterogeneous packet dropout rates to simplify the equation. Replacing γ_1 with $(1-\partial)(H \otimes I_3)$, γ_2 with $\partial(H \otimes I_3)$. Substituting (5.70) into (5.72), (5.72) can be rewritten as:

$$\begin{aligned} \Delta V(k) = {} & \big[\bar{\mathrm{Z}}_1 E(k) + \bar{\mathrm{Z}}_2 E(k-1) + \bar{\mathrm{Z}}_3\widetilde{W}(k)\big]^T P[\bar{\mathrm{Z}}_1 E(k) + \bar{\mathrm{Z}}_2 E(k-1) + \bar{\mathrm{Z}}_3\widetilde{W}(k)] \\ & + E^T(k)RE(k) - E^T(k)P\,E(k) - E^T(k-1)RE(k-1) \end{aligned}$$

(5.73)

where

$$H_D = H \otimes I_3$$

$$\bar{\mathrm{Z}}_1 = A_D - B_{D1}(K_D H_D B_{D1})^{-1}[K_D H_D A_D - (I_N - Q\mathcal{T})K_D H_D] + B_{D1}\frac{1-2\partial}{1-\partial}(K_D H_D B_{D1})^{-1}K_D H_D$$

$$\bar{\mathrm{Z}}_2 = B_{D1}\frac{\partial}{1-\partial}(K_D H_D B_{D1})^{-1}(I_N - Q\mathcal{T})K_D\, H_D$$

$$\bar{\mathrm{Z}}_3 = [-B_{D1}(K_D H_D B_{D1})^{-1}, -B_{D1}(K_D H_D B_{D1})^{-1}K_D H_D B_{D2} + B_{D2}\,, -B_{D1}(K_D H_D B_{D1})^{-1}K_D H_D B_{D3} + B_{D3}]$$

(5.74)

Taking the expectation value, (5.73) is converted into:

$$\mathbb{E}\{\Delta V(k)\} = \mathbb{E}[E^T(k) \quad E^T(k-1) \quad \widetilde{W}^T(k)] \times \begin{bmatrix} \mathrm{Z}_1{}^T P \mathrm{Z}_1 + R - P & \mathrm{Z}_1{}^T P \mathrm{Z}_2 & \mathrm{Z}_1{}^T P \mathrm{Z}_3 \\ * & \mathrm{Z}_2{}^T P \mathrm{Z}_2 - R & \mathrm{Z}_2{}^T P \mathrm{Z}_3 \\ * & * & \mathrm{Z}_3{}^T P \mathrm{Z}_3 \end{bmatrix} \times \mathbb{E}\begin{bmatrix} E(k) \\ E(k-1) \\ \widetilde{W}(k) \end{bmatrix}$$

(5.75)

The aim is to find sufficient LMIs to prove the following condition according to *Lemma 5.1*:

$$V(k+1) - V(k) + Y^T(k)Y(k) - \gamma^2 \widetilde{W}^T(k)\widetilde{W}(k) < 0$$

(5.76)

Taking the expectation value of (5.76), the following LMI holds:

$$\mathbb{E}\{\Delta V(k)\} + \mathbb{E}\{Y(k)Y(k) - \gamma^2 \widetilde{W}^T(k)\widetilde{W}(k)\} < 0$$

(5.77)

It can be obtained that:

$$\mathbb{E}\{Y^T(k)Y(k) - \gamma^2 \widetilde{W}^T(k)\widetilde{W}(k)\}$$

$$= \mathbb{E}[E^T(k) \quad E^T(k-1) \quad \widetilde{W}^T(k)] \times \begin{bmatrix} B_{D4}{}^T B_{D4} & 0 & 0 \\ * & 0 & 0 \\ * & * & -\gamma^2 \end{bmatrix} \times \mathbb{E}\begin{bmatrix} E(k) \\ E(k-1) \\ \widetilde{W}(k) \end{bmatrix}$$

(5.78)

Combining (5.75) with (5.78), (5.77) can be converted into:

$$\begin{bmatrix} \bar{\mathrm{Z}}_1{}^T P \bar{\mathrm{Z}}_1 + R - P + B_{D4}{}^T B_{D4} & \bar{\mathrm{Z}}_1{}^T P \bar{\mathrm{Z}}_2 & \bar{\mathrm{Z}}_1{}^T P \bar{\mathrm{Z}}_3 \\ * & \bar{\mathrm{Z}}_2{}^T P \bar{\mathrm{Z}}_2 - R & \bar{\mathrm{Z}}_2{}^T P \bar{\mathrm{Z}}_3 \\ * & * & \bar{\mathrm{Z}}_3{}^T P \bar{\mathrm{Z}}_3 - \gamma^2 I_{3N} \end{bmatrix} < 0$$

(5.79)

Using matrix factorisation method, (5.79) can be rewritten as:

$$\begin{bmatrix} R-P & 0 & 0 \\ * & -R & 0 \\ * & * & -\gamma^2 \end{bmatrix} + \begin{bmatrix} B_{D4}{}^T \\ 0 \\ 0 \end{bmatrix}[B_{D4} \quad 0 \quad 0] + \begin{bmatrix} \bar{\mathrm{Z}}_1{}^T \\ \bar{\mathrm{Z}}_2{}^T \\ \bar{\mathrm{Z}}_3{}^T \end{bmatrix} P [\bar{\mathrm{Z}}_1 \quad \bar{\mathrm{Z}}_2 \quad \bar{\mathrm{Z}}_3] < 0$$

(5.80)

Applying Schur complement [111] to (5.80) yields:

$$\begin{bmatrix} R-P & * & * & * & * \\ 0 & -R & * & * & * \\ 0 & 0 & -\gamma^2 & * & * \\ \bar{Z}_1 & \bar{Z}_2 & \bar{Z}_3 & -P^{-1} & * \\ B_{D4} & 0 & 0 & 0 & I_{3N} \end{bmatrix} < 0$$

(5.81)

Multiply both sides by $diag\{P^{-1}, P^{-1}, I_{3N}, I_{3N}, I_{3N}\}$. By defining $P^{-1}RP^{-1} = M, P^{-1} = \bar{P}, R^{-1} = \bar{R}$, new LMIs can be computed as follows:

$$\begin{bmatrix} -M & \bar{P} \\ * & -\bar{R} \end{bmatrix} \leq 0$$

(5.82)

$$\begin{bmatrix} M-\bar{P} & * & * & * & * \\ 0 & -M & * & * & * \\ 0 & 0 & -\gamma^2 & * & * \\ \bar{Z}_1\bar{P} & \bar{Z}_2\bar{P} & \bar{Z}_3 & -\bar{P} & * \\ B_{D4}\bar{P} & 0 & 0 & 0 & I_{3N} \end{bmatrix} < 0$$

(5.83)

Therefore, the sufficient condition for achieving string stability is described by (5.82-5.83). By finding feasible $\bar{P} = \bar{P}^T > 0 \in \mathbb{R}^{3N\times 3N}$, $\bar{R} = \bar{R}^T > 0 \in \mathbb{R}^{3N\times 3N}$, $M = \bar{P}R^{-1}\bar{P} \in \mathbb{R}^{3N\times 3N}$, scalar γ, and appropriate matrices K_D and H_D for LMIs (5.82-5.83), the platoon is guaranteed to be input-to-output $\mathcal{L}_2$ string stable.

Here are some remarks about the controller's configurable parameters K, q, ϵ, and σ. Table 5.6 displays the final values chosen after tuning.

Remark 1: K is the controller's gain that indicates the strength of the controller's response. Increasing the magnitude of K can increase control strength and precision. However, it also increases the system's computing complexity. K is chosen according to inequalities (5.82-5.83) to assure the platoon's string stability.

Remark 2: q substantially affects the controller's reaching speed and control precision. When q equals $\frac{1}{T}$, the approaching speed of the sliding surface reaches its fastest [112]. Therefore, a suitable value of q must be tuned to strike a balance between approaching speed and control precision.

Remark 3: ϵ also has a considerable effect on the approaching speed of the sliding surface. A higher value of ϵ improves the control accuracy while decreasing the computational difficulty. ϵ needs to be tuned according to the value of q and inequalities (5.65) to ensure the platoon's asymptotic stability.

Remark 4: σ is utilised in the $sign$ function and intended to eliminate the controller's chatter. The choice of σ represents a trade-off between control precision and chattering. Increased σ can reduce chattering at the expense of low control accuracy.

Remark 5: In conclusion, the controller's configurable parameters face a trade-off between control precision and the system's computing complexity. Firstly, a relatively large value for K should be chosen to ensure control accuracy, then q and ϵ should be tuned to increase the

controller's reaching speed while not compromising its performance. Finally, σ should be tuned to reduce chattering as much as possible.

Table 5.6 Controller's parameters

ϵ	K	q	σ	SDE	SVE
1.5	[-5,-10,-5]	0.05	6	50	20

Figure 5.4 summarises the overall framework of the proposed controller. The vehicle model, topology selection, and controller design are all illustrated in it.

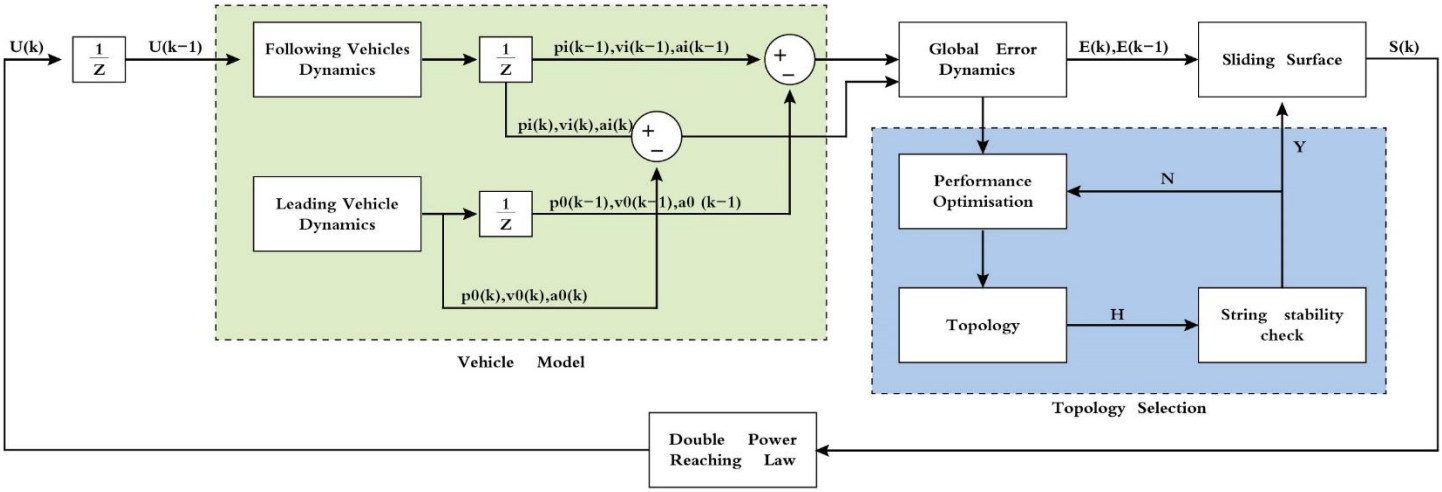

Figure 5.4 Controller's block diagram

5.3.3 Two-step Topology Switching Framework

The platoon's performance optimisation considers tracking ability, fuel economy, and driving comfort, which are the same as (3.5-3.9) in Chapter 3. The overall control objective is the same as (5.37) in Section 5.2.4. The proposed two-step topology switching framework is similar to the framework in Section 5.2.4. However, this section introduces a modified MOEA/D to improve the offline searching performance. MOEA/D has the benefit of being computationally efficient. However, premature convergence is quite common in MOEA/D when dealing with a substantial number of input variables. Inspired by [113], this section boosts the genetic operator of MOEA/D with two opposing adaptive mechanisms. The goal is to increase crossover and mutation rates when a superior solution is obtained. The opposing adaptive mechanism can successfully prevent the premature convergence problem. It promotes the concept that superior solutions can generate better solutions. The crossover rate P_{rc} and mutation rate P_{rm} update are as follows:

$$P_{rc} = \begin{cases} k_c \dfrac{\bar{f} - f_{min}}{f_c - f_{min}} & f_c \le \bar{f} \\ k_c & f_c > \bar{f} \end{cases} \tag{5.84}$$

$$P_{rm} = \begin{cases} k_m \dfrac{\bar{f} - f_{min}}{f_m - f_{min}} & f_m \le \bar{f} \\ k_m & f_m > \bar{f} \end{cases} \tag{5.85}$$

where k_c and k_m are the original crossover rate and mutation rate, they are set to be 0.3 and 0.2, respectively. $\bar{f}$ and f_{min} are the average and minimum fitness values of the population. f_c is the fitness value of the solution to be crossed, and f_m is the fitness value of the solution to be mutated.

Several common communication failure situations are predicted throughout the offline topology optimisation process. It includes vehicles encountering packet loss, unforeseen external disturbances, or losing connection with the leader. First, the system does an offline Pareto optimal topology search based on the anticipated communication failure situations. Then, a Pareto optimal topology is determined for each scenario, which will be utilised as candidates for online searching in the following step. When the platoon operates in real-time, the system conducts an online search within the Pareto optimal topology candidates. The online search is entirely based on the weighted sum approach described in (5.37), which is used to decide the ideal topology with minimal control cost.

5.3.4 Simulation Results

The hardware setup is the same as in Chapter 2. The proposed strategy and a robust discrete sliding mode controller [114] are tested and compared to prove the effectiveness of the proposed framework. Considering the urban road traffic scenario, the kinematic profile for the leader is the same as (5.38) in Section 5.2.5. The sampling period is set to be $\mathcal{T} = 0.1s$. Table 5.7 displays the starting location, velocity, and required distance between each vehicle and the leading vehicle.

Table 5.7 Initial states and desired gaps of each vehicle

Vehicle	Position (m)	Velocity (m/s)	Desired gap (m)
Leader	0	5	0
Vehicle 1	-18	4.8	-20
Vehicle 2	-41	5.2	-40
Vehicle 3	-63	4.7	-60
Vehicle 4	-79	4.5	-80
Vehicle 5	-97	5.5	-100
Vehicle 6	-121	4.6	-120
Vehicle 7	-142	4.7	-140
Vehicle 8	-157	5.4	-160
Vehicle 9	-178	5.1	-180
Vehicle 10	-201	4.9	-200

All vehicles in the platoon experience packet loss. The packet dropout rate between one

vehicle and the other increases as their physical distance increases. The upper bound of all packet dropout rates is set to be $\partial = 0.2$. They are updated at each discrete signal. The communication scenarios are designed the same as (5.39) in Section 5.2.5. The predecessor-leader following (PLF) topology is chosen for the robust discrete sliding mode controller [114]. It is widely used and has proven to be the effective in most research. For the proposed controller, Pareto optimal topology for each time interval is determined using the proposed framework. Table 5.8 displays the resultant Pareto optimal topology $\mho$.

Table 5.8 Pareto optimal information flow topology $\mho$ obtained offline

$$\mho_1 = \begin{bmatrix} 1 & 0 & 0 & 0 & 0 & 0 & 0 & 0 & 0 & 0 \\ 1 & 0 & 0 & 0 & 0 & 0 & 0 & 0 & 0 & 0 \\ 0 & 0 & 1 & 0 & 0 & 0 & 0 & 0 & 0 & 0 \\ 0 & 1 & 1 & 1 & 0 & 0 & 0 & 0 & 0 & 0 \\ 1 & 0 & 0 & 0 & 0 & 0 & 0 & 0 & 0 & 0 \\ 1 & 0 & 1 & 1 & 0 & 1 & 0 & 0 & 0 & 0 \\ 1 & 1 & 1 & 1 & 0 & 0 & 1 & 0 & 0 & 0 \\ 1 & 0 & 0 & 1 & 1 & 1 & 1 & 0 & 0 & 0 \\ 1 & 0 & 1 & 1 & 1 & 0 & 0 & 0 & 1 & 0 \\ 1 & 0 & 1 & 1 & 0 & 1 & 1 & 1 & 1 & 0 \end{bmatrix} \quad \mho_2 = \begin{bmatrix} 1 & 0 & 0 & 0 & 0 & 0 & 0 & 0 & 0 & 0 \\ 1 & 1 & 0 & 0 & 0 & 0 & 0 & 0 & 0 & 0 \\ 0 & 0 & 1 & 0 & 0 & 0 & 0 & 0 & 0 & 0 \\ 0 & 1 & 0 & 1 & 0 & 0 & 0 & 0 & 0 & 0 \\ 1 & 0 & 0 & 0 & 0 & 0 & 0 & 0 & 0 & 0 \\ 1 & 0 & 0 & 0 & 0 & 1 & 0 & 0 & 0 & 0 \\ 0 & 1 & 0 & 1 & 0 & 0 & 0 & 0 & 0 & 0 \\ 0 & 0 & 0 & 0 & 1 & 1 & 0 & 0 & 0 & 0 \\ 1 & 1 & 0 & 0 & 0 & 0 & 0 & 0 & 1 & 0 \\ 0 & 0 & 0 & 1 & 1 & 0 & 1 & 0 & 1 & 1 \end{bmatrix}$$

$$\mho_3 = \begin{bmatrix} 1 & 0 & 0 & 0 & 0 & 0 & 0 & 0 & 0 & 0 \\ 1 & 0 & 0 & 0 & 0 & 0 & 0 & 0 & 0 & 0 \\ 0 & 0 & 1 & 0 & 0 & 0 & 0 & 0 & 0 & 0 \\ 0 & 1 & 0 & 1 & 0 & 0 & 0 & 0 & 0 & 0 \\ 1 & 0 & 0 & 0 & 0 & 0 & 0 & 0 & 0 & 0 \\ 0 & 0 & 0 & 1 & 0 & 1 & 0 & 0 & 0 & 0 \\ 0 & 1 & 0 & 1 & 1 & 0 & 1 & 0 & 0 & 0 \\ 0 & 1 & 0 & 0 & 1 & 0 & 0 & 1 & 0 & 0 \\ 1 & 0 & 0 & 1 & 1 & 0 & 1 & 0 & 1 & 0 \\ 0 & 0 & 1 & 1 & 1 & 0 & 1 & 0 & 0 & 1 \end{bmatrix} \quad \mho_4 = \begin{bmatrix} 1 & 0 & 0 & 0 & 0 & 0 & 0 & 0 & 0 & 0 \\ 1 & 0 & 0 & 0 & 0 & 0 & 0 & 0 & 0 & 0 \\ 0 & 0 & 1 & 0 & 0 & 0 & 0 & 0 & 0 & 0 \\ 1 & 1 & 1 & 0 & 0 & 0 & 0 & 0 & 0 & 0 \\ 1 & 0 & 0 & 0 & 1 & 0 & 0 & 0 & 0 & 0 \\ 1 & 0 & 1 & 1 & 0 & 1 & 0 & 0 & 0 & 0 \\ 1 & 0 & 1 & 0 & 0 & 0 & 0 & 0 & 0 & 0 \\ 1 & 0 & 1 & 0 & 1 & 1 & 0 & 0 & 0 & 0 \\ 1 & 0 & 1 & 0 & 0 & 1 & 0 & 1 & 1 & 0 \\ 0 & 0 & 1 & 0 & 0 & 0 & 1 & 1 & 0 & 0 \end{bmatrix}$$

Table 5.8 shows the offline Pareto optimal topology searching results for each time interval. The resulting topologies avoided the anticipated communication failure to some extent. For example, Vehicle 3 was subjected to external disturbances from $t = 250s$ to $t = 400s$, the Pareto optimal topology $\mho_2$ demonstrates that no following vehicles chose to receive information from Vehicle 3 in the period mentioned above. Vehicle 6 was also subjected to external disturbances from $t = 400s$ to $t = 500s$. Similarly, $\mho_3$ shows that no following vehicles chose to connect with Vehicle 6 over the period mentioned above. Apart from Vehicle 3 and Vehicle 6, the rest of the platoon is completely uninfected by external disturbances due to switching topology. It dramatically reduced the negative impact of external disturbances on the platoon. Vehicle 2 and vehicle 4 lost contact with the leader from $t = 500s$ to $t = 600s$. $\mho_4$ shows that only vehicle 4 chose to receive information from Vehicle 2, and only Vehicle 6 chose to receive information from vehicle 4. To avoid the negative communication impact, all other vehicles in the platoon avoided making connections with Vehicle 2 and Vehicle 4.

The platoon's trajectory with the proposed switching topology strategy is presented in Figure

5.5. The platoon travelled over $6000m$ from its starting point. It went through several stages of acceleration and deceleration. Nevertheless, it kept desired inter-vehicle gaps the whole time. Figure 5.6 depicts the platoon's velocity profile when using the proposed approach. The platoon accelerated from $t = 300s$, reached its maximum velocity at $t = 350s$ and travelled at high speed for 200 seconds. It slowed down at $t = 550s$ and maintained a low and constant speed at $t = 600s$. CAVs' velocities varied in the first five seconds because of the different initial state values but quickly reached consensus in the next five seconds. After that, they converged to the leader's velocity with slight variation throughout the entire time. The smoothness of the platoon's trajectory and velocity profile demonstrate the efficacy of the proposed strategy.

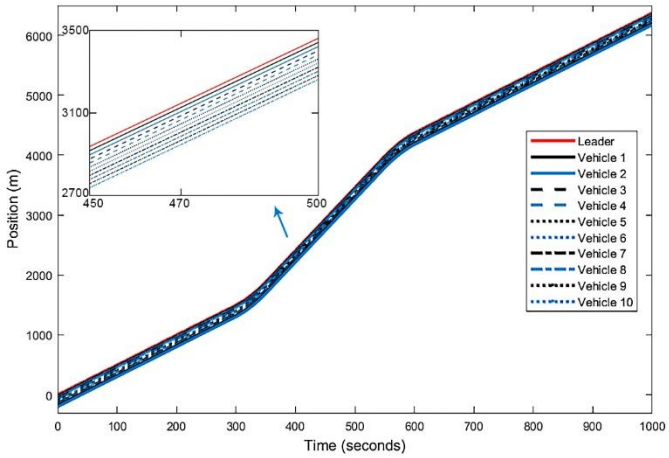

Figure 5.5 Platoon's trajectory with proposed strategy

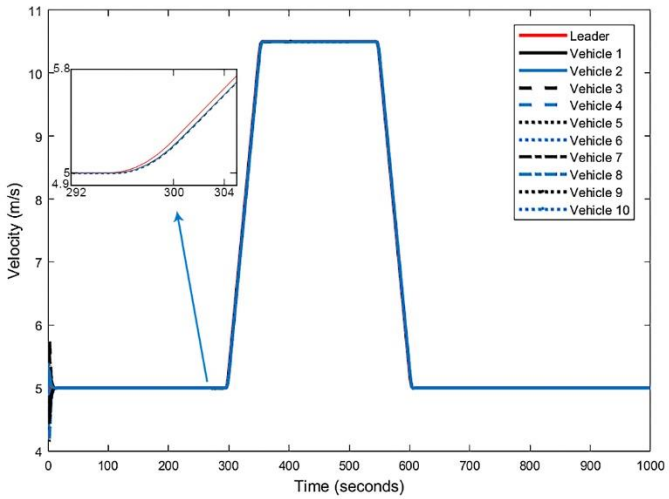

Figure 5.6 Platoon's velocity profile with proposed strategy

Figure 5.7 depicts the platoon's spacing error for the proposed method and the robust discrete sliding mode controller [114]. The robust controller [114] effectively managed the spacing errors until $t = 250s$. From $t = 250s$ to $t = 550s$, all spacing errors exhibited substantial fluctuation and poor converging ability. Vehicle 3 and Vehicle 6 performed the worst due to external disturbances. Their spacing errors converged to $-2m$, while the rest of the platoon converged to $-1m$. all spacing errors were reduced and converged to $\pm 0.1m$ after $t = 610s$. The robust

controller [114] was ineffective when dealing with external disturbance. On the other hand, the proposed strategy significantly reduced all spacing errors. From $t = 250s$ to $t = 600s$, spacing errors significantly decreased, with all values converging to $\pm 0.1m$. Although the impact of external disturbances on Vehicle 3 and Vehicle 6 was still visible but kept to a manageable and acceptable level. The switching topology process also reduced the influence of Vehicle 3 and Vehicle 6 on the rest of the platoon.

Figure 5.8 depicts the platoon's velocity error for the robust discrete sliding mode controller [114] and the proposed method. The variations of velocity errors with the two controllers were similar. First, the velocity errors increased at $t = 300s$, converged to a small negative constant, decreased at $t = 350s$, and fluctuated around 0 until $t = 550s$. Then, the velocity errors increased again and converged to a small positive constant until $t = 600s$. After that, the velocity errors decreased and converged to almost zero till the end.

However, the velocity error curves for the two controllers substantially differed. The robust controller [114] produced abrupt and sharp velocity errors in Vehicle 3 and Vehicle 6 at $t = 250s$, $t = 400s$, and $t = 500s$. In contrast, the proposed controller always kept them within a reasonable range. It demonstrates that vehicles with external disturbances were susceptible to the leader's change in speed with the robust controller [114], which caused unnecessary jerks in the velocity profile. The proposed controller overcame the shortcoming. It generated smoother curves for all vehicles in the platoon, which benefits safety and driving comfort. In conclusion, the proposed method helps maintain stability and lower platoon spacing and velocity errors. It is especially beneficial when dealing with external disruptions.

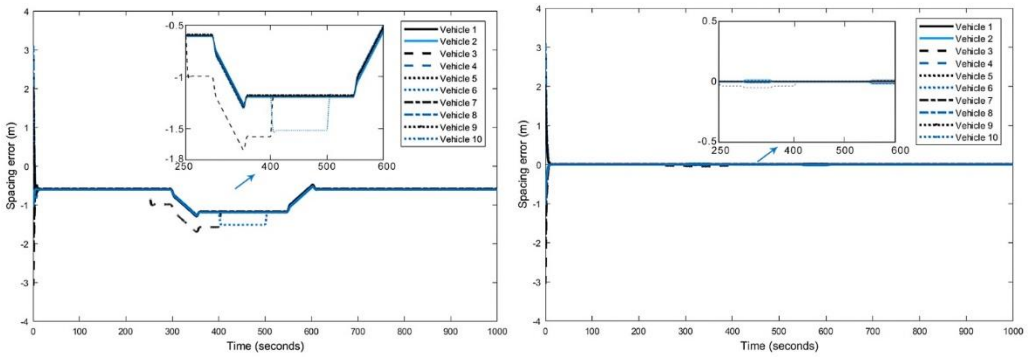

(a) (b)

Figure 5.7 Spacing errors. (a) Robust controller [114]; (b) Proposed controller

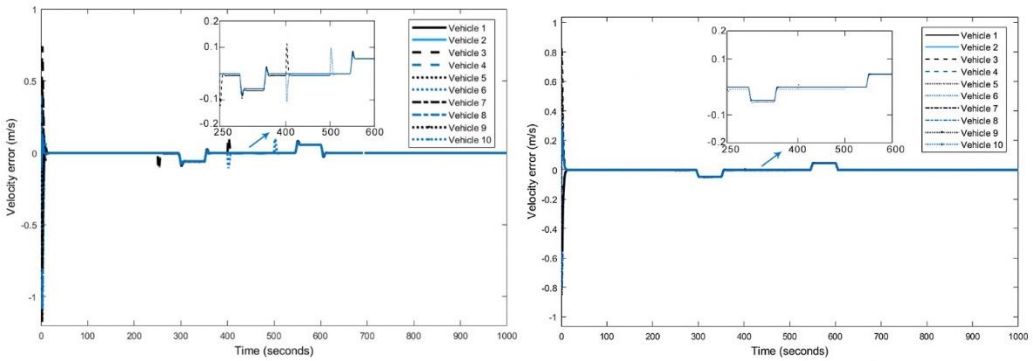

(a) (b)

Figure 5.8 Velocity errors. (a) Robust controller [114]; (b) Proposed controller

Table 5.9 compares three performance indices between the robust method [114] and the proposed method, using Vehicles 1, 5, and 10 as examples. Table 5.10 summarises the platoon's performance in each time interval using the switching topology approach.

Table 5.9 Performance comparison for different controllers

Performance Index	Information flow topology	Vehicle 1	Vehicle 5	Vehicle 10	Platoon Overall
TI	Robust	37.77	37.56	38.1	382
	Proposed	**0.6969**	**1.099**	**0.6168**	**8.655**
FC	Robust	0.6059	0.6054	0.6055	6.664
	Proposed	**0.5538**	**0.5115**	**0.5205**	**6**
ASD	Robust	0.0422	0.0605	0.0369	0.0446
	Proposed	**0.0257**	**0.0719**	**0.0168**	**0.0356**
Control Cost	Robust	1141.3	1129.6	1161.3	11674
	Proposed	**0.419**	**0.993**	**0.331**	**63.53**

Table 5.10 Performance under switching topology in each time interval

Time / Criterion	0-250 (s)	250-400 (s)	400-500 (s)	500-600 (s)	600-1000 (s)
TI	3.4221	4.2099	3.2062	3.8157	8.6547
FC	1.6561	1.0231	0.6637	0.6624	5.999
ASD	0.0451	0.0805	0.0712	0.0936	0.0356
Cost	**9.6431**	**14.2838**	**8.2681**	**11.6926**	**63.5233**

Table 5.9 shows that switching topology significantly reduced all vehicles and the platoon's tracking index, resulting in stronger tracking ability. In addition, all vehicles and the platoon consumed less fuel, demonstrating superior fuel efficiency. Furthermore, they all had lower acceleration standard deviation values, indicating improved driving comfort. In conclusion, the proposed method improved tracking ability, fuel consumption and driving comfort by 97.73 percent, 9.96 percent, and 20.18 percent, respectively. Moreover, it has the most significant impact on tracking ability. Table 5.10 summarises the platoon's performance over various time intervals. Tracking ability, fuel economy, and driving comfort are all superior and consistent with switching topology. Furthermore, when communication is normal, driving comfort is optimal.

5.4 Conclusion

This section consists of two parts. The first part investigates a nonlinear platoon with actuator faults. The second part studies a discrete nonlinear platoon with packet loss. By introducing switching topology, multi-objective switching topology sliding mode controllers for CAVs are proposed. This chapter develops a topology switching framework that deals with poor communication and improves the platoon's overall performance. Firstly, it searches for Pareto optimal topology offline with predicted imperfect communication scenarios. Then, the platoon's overall performance is optimised using modified MOEA/D. The optimal topology is selected and switched in real-time to reduce the control cost. The proposed method maximises the advantages of information flow topology. The modified MOEA/D overcomes the sensitivity and optimality barriers while giving flexible solutions that adapt to the platoon's priorities. The simulation is performed on a platoon of eleven heterogeneous vehicles. It compared the proposed approach to a robust sliding mode controller and fixed information flow topology to demonstrate the advantage. Poor communication situations, such as persistent packet loss, external disruptions, and disconnection from the leader, are anticipated and applied to different time intervals. The proposed approach is suitable for road segments where traffic and weather conditions are predictable over a specific time. The results indicate that the proposed strategy efficiently reduced spacing and velocity errors while enhancing the platoon's overall performance. The next chapter introduces all experiments conducted.

Chapter 6

Experiments

6.1 Introduction

The previous chapter proposes a two-step information flow topology switching framework. First, advanced sliding mode controllers and modified MOEA/D are proposed to deal with the platoon with actuator faults and packet loss. As a result, the proposed method can effectively deal with anticipated poor communication situations, such as persistent packet loss, external disruptions, and disconnection from the leader. Next, this chapter details the experiments conducted using an Arduino robot car. Hardware components are introduced at first. Then this chapter presents the results of the experiments from validating some chapters in this thesis.

6.2 Experimental Setup

Figure 6.1 shows the experiment setup, which is an Arduino robot car. It moves automatically with programming codes in the microcontroller. It can also communicate with other Arduino robot cars with wireless communication sensors. Therefore, it is selected as the experiment equipment. The motors enable motions in different directions. The battery provides a power supply on demand. The wireless communication sensor achieves wireless communication between different Arduino robot cars. The Ultrasonic sensor measures the spacing error, and a servo motor is attached, which turns the position of the ultrasonic sensor in case of curve motion. The accelerometer and gyroscope sensor is used to facilitate linear motion. It measures the pitch, roll, and yaw data, enabling a closed-loop control to ensure the Arduino robot car moves in a straight line precisely. The line tracking sensor controls lateral motion and checks if the Arduino robot car leaves the ground. Finally, the Arduino Uno Board is used as the microcontroller, with an expansion board that stacks on top of it to expand the number of interface pins for practicality purposes. Figure 6.2 presents the Arduino robot car in more views.

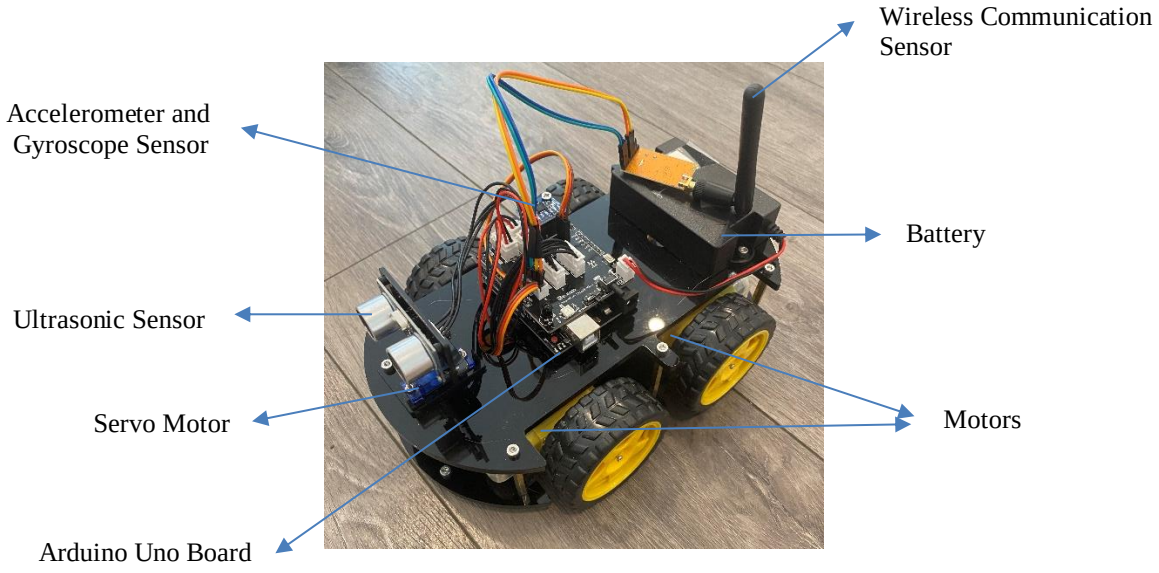

Figure 6.1 Arduino robot car

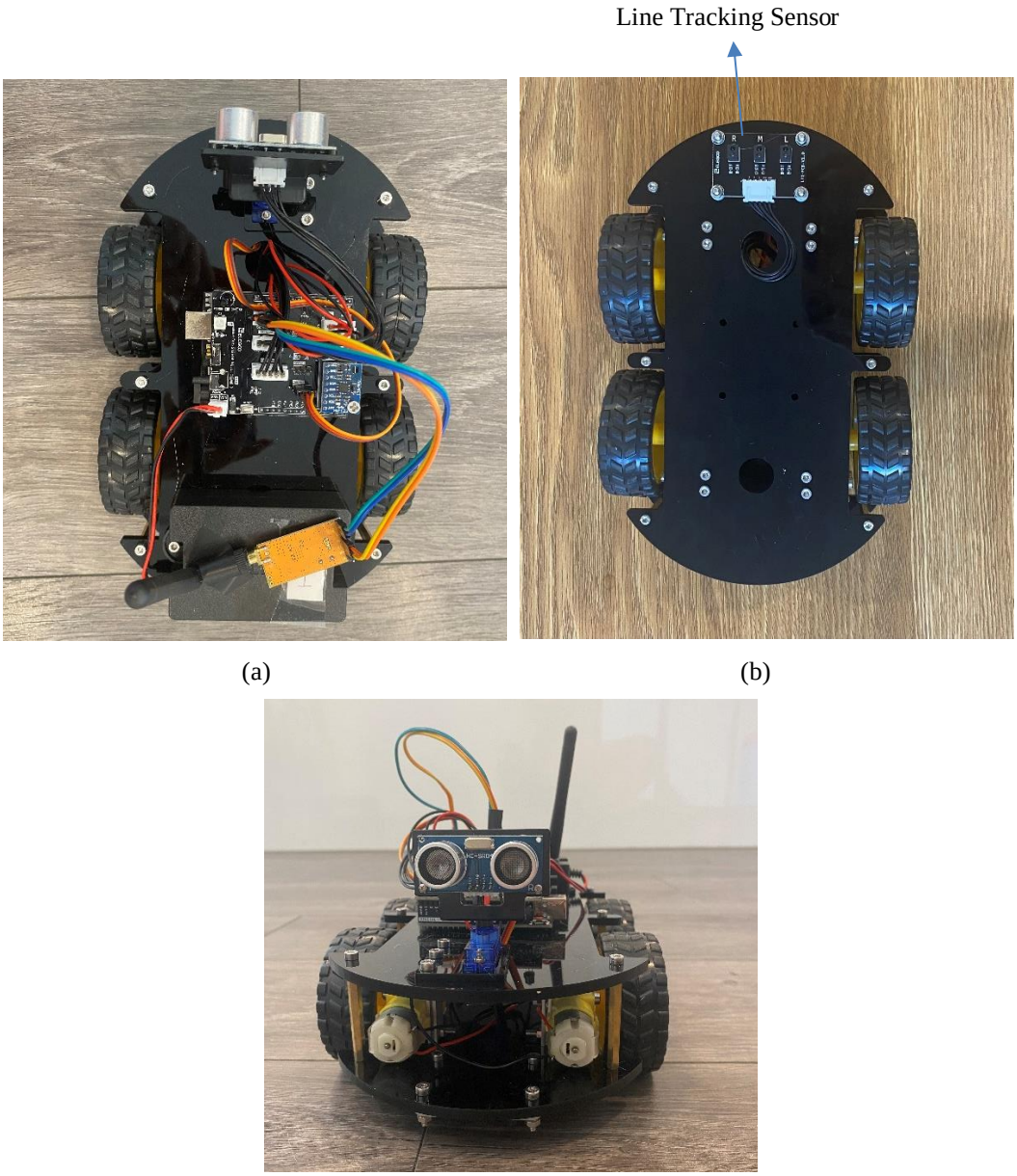

Figure 6.2 Arduino robot car in more views. (a) Top view; (b) Bottom view; (c) Front view

Here are detailed descriptions of some of the most critical hardware components. In motion control, the Direct Current (DC) motor driver is attached to the expansion board of the Arduino Uno board. It supplies direct current to two motors simultaneously. With different numbers applied to pins AIN1 and BIN1, the Arduino robot car can move in eight different directions, including forward, backward, left, right, left forward, left backward, right forward, and right backward. Pins PWMA and PWMB control the speed of the motion. An accelerometer and gyroscope sensor are used to ensure the car moves in a straight line. The angular velocity can be obtained with the original sensor data and the sensitivity scaling factor. Then the yaw value can be computed. With a closed-loop controller, the motion is constantly corrected by controlling the yaw

value. Therefore, the car moves straightly precisely.

In terms of lateral motion control, a line tracking sensor is attached to the middle of the bottom of the Arduino robot car. The sensor consists of an infrared pair tube and an NPN silicon phototransistor. It detects the change of ground light and the presence of close objects. It is displayed in Figure 6.2 (b), where the letters R, M, and L stand for Right, Middle, and Left photoelectric sensors. They are directly connected to three analog pins, A0, A1 and A2. Each photoelectric sensor returns data based on the light and shade it detected. The line tracking sensor is used to check if the Arduino robot car leaves the ground and whether the middle of the sensor is on the black line. By predefining the range limits of the data from photoelectric sensors, the Arduino robot car is programmed to move right if it is on the left side of the black line and move left if it is on the right side of the black line. Therefore, the line tracking sensor can achieve lateral motion control by ensuring the middle of the Arduino robot car consistently stays on the black line.

In terms of measuring distance, the ultrasonic sensor is in use. It can be seen from Figure 6.2 (c) that it is located at the front of the Arduino robot car. Pins D12 and D13 are defined as the trigger pin and echo pin, respectively. The ultrasonic sensor emits ultrasonic waves, which travel and return as soon as it encounters obstacles. Therefore, the distance between the ultrasonic sensor and the closest obstacle can be computed according to the ultrasonic propagation speed and the recorded time. Therefore, it can be used to measure the spacing errors in the platoon between two consecutive cars.

Regarding wireless communication within the platoon, multiple wireless communication sensors are used to establish information exchange between the Arduino robot cars or between the Arduino robot car and the computer. It is a highly integrated semi-duplex low-power transceiver module that comes in pairs. By connecting the RXD and TXD pins correctly in the Arduino Uno board and setting up the same serial baud rate in the Arduino interface, the wireless communication sensor can transmit and receive data between Arduino robot cars. Likewise, by plugging it into the computer via USB and setting up the same serial baud rate, the computer can send to or receive data from the Arduino robot car. Table 6.1 summarises all hardware components, their models, and their brief descriptions.

Table 6.1 List of hardware

Hardware Component	Model	Description
Direct Current (DC) motor driver device	TB6612	It supplies direct current to two motors simultaneously.
Accelerometer and gyroscope sensor	MPU6050	It measures pitch, roll, and yaw data.
Line tracking sensor	ITR20001	It detects the change of ground light and the presence of close objects.
Ultrasonic Sensor	HC-SR04	It emits ultrasonic waves and records the time.
Wireless communication sensor	APC220	It transmits and receives data.
Arduino board	Uno	It is the microcontroller.

Lithium battery with cell box	-	It supplies direct current, and it is chargeable.
Servo motor	SG90 9g	It rotates 180 degrees.

6.3 Experiments Results

This section uses experiments to validate the theory proposed in Section 4.3 and Section 5.2. All codes are programmed in C++ language in the Arduino interface. The platoon consists of three Arduino robot cars, with one leader and two followers. The line tracking sensor conducts lateral motion control, where all Arduino robot cars follow the black line consistently. Regarding the longitudinal motion, the controllers (4.65,5.12) proposed in Section 4.3 and Section 5.2 are in use. The following cars are expected to track the leading car at a constant speed of $10\ cm/s$, the inter-vehicle gap should be kept at $20\ cm$.

The PLF information flow topology is used to validate the controller (4.65) proposed in Section 4.3. In addition, a simulation was run prior to the experiment to discover the heterogeneous Pareto optimal asymmetric degrees for Vehicles 1 and 2. They are 5.8978% and 12.6523%, respectively. Finally, the platoon with symmetric and asymmetric control strategies under PLF topology is tested and compared.

Figure 6.3 shows the spacing and velocity errors under the symmetric controller, while figure 6.4 shows the same under the heterogeneous asymmetric controller. For spacing error, it can be seen that Vehicle 1 has better tracking ability than Vehicle 2 in general. Vehicle 1 displays some fluctuations in the spacing error around $4s$ to $6s$ with the symmetric controller, while it gets reduced to zero in the same time interval with the asymmetric controller. On the other hand, Vehicle 2 has negative spacing errors almost the entire time with the symmetric controller, which indicates that it follows Vehicle 1 too close and might compromise the platoon's safety in the long run. However, the spacing error of Vehicle 2 fluctuates around $-3cm$ to $4cm$ with the asymmetric controller, indicating its fast response to the controller. Regarding velocity error, the asymmetric controller performs better than the symmetric controller. Vehicle 1 has a perfect velocity tracking record for more than half of the experiment time with the asymmetric controller, where the velocity error is zero. Vehicle 2 performs differently with the two controllers. It is faster than the desired speed most of the time, which can be undesirable for safety concerns. With the asymmetric controller, it is faster than the desired speed at first, then quickly reaches consensus after $6s$, and experiences slight fluctuations at the end. In conclusion, the heterogeneous Pareto optimal asymmetric controller generally reduces the platoon's spacing and velocity errors. It also improves the platoon's safety.

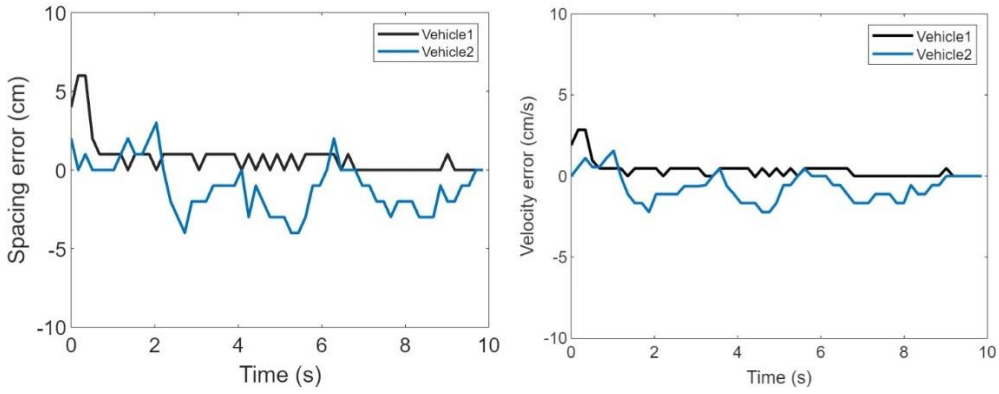

(a) (b)

Figure 6.3 Symmetric controller. (a) Spacing error; (b) Velocity error

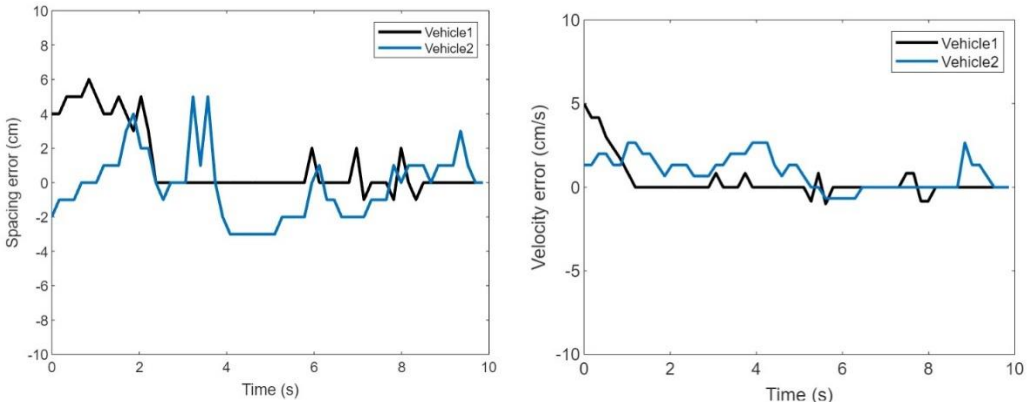

(a) (b)

Figure 6.4 Asymmetric controller. (a) Spacing error; (b) Velocity error

The accumulations of the spacing and velocity errors are displayed in Table 6.2 to study the experiment results quantitatively. According to the results shown in Table 6.2, it can be concluded that both vehicles' spacing and velocity errors are reduced with the asymmetric controller. Therefore, the effectiveness of the controller (4.65) proposed in Section 4.3 is proven.

Table 6.2 Accumulations of the spacing and velocity errors for Section 4.3

	Accumulation of the spacing error		Accumulation of the velocity error	
Vehicle number / Controller	Vehicle 1	Vehicle 2	Vehicle 1	Vehicle 2
Symmetric	69	92	26.33	57.33
Asymmetric	44	86	21.45	51.6

The controller (5.12) proposed in Section 5.2 is tested here. The desired constant speed and inter-vehicle gap are the same as before. Given that the platoon size is small, only external disturbance (5.39) is applied to Vehicle 1 in the first 5 seconds. Therefore, Vehicles 1 and 2 normally communicate with the leading vehicle during the experiment. PF information flow topology is used as the fixed topology and tested first. For the proposed framework, a simulation

was run prior to the experiment to discover the Pareto optimal information flow topology, which is the PLF topology in this case particularly. Therefore, PLF topology will apply to the platoon in the first five seconds. Then the platoon uses PF topology for the remaining experiment. Comparisons are made to highlight the advantages of the proposed two-step topology switching framework.

Figure 6.5 shows the spacing and velocity errors under the fixed, while Figure 6.6 shows the same under the switching topology. It can be observed that Vehicle 2 performs better than Vehicle 1 in general because Vehicle 1 suffers from the external disturbance in the first five seconds. Regarding the spacing error, Vehicle 2 generates smoothers curves with less fluctuation under the switching information flow topology, where the spacing error is reduced to zero from $3s$ to $4s$ and from $6s$ to $7s$. On the other hand, Vehicle 2 has more abrupt changes in its spacing error under the fixed information flow topology, indicating weak tracking ability. Vehicle 1 also generates smoother curves with switching topology. In terms of velocity error, it can be observed that, with switching topology, both Vehicles 1 and 2 can reach consensus for almost half of the time, while Vehicle 1 is shown to be slower than the desired speed, and Vehicle 2 is shown to be faster than the desires speed for the majority of the time. It can be concluded from Figure 6.6 that the spacing and velocity errors are reduced to an extent after $5s$, where the topology is switched from PF to PLF information flow topology, proving the proposed framework's effectiveness.

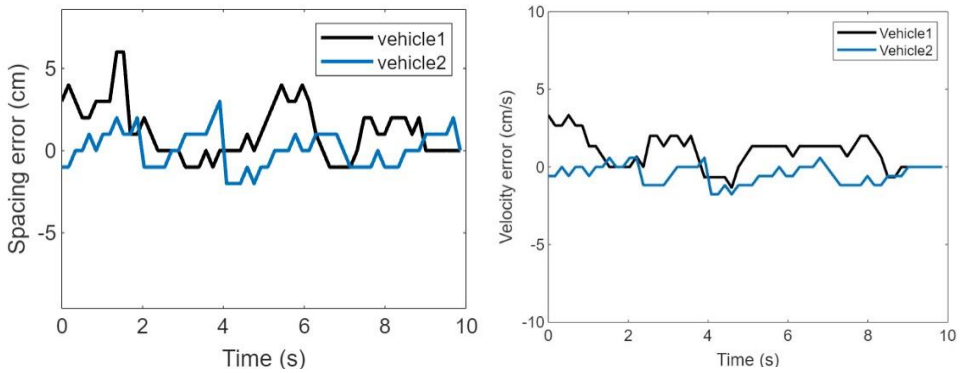

(a) (b)

Figure 6.5 Fixed information flow topology. (a) Spacing error; (b) Velocity error

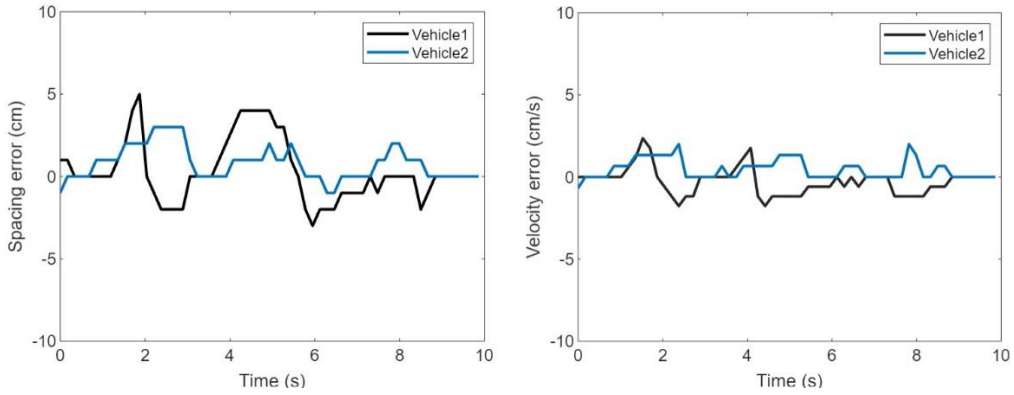

(a) (b)

Figure 6.6 Switching information flow topology. (a) Spacing error; (b) Velocity error

The accumulations of the spacing and velocity errors are displayed in Table 6.3 to investigate the experiment results. According to Table 6.3, it can be seen that both vehicles' spacing and velocity errors are reduced with the switching information flow topology. Moreover, the velocity error of Vehicle 2 is reduced significantly, which proves the effectiveness of the controller (5.12) proposed in Section 5.2 is proven. Figure 6.7 shows the platoon with three Arduino robot cars during the experiment.

Table 6.3 Accumulations of the spacing and velocity errors for Section 5.2

	Accumulation of the spacing error		Accumulation of the velocity error	
Vehicle number / IFT	Vehicle 1	Vehicle 2	Vehicle 1	Vehicle 2
Fixed	86.5	52.5	55.3	33.24
Switching	74.5	51.5	35.29	28.33

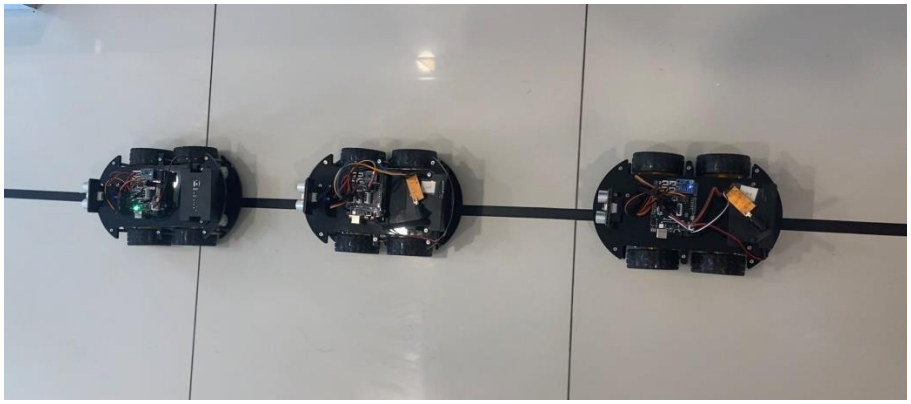

Figure 6.7 Platoon in the experiment

6.4 Conclusion

This chapter details the experiments conducted in this study. Firstly, the Arduino robot car is introduced, and detailed descriptions of crucial sensors are given, including the line tracking sensor, the wireless communication sensor, the ultrasonic sensor, the DC motor driver, and the accelerometer and gyroscope sensor. Then, a platoon consisting of three Arduino robot cars is presented in the experiment, where each Arduino robot car represents a CAV in the study. Next, two experiments are conducted to validate the controller (4.65,5.12) proposed in Section 4.3 and Section 5.2. The resulting figures regarding the spacing and velocity errors are displayed. Two tables show the accumulations of the spacing and velocity errors in both experiments. As a result, the proposed controllers can reduce spacing and velocity errors effectively. The next chapter gives conclusions and implications of the study and then makes future recommendations.

Chapter 7

Conclusion and Future Work

7.1 Introduction

The previous chapter introduces some experiments conducted. This chapter gives some discussion and conclusion, details the contribution and implications of this research, and discusses the future research direction.

7.2 Discussion and Conclusion

This thesis focuses on the information flow topology of CAVs, where the fixed, asymmetric, and switching information flow topologies are studied and sliding mode controllers that deal with different problems of the platoon are proposed. Some discussion and conclusion of each part of this research are listed as follows:

Firstly, information flow topology has always been regarded as one of the most critical aspects of the platoon. It significantly impacts the platoon's convergence time, stability, and scalability. However, studies have yet to examine the influence of information flow topology on the platoon's performance systematically and quantitatively. Chapter 3 fills the gap by investigating the impact of both conventional and innovative topologies on the platoon's performance and uses multiple evaluation criteria to assess the platoon's performance. As a result, the platoon's performance regularities were discovered and concluded in a broad view with clear evidence of consistency. For example, the smoothness of the velocity profile and fuel economy are consistent, whereas driving comfort, fuel efficiency and communication efficiency are in direct opposition to tracking ability.

Secondly, most studies design the controller based on one or a few fixed information flow topologies, which is not practical in real-world applications. For example, if communication gets interrupted unexpectedly, which is very common in real life, the controller will break down immediately. Therefore, it is vital to design a controller that supports the majority of information flow topologies to avoid the above situation. Although switching information flow topology research has grown in popularity in recent years, previous studies focused solely on switching among a few traditional topologies with random switching signals, compromising the platoon's performance and posing unnecessary risks to its stability. Other studies conduct the topology switching process entirely offline, reducing its practicality while proving energy-consuming. Chapter 5 proposed a two-step framework to balance the trade-off between online and offline searching. When both searching processes are combined, superior topology solutions are preserved with offline searching first. Computation time and energy are significantly reduced with online searching. The proposed framework can quickly deal with predictable imperfect communication scenarios in real time while providing a satisfying topology switching solution. Moreover, the advantages of information flow topologies should be utilised fully. Thus, the Pareto

optimal information flow topology concept is introduced in Chapters 3, 4, and 5. Rather than studying a few fixed topologies or artificially creating a new topology, Chapters 3, 4, and 5 find the Pareto optimal information flow topology to improve the platoon's overall performance.

Thirdly, the state-of-the-art has several drawbacks in the context of the platoon's multi-objective optimisation. MPC is the most frequently used strategy, but it still has limitations. A limited number of fixed weighting coefficients face the trade-off between sensitivity and optimality. Then, dynamic weighting coefficients heavily rely on the inter-vehicle states, which means the platoon might be compromised with any information feedback delay. Moreover, using normalisation in optimisation problems, such as the utopia point, can only obtain a single optimal solution. What is more, it is impossible to find the optimal information flow topology based on traditional methods since there is no linear mathematical model and regularity between all input variables and the resulting topological matrix eigenvalue. Thus, this problem cannot use any heuristic solutions. This research uses evolutionary algorithms to overcome the above limitations. As a metaheuristic method, the evolutionary algorithm has been famous for solving complex problems that cannot use heuristic solutions. The primary principle of the evolutionary algorithm is that only the fittest individual survives. Besides, evolutionary algorithms have many advantages, including flexibility, robustness, and human expertise independence. Chapter 3 and 4 uses NSGA-II to find the Pareto optimal information flow topology with asymmetric degrees. A modified MOEA/D that incorporates two opposing adaptive mechanisms is in use in Chapter 5 to improve the search strategy. The proposed strategy obtains the entire Pareto front with multiple Pareto optimal solutions. It can better balance the trade-off and provide flexible optimal solutions that can adjust to the platoon's priority in different scenarios.

Fourthly, in the context of the platoon's controller, the traditional distributed feedback controller suffers from slow convergence speed, and the traditional sliding mode controller lacks scientific evidence when choosing control parameters. However, past studies selected the controller's gains arbitrarily within a wide range by the transfer function method. To bridge the gap, Chapters 4 and 5 employ a Riccati inequality-based sliding mode control strategy to calculate the feasible controller's gains. As a result, the closed-loop stability theorem for a nonlinear heterogeneous platoon interconnected is derived using the Lyapunov analysis. Therefore, the advantage of fast convergence speed is preserved while the platoon's stability is ensured.

Finally, many communication failures occur in the platoon, which should be considered in the CAVs control problem. For example, Section 4.2 deals with the platoon with a time delay. Section 5.2 handles the platoon with actuator faults. The latest research on the platoon's packet loss was based primarily on a third-order linearised vehicle dynamic model that only addressed powertrain time lag. Section 5.3 proposes a discrete sliding mode controller based on a nonlinear vehicle dynamic model to deal with packet loss for practicality. Moreover, a third-order nonlinear heterogeneous model is considered in Section 4.3 and Section 5.

To sum up, this research studies the information flow topology of CAVs, and proposes advanced sliding mode controllers to deal with the platoon with various communication failures while using evolutionary algorithms to find the Pareto optimal information flow topology and

improve the platoon’s performance systematically. The proposed strategies are proved to be effective with simulations, and experiments also verify some.

7.3 Originalities of Research

1) This research examines the impact of both conventional and innovative topologies on the platoon's performance systematically and quantitatively, using multiple evaluation criteria to investigate the platoon's performance. The platoon's performance regularities were discovered and concluded in a broad view with clear evidence of consistency.

2) This research employs a Riccati inequality-based sliding mode control strategy and establishes a closed-loop stability theorem for a nonlinear heterogeneous platoon interconnected by asymmetric topologies. As a result, the advantage of fast convergence speed is preserved while the platoon's stability is ensured.

3) To deal with packet loss, this research proposes a discrete sliding mode controller based on a nonlinear vehicle dynamic model instead of a third-order linearised vehicle dynamic model that only addresses powertrain time lag. Therefore, it is more practical and suitable for platoons in real-world applications.

4) This research utilises NSGA-II and modified MOEA/D to find the Pareto optimal information flow topology and an optimal asymmetric degree in the topological matrix. It balances the trade-off and provides flexible optimal solutions that can adjust to the platoon's priority in different scenarios. It optimises the platoon's multi-objectives in complex control problems with varying vehicle dynamics, information feedback delay, and external disturbances.

5) This research proposes a two-step framework to balance the trade-off between online and offline information flow topology searching. Superior topology solutions are preserved, while computation time and energy are significantly reduced. It deals with predictable imperfect communication scenarios in real-time while providing a satisfying topology-switching solution.

7.4 Some Future Work

Several controllers related to information flow topology are proposed in this research, but some interesting research topics are worth investigating in the field of CAVs. Some possible future works are listed as follows:

1) Increasing communication links lead to better tracking ability, however, at the cost of communication cost. Therefore, the trade-off between the communication cost of optimal information flow topology and its tracking ability should be investigated.

2) Using evolutionary algorithms to search for the Pareto optimal information flow topology

can be time and energy-consuming. Although a two-step topology switching framework is proposed to move the searching process offline, other computationally effective algorithms should be considered for online optimisation.

3) Regarding the platoon's multi-objective optimisation, the current approach considers tracking ability, fuel economy, and driving comfort. In addition, other critical platoon performance evaluation indices, such as the safety index, could be considered.

4) The proposed two-step topology switching framework works for predictable weather and traffic. However, an event-triggered topology switching approach could be investigated for unpredictable weather and traffic conditions in the future.

5) Regarding the traffic system, the current research considers only CAVs. However, a mixed traffic scenario where HDVs and CAVs co-exist is also -worth studying, where the impact of the platoon could be investigated in a mixed traffic scenario [115-117].

6) The proposed approach optimises the platoon's performance to a great extent. However, it should be noted that it comes with a high communication cost. Therefore, the balance between the platoon's performance optimisation and communication cost should be considered in the future.

Bibliography

[1] Zheng, Y., Li, S.E., Wang, J. and Li, K., 2014, October. Influence of information flow topology on closed-loop stability of vehicle platoon with rigid formation. In *17th International IEEE Conference on Intelligent Transportation Systems (ITSC)* (pp. 2094-2100). IEEE.

[2] Petrillo, A., Pescapé, A. and Santini, S., 2018. A collaborative approach for improving the security of vehicular scenarios: The case of platooning. *Computer Communications*, *122*, pp.59-75.

[3] Ramezani, M. and Ye, E., 2019. Lane density optimisation of automated vehicles for highway congestion control. *Transportmetrica B: Transport Dynamics*, *7*(1), pp.1096-1116.

[4] Montanaro, U., Dixit, S., Fallah, S., Dianati, M., Stevens, A., Oxtoby, D. and Mouzakitis, A., 2019. Towards connected autonomous driving: review of use-cases. *Vehicle system dynamics*, *57*(6), pp.779-814.

[5] Zhu, Y., Wu, J. and Su, H., 2020. V2V-based cooperative control of uncertain, disturbed and constrained nonlinear CAVs platoon. *IEEE Transactions on Intelligent Transportation Systems*.

[6] Li, Y., Tang, C., Peeta, S. and Wang, Y., 2018. Nonlinear consensus-based connected vehicle platoon control incorporating car-following interactions and heterogeneous time delays. *IEEE Transactions on Intelligent Transportation Systems*, *20*(6), pp.2209-2219.

[7] Su, D. and Ahn, S., 2017. In-vehicle sensor-assisted platoon formation by utilizing vehicular communications. *International Journal of Distributed Sensor Networks*, *13*(7), p.1550147717718756.

[8] He, D., Qiu, T. and Luo, R., 2020. Fuel efficiency-oriented platooning control of connected nonlinear vehicles: a distributed economic MPC approach. *Asian Journal of Control*, *22*(4), pp.1628-1638.

[9] Zheng, Y., Li, S.E., Li, K. and Wang, L.Y., 2015. Stability margin improvement of vehicular platoon considering undirected topology and asymmetric control. *IEEE Transactions on Control Systems Technology*, *24*(4), pp.1253-1265.

[10] Wang, W., Wang, C., Guo, Y., Luo, X. and Gao, Y., 2020. Self-triggered consensus of vehicle platoon system with time-varying topology. *Frontiers in Neurorobotics*, *14*, p.53.

[11] Musa, M.J., Sudin, S., Mohammed, Z. and Sha'aban, Y.A., 2019, March. Model predictive control for an improved vehicle convoy communication. In *Proc. IEEE 1st Int. Conf. Mechatronics, Automat. Cyber-Phys. Comput. Syst.* (pp. 1-6).

[12] Halder, K., Montanaro, U., Dixit, S., Dianati, M., Mouzakitis, A. and Fallah, S., 2020. Distributed H∞ controller design and robustness analysis for vehicle platooning under random packet drop. *IEEE Transactions on Intelligent Transportation Systems*.

[13] Feng, S., Song, Z., Li, Z., Zhang, Y. and Li, L., 2021. Robust platoon control in mixed traffic flow based on tube model predictive control. *IEEE Transactions on Intelligent Vehicles*, 6(4), pp.711-722.

[14] Ma, F., Wang, J., Zhu, S., Gelbal, S.Y., Yang, Y., Aksun-Guvenc, B. and Guvenc, L., 2020. Distributed control of cooperative vehicular platoon with nonideal communication condition. *IEEE Transactions on Vehicular Technology*, *69*(8), pp.8207-8220.

[15] Wang, J., Ma, F., Yang, Y., Nie, J., Aksun-Guvenc, B. and Guvenc, L., 2020. Adaptive event-

triggered platoon control under unreliable communication links. *IEEE Transactions on Intelligent Transportation Systems*.

[16] Zheng, Y., Li, S.E., Wang, J., Cao, D. and Li, K., 2015. Stability and scalability of homogeneous vehicular platoon: Study on the influence of information flow topologies. *IEEE Transactions on intelligent transportation systems*, *17*(1), pp.14-26.

[17] Zhu, Y. and Zhu, F., 2018. Distributed adaptive longitudinal control for uncertain third-order vehicle platoon in a networked environment. *IEEE Transactions on Vehicular Technology*, 67(10), pp.9183-9197.

[18] Zhu, Y., He, H. and Zhao, D., 2019. LMI-based synthesis of string-stable controller for cooperative adaptive cruise control. *IEEE Transactions on Intelligent Transportation Systems*, 21(11), pp.4516-4525.

[19] Wei, S., Zou, Y., Zhang, T., Zhang, X. and Wang, W., 2018. Design and experimental validation of a cooperative adaptive cruise control system based on supervised reinforcement learning. *Applied sciences*, 8(7), p.1014.

[20] Xin, Q., Fu, R. and Ukkusuri, S.V., 2022. Safe and sub-optimal CAV platoon longitudinal control protocol accounting for state constraints and uncertain vehicle dynamics. *Journal of the Franklin Institute*, 359(15), pp.7866-7892.

[21] Rizk, H., Chaibet, A. and Kribèche, A., 2023. Model-Based Control and Model-Free Control Techniques for Autonomous Vehicles: A Technical Survey. *Applied Sciences*, *13*(11), p.6700.

[22] Li, D. and Guo, G., 2020. Prescribed performance concurrent control of connected vehicles with nonlinear third-order dynamics. *IEEE Transactions on Vehicular Technology*, 69(12), pp.14793-14802.

[23] Gkizas, G., Yfoulis, C., Amanatidis, C., Stergiopoulos, F., Giaouris, D., Ziogou, C., Voutetakis, S. and Papadopoulou, S., 2018. Digital state-feedback control of an interleaved DC–DC boost converter with bifurcation analysis. *Control Engineering Practice*, 73, pp.100-111.

[24] Ma, W. and Ouyang, S., 2019. Control strategy for inverters in microgrid based on repetitive and state feedback control. *International Journal of Electrical Power & Energy Systems*, 111, pp.447-458.

[25] Sawant, J. and Chaskar, U., 2021, February. State Feedback Control of a Platoon in the Presence of Parametric Uncertainty and Communication Delay. In *2021 International Conference on Computing, Communication, and Intelligent Systems (ICCCIS)* (pp. 845-850). IEEE.

[26] Wang, Y., Su, R. and Wang, B., 2022. Optimal control of interconnected systems with time-correlated noises: Application to vehicle platoon. *Automatica*, 137, p.110018.

[27] Zhang, D., Shen, Y.P., Zhou, S.Q., Dong, X.W. and Yu, L., 2020. Distributed secure platoon control of connected vehicles subject to DoS attack: Theory and application. *IEEE Transactions on Systems, Man, and Cybernetics: Systems*, 51(11), pp.7269-7278.

[28] Liu, C., Yue, X., Shi, K. and Sun, Z., 2022. *Spacecraft Attitude Control: A Linear Matrix Inequality Approach*. Elsevier.

[29] Graham C. Goodwin, Stefan F. Graebe, and Mario E. Salgado. 2000. Control System Design (1st. ed.). *Prentice Hall PTR*, USA.

[30] Feng, G., Dang, D. and He, Y., 2020. Robust coordinated control of nonlinear heterogeneous platoon interacted by uncertain topology. *IEEE Transactions on Intelligent Transportation Systems*.

[31] Xu, L., Zhuang, W., Yin, G. and Bian, C., 2018. Stable longitudinal control of heterogeneous vehicular platoon with disturbances and information delays. *IEEE Access*, 6, pp.69794-69806.

[32] Wu, Y., Li, S.E., Cortés, J. and Poolla, K., 2019. Distributed sliding mode control for nonlinear heterogeneous platoon systems with positive definite topologies. *IEEE Transactions on Control Systems Technology*, *28*(4), pp.1272-1283.

[33] Guo, J., Luo, Y. and Li, K., 2017. Adaptive fuzzy sliding mode control for coordinated longitudinal and lateral motions of multiple autonomous vehicles in a platoon. *Science China Technological Sciences*, *60*(4), pp.576-586.

[34] Song, J.C. and Ju, Y.F., 2020. Distributed adaptive sliding mode control for vehicle platoon with uncertain driving resistance and actuator saturation. *Complexity*, *2020*.

[35] Guo, G. and Li, D., 2018. PMP-based set-point optimization and sliding-mode control of vehicular platoons. *IEEE Transactions on Computational Social Systems*, *5*(2), pp.553-562.

[36] Bajoria, N., Sahu, P., Nema, R.K. and Nema, S., 2016, December. Overview of different control schemes used for controlling of DC-DC converters. In *2016 International Conference on Electrical Power and Energy Systems (ICEPES)* (pp. 75-82). IEEE.

[37] Uçak, K. and Öke Günel, G., 2020. An adaptive sliding mode controller based on online support vector regression for nonlinear systems. *Soft Computing*, 24(6), pp.4623-4643.

[38] Herman, I., Martinec, D., Hurák, Z. and Sebek, M., 2014, June. Harmonic instability of asymmetric bidirectional control of a vehicular platoon. In *2014 American Control Conference* (pp. 5396-5401). IEEE.

[39] Herman, I. and Sebek, M., 2016, December. Optimal distributed control with application to asymmetric vehicle platoons. In *2016 IEEE 55th Conference on Decision and Control (CDC)* (pp. 4340-4345). IEEE.

[40] Li, Y., Li, K., Zheng, T., Hu, X., Feng, H. and Li, Y., 2016. Evaluating the performance of vehicular platoon control under different network topologies of initial states. *Physica A: Statistical Mechanics and its Applications*, *450*, pp.359-368.

[41] Wu, J., Wang, Y., Wang, L., Shen, Z. and Yin, C., 2018. Consensus-based platoon forming for connected autonomous vehicles. *IFAC-PapersOnLine*, *51*(31), pp.801-806.

[42] Li, Y., Tang, C., Li, K., He, X., Peeta, S. and Wang, Y., 2018. Consensus-based cooperative control for multi-platoon under the connected vehicles environment. *IEEE Transactions on Intelligent Transportation Systems*, *20*(6), pp.2220-2229.

[43] Chen, D., Ahn, S., Chitturi, M. and Noyce, D., 2018. Truck platooning on uphill grades under cooperative adaptive cruise control (CACC). *Transportation research part C: emerging technologies*, *94*, pp.50-66.

[44] Li, S.E., Wang, Z., Zheng, Y., Yang, D. and You, K., 2020. Stability of general linear dynamic multi-agent systems under switching topologies with positive real eigenvalues. *Engineering*, *6*(6), pp.688-694.

[45] Chehardoli, H. and Ghasemi, A., 2018. Adaptive centralized/decentralized control and identification of 1-D heterogeneous vehicular platoons based on constant time headway policy. *IEEE Transactions on Intelligent Transportation Systems*, *19*(10), pp.3376-3386.

[46] Li, Y., Tang, C., Li, K., Peeta, S., He, X. and Wang, Y., 2018. Nonlinear finite-time consensus-based connected vehicle platoon control under fixed and switching communication topologies. *Transportation Research Part C: Emerging Technologies*, *93*, pp.525-543.

[47] Gao, F., Lin, F.X. and Liu, B., 2020. Distributed H∞ control of platoon interacted by switching and undirected topology. *International Journal of Automotive Technology*, 21(1), pp.259-268.

[48] Li, Y., Tong, S., Liu, L. and Feng, G., 2017. Adaptive output-feedback control design with prescribed performance for switched nonlinear systems. *Automatica*, *80*, pp.225-231.

[49] Li, Y. and Tong, S., 2016. Command-filtered-based fuzzy adaptive control design for MIMO-switched nonstrict-feedback nonlinear systems. *IEEE Transactions on Fuzzy Systems*, *25*(3), pp.668-681.

[50] Hu, M., Li, C., Bian, Y., Zhang, H., Qin, Z. and Xu, B., 2022. Fuel economy-oriented vehicle platoon control using economic model predictive control. *IEEE Transactions on Intelligent Transportation Systems*, 23(11), pp.20836-20849.

[51] Qin, R., Lu, Y., Guan, J. and Ji, C., 2021, December. Eco-driving speed optimization model of urban intelligent connected vehicle platoon considering driver's comfort level. In 2*021 2nd International Conference on Electronics, Communications and Information Technology (CECIT)* (pp. 532-537). IEEE.

[52] Zhang, X., Li, L. and Zhu, X., 2020. Computation of Time Delay Stability Margin for the Automated Vehicular Platoon. *Complexity*, *2020*.

[53] Chanfreut, P., Keijzer, T., Ferrari, R.M. and Maestre, J.M., 2020. A topology-switching coalitional control and observation scheme with stability guarantees. *IFAC-PapersOnLine*, *53*(2), pp.6477-6482.

[54] Li, S.E., Zheng, Y., Li, K., Wu, Y., Hedrick, J.K., Gao, F. and Zhang, H., 2017. Dynamical modeling and distributed control of connected and automated vehicles: Challenges and opportunities. *IEEE Intelligent Transportation Systems Magazine*, *9*(3), pp.46-58.

[55] Wang, C., Dai, Y. and Xia, J., 2020. A CAV platoon control method for isolated intersections: guaranteed feasible multi-objective approach with priority. *Energies*, *13*(3), p.625.

[56] Yang, X.T., Huang, K., Zhang, Z., Zhang, Z.A. and Lin, F., 2020. Eco-driving system for connected automated vehicles: multi-objective trajectory optimization. *IEEE Transactions on Intelligent Transportation Systems*, *22*(12), pp.7837-7849.

[57] Luo, J., He, D., Zhu, W. and Du, H., 2022. Multiobjective Platooning of Connected and Automated Vehicles Using Distributed Economic Model Predictive Control. *IEEE Transactions on Intelligent Transportation Systems*.

[58] Zheng, Y., Li, S.E., Li, K., Borrelli, F. and Hedrick, J.K., 2016. Distributed model predictive control for heterogeneous vehicle platoons under unidirectional topologies. *IEEE Transactions on Control Systems Technology*, *25*(3), pp.899-910.

[59] Arnold, M., Negenborn, R.R., Andersson, G. and De Schutter, B., 2009, August. Multi-area predictive control for combined electricity and natural gas systems. In *2009 European Control Conference (ECC)* (pp. 1408-1413). IEEE.

[60] Grodzevich, O. and Romanko, O., 2006. Normalization and other topics in multi-objective optimization.

[61] Yu, G., Wong, P.K., Zhao, J., Mei, X., Lin, C. and Xie, Z., 2021. Design of an acceleration redistribution cooperative strategy for collision avoidance system based on dynamic weighted multi-objective model predictive controller. *IEEE Transactions on Intelligent Transportation Systems*.

[62] Zhao, R.C., Wong, P.K., Xie, Z.C. and Zhao, J., 2017. Real-time weighted multi-objective model predictive controller for adaptive cruise control systems. *International journal of automotive technology*, *18*(2), pp.279-292.

[63] He, D., Shi, Y. and Song, X., 2019. Weight-free multi-objective predictive cruise control of autonomous vehicles in integrated perturbation analysis and sequential quadratic programming optimization framework. *Journal of Dynamic Systems, Measurement, and Control*, *141*(9).

[64] Deb, K., Pratap, A., Agarwal, S. and Meyarivan, T.A.M.T., 2002. A fast and elitist multiobjective genetic algorithm: NSGA-II. *IEEE transactions on evolutionary computation*, *6*(2), pp.182-197.

[65] Zhang, Q. and Li, H., 2007. MOEA/D: A multiobjective evolutionary algorithm based on decomposition. *IEEE Transactions on evolutionary computation*, *11*(6), pp.712-731.

[66] Ma, F., Wang, J., Yang, Y., Wu, L., Zhu, S., Gelbal, S.Y., Aksun-Guvenc, B. and Guvenc, L., 2020. Stability design for the homogeneous platoon with communication time delay. *Automotive Innovation*, 3(2), pp.101-110.

[67] Resmi, R., Mija, S.J. and Jacob, J., 2022. Discrete Laguerre-based model predictive control for dynamic consensus of a vehicle platoon with time delay. *International Journal of Systems Science*, pp.1-18.

[68] Yang, P., Tang, Y., Yan, M. and Zhu, X., 2019. Consensus based control algorithm for nonlinear vehicle platoons in the presence of time delay. *International Journal of Control, Automation and Systems*, 17(3), pp.752-764.

[69] Zhou, Z., Zhu, F., Xu, D., Guo, S. and Zhao, Y., 2022. Attack resilient control for vehicle platoon system with full states constraint under actuator faulty scenario. *Applied Mathematics and Computation*, 419, p.126874.

[70] Pan, C., Chen, Y., Liu, Y. and Ali, I., 2021. Adaptive resilient control for interconnected vehicular platoon with fault and saturation. *IEEE Transactions on Intelligent Transportation Systems*.

[71] Han, J., Zhang, J., He, C., Lv, C., Hou, X. and Ji, Y., 2022. Distributed finite-time safety consensus control of vehicle platoon with senor and actuator failures. *IEEE Transactions on Vehicular Technology*.

[72] Wen, S. and Guo, G., 2018. Cooperative control and communication of connected vehicles considering packet dropping rate. *International Journal of Systems Science*, *49*(13), pp.2808-2825.

[73] Elahi, A., Alfi, A. and Modares, H., 2021. H∞ consensus of homogeneous vehicular platooning systems with packet dropout and communication delay. *IEEE Transactions on Systems, Man, and Cybernetics: Systems*, *52*(6), pp.3680-3691.

[74] Orki, O. and Arogeti, S., 2019, November. Control of mixed platoons consist of automated and manual vehicles. In *2019 IEEE International Conference on Connected Vehicles and Expo (ICCVE)* (pp. 1-6). IEEE.

[75] Zheng, Y., Li, S.E., Li, K. and Ren, W., 2017. Platooning of connected vehicles with undirected topologies: Robustness analysis and distributed H-infinity controller synthesis. *IEEE Transactions on Intelligent Transportation Systems*, *19*(5), pp.1353-1364.

[76] Tang, Z., Xu, L., Yin, G. and Liu, H., 2019, June. L 2 String Stability of Heterogeneous Platoon under Disturbances and Information Delays. In *2019 Chinese Control And Decision Conference (CCDC)* (pp. 5472-5477). IEEE.

[77] Rakha, H., Lucic, I., Demarchi, S.H., Setti, J.R. and Aerde, M.V., 2001. Vehicle dynamics model for predicting maximum truck acceleration levels. *Journal of transportation engineering*, *127*(5), pp.418-425.

[78] Ma, Y. and Wang, J., 2020. Energetic impacts evaluation of eco-driving on mixed traffic with driver behavioral diversity. *IEEE Transactions on Intelligent Transportation Systems*, *23*(4), pp.3406-3417.

[79] Musa, M.A.J., Sudin, S., Mohamed, Z. and Nawawi, S.W., 2017, August. Novel information flow topology for vehicle convoy control. In *Asian Simulation Conference* (pp. 323-335). Springer, Singapore.

[80] Gong, S., Zhou, A. and Peeta, S., 2019. Cooperative adaptive cruise control for a platoon of connected and autonomous vehicles considering dynamic information flow topology. *Transportation research record*, *2673*(10), pp.185-198.

[81] Chehardoli, H., Ghasemi, A. and Najafi, A., 2019. Centralized and decentralized distributed control of longitudinal vehicular platoons with non-uniform communication topology. *Asian Journal of Control*, *21*(6), pp.2691-2699.

[82] Zhao, H., Dai, X., Zhang, Q. and Ding, J., 2020. Robust event-triggered model predictive control for multiple high-speed trains with switching topologies. *IEEE Transactions on Vehicular Technology*, *69*(5), pp.4700-4710.

[83] Zakwan, M., Ahmed, S. and Bajcinca, N., 2020. On output feedback stabilization of time-varying decomposable systems with switching topology and delay. *IFAC-PapersOnLine*, *53*(2), pp.4713-4718.

[84] Ucar, S., Higuchi, T. and Altintas, O., 2019, December. Platoon as a mobile vehicular cloud. In *2019 IEEE Globecom Workshops (GC Wkshps)* (pp. 1-6). IEEE.

[85] Jin, Y., Wang, H., Chugh, T., Guo, D. and Miettinen, K., 2018. Data-driven evolutionary optimization: An overview and case studies. *IEEE Transactions on Evolutionary Computation*, *23*(3), pp.442-458.

[86] Ding, J., Pei, H., Hu, J. and Zhang, Y., 2018, November. Cooperative adaptive cruise control in vehicle platoon under environment of i-VICS. In *2018 21st International Conference on*

Intelligent Transportation Systems (ITSC) (pp. 1246-1251). IEEE.

[87] Zheng, Y., Bian, Y., Li, S. and Li, S.E., 2019. Cooperative control of heterogeneous connected vehicles with directed acyclic interactions. *IEEE Intelligent Transportation Systems Magazine*, *13*(2), pp.127-141.

[88] Xu, H. and Lu, C., 2020, September. Design of switched fuzzy adaptive double coupled sliding mode control for vehicles platoon. In *2020 5th International Conference on Automation, Control and Robotics Engineering (CACRE)* (pp. 422-426). IEEE.

[89] Li, Y., Tang, C., Peeta, S. and Wang, Y., 2018. Integral-sliding-mode braking control for a connected vehicle platoon: Theory and application. *IEEE Transactions on Industrial Electronics*, *66*(6), pp.4618-4628.

[90] Li, H., Chen, Z., Fu, B., Wu, Z., Ji, X. and Sun, M., 2021. Event-triggered vehicle platoon control under random communication noises. *IEEE Access*, *9*, pp.51722-51733.

[91] Yue, W., Guo, G., Wang, L. and Wang, W., 2015. Nonlinear platoon control of Arduino cars with range-limited sensors. *International Journal of Control*, 88(5), pp.1037-1050.

[92] Ma, F., Yang, Y., Wang, J., Liu, Z., Li, J., Nie, J., Shen, Y. and Wu, L., 2019. Predictive energy-saving optimization based on nonlinear model predictive control for cooperative connected vehicles platoon with V2V communication. *Energy*, 189, p.116120.

[93] Guo, H., Liu, J., Dai, Q., Chen, H., Wang, Y. and Zhao, W., 2020. A distributed adaptive triple-step nonlinear control for a connected automated vehicle platoon with dynamic uncertainty. *IEEE Internet of Things Journal*, 7(5), pp.3861-3871.

[94] Li, S.E., Qin, X., Zheng, Y., Wang, J., Li, K. and Zhang, H., 2017. Distributed platoon control under topologies with complex eigenvalues: Stability analysis and controller synthesis. *IEEE Transactions on Control Systems Technology*, *27*(1), pp.206-220.

[95] Feng, S., Zhang, Y., Li, S.E., Cao, Z., Liu, H.X. and Li, L., 2019. String stability for vehicular platoon control: Definitions and analysis methods. *Annual Reviews in Control*, *47*, pp.81-97.

[96] Coutinho, D.F., Fu, M., Trofino, A. and Danes, P., 2008. $\mathscr{L}2$-Gain analysis and control of uncertain nonlinear systems with bounded disturbance inputs. *International Journal of Robust and Nonlinear Control: IFAC-Affiliated Journal*, *18*(1), pp.88-110.

[97] Liu, B., Gao, F., He, Y. and Wang, C., 2019. Robust control of heterogeneous vehicular platoon with non-ideal communication. *Electronics*, *8*(2), p.207.

[98] Dai, S.L., He, S., Lin, H. and Wang, C., 2017. Platoon formation control with prescribed performance guarantees for USVs. *IEEE Transactions on Industrial Electronics*, *65*(5), pp.4237-4246.

[99] Liu, Y., Zong, C. and Zhang, D., 2019. Lateral control system for vehicle platoon considering vehicle dynamic characteristics. *IET intelligent transport systems*, *13*(9), pp.1356-1364.

[100] Wang, D., Fu, M., Ge, S.S. and Li, D., 2020. Velocity free platoon formation control for unmanned surface vehicles with output constraints and model uncertainties. *Applied Sciences*, *10*(3), p.1118.

[101] Zuo, L., Wang, P., Yan, M. and Zhu, X., 2022. Platoon Tracking Control With Road-

Friction Based Spacing Policy for Nonlinear Vehicles. *IEEE Transactions on Intelligent Transportation Systems*.

[102] Wen, S. and Guo, G., 2019. Sampled-data control for connected vehicles with Markovian switching topologies and communication delay. *IEEE Transactions on Intelligent Transportation Systems*, *21*(7), pp.2930-2942.

[103] Salvi, A., Santini, S. and Valente, A.S., 2017. Design, analysis and performance evaluation of a third order distributed protocol for platooning in the presence of time-varying delays and switching topologies. *Transportation Research Part C: Emerging Technologies*, *80*, pp.360-383.

[104] Chen, J., Liang, H., Li, J. and Lv, Z., 2020. Connected automated vehicle platoon control with input saturation and variable time headway strategy. *IEEE Transactions on Intelligent Transportation Systems*, *22*(8), pp.4929-4940.

[105] Wang, P., Deng, H., Zhang, J., Wang, L., Zhang, M. and Li, Y., 2021. Model predictive control for connected vehicle platoon under switching communication topology. *IEEE Transactions on Intelligent Transportation Systems*.

[106] Qin, J., Zhang, G., Zheng, W.X. and Kang, Y., 2018. Adaptive sliding mode consensus tracking for second-order nonlinear multiagent systems with actuator faults. *IEEE Transactions on Cybernetics*, *49*(5), pp.1605-1615.

[107] Hu, Z., Huang, J., Yang, D. and Zhong, Z., 2021. Constraint-tree-driven modeling and distributed robust control for multi-vehicle cooperation at unsignalized intersections. *Transportation Research Part C: Emerging Technologies*, *131*, p.103353.

[108] Gajic, Z., 2003. *Linear dynamic systems and signals*. Upper Saddle River: Prentice Hall/Pearson Education.

[109] Tan, D. and Chen, Z., 2012. On a general formula of fourth order Runge-Kutta method. *Journal of Mathematical Science & Mathematics Education*, *7*(2), pp.1-10.

[110] Patel, K. and Mehta, A., 2020. Discrete-time sliding mode protocols for leader-following consensus of discrete multi-agent system with switching graph topology. *European Journal of Control*, *51*, pp.65-75.

[111] VanAntwerp, J.G. and Braatz, R.D., 2000. A tutorial on linear and bilinear matrix inequalities. *Journal of process control*, *10*(4), pp.363-385.

[112] Zhao, Y.X., Wu, T. and Ma, Y., 2013. A double power reaching law of sliding mode control based on neural network. *Mathematical Problems in Engineering*, *2013*.

[113] Li, J., Chen, J., Xin, B. and Dou, L., 2015, May. Solving multi-objective multi-stage weapon target assignment problem via adaptive NSGA-II and adaptive MOEA/D: A comparison study. In *2015 IEEE Congress on Evolutionary Computation (CEC)* (pp. 3132-3139). IEEE.

[114] Khandekar, A.A. and Patre, B.M., 2014. Discrete sliding mode control for robust tracking of time-delay systems. *Systems Science & Control Engineering: An Open Access Journal*, *2*(1), pp.457-464.

[115] Stern, R.E., Cui, S., Delle Monache, M.L., Bhadani, R., Bunting, M., Churchill, M., Hamilton, N., Pohlmann, H., Wu, F., Piccoli, B. and Seibold, B., 2018. Dissipation of stop-and-go waves via control of autonomous vehicles: Field experiments. *Transportation Research Part C:*

Emerging Technologies, *89*, pp.205-221.

[116] Zheng, Y., Wang, J. and Li, K., 2020. Smoothing traffic flow via control of autonomous vehicles. *IEEE Internet of Things Journal*, *7*(5), pp.3882-3896.

[117] Wang, J., Zheng, Y., Chen, C., Xu, Q. and Li, K., 2021. Leading cruise control in mixed traffic flow: System modeling, controllability, and string stability. *IEEE Transactions on Intelligent Transportation Systems*, *23*(8), pp.12861-12876.